UNIVERSITÀ DEGLI STUDI DI TORINO

Dipartimento di Scienze Biomediche ed Oncologia

Dipartimento di Scienze della Sanità Pubblica e Pediatriche

Dottorato di Ricerca in Scienze Biomediche ed Oncologia

Curriculum di Pediatria Sperimentale

Ciclo XXXIII

TESI DI DOTTORATO

Genomic Approach among Children with Medical Complexity: from Diagnosis to Therapy

Tesi presentata da: Dott.ssa Diana Carli

Tutor: Prof. Giovanni Battista Ferrero

Coordinatore del Dottorato: Prof. Emilio Hirsch

Anno Accademico: 2020/2021

Settori scientifico-disciplinare di afferenza: MED/03 Genetica Medica; MED/38 Pediatria Generale E Specialistica

Contents

1 Abstract

In recent years, clinical genetics has witnessed a rapid evolution that has revolutionized the approach to the patient with suspected genetic disease from diagnosis to therapy. The massive use of next-generation sequencing (NGS) techniques has allowed to achieve an etiological diagnosis in an increasing number of patients and has accelerated the discovery of new disease-associated genes. The etiological diagnosis is the starting point for the understanding of the natural history of the disease and for the definition of genotype-phenotype correlations through deep phenotyping. Knowledge deriving from deep phenotyping is paramount for the development of clinical guidelines, shared follow-up pathways and specific therapies. Clinical genetics is an evolving field, currently engaged on several fronts from diagnosis to therapy. This study aims to provide an overview of the manifold aspects of clinical genetics. A cohort of patients with suspected genetic disease analyzed with exome sequencing at the Regina Margherita Children's Hospital of Torino in the years 2015-2020, will be discussed. An example of description of a new disease-associated gene, discovered in this cohort and studied through an international collaboration, will be presented. Namely, the *H3F3A* and *H3F3B* genes are the cause of a new genetic condition characterized by intellectual disability and neurological regression. Subsequently, two examples of deep phenotyping will be discussed: the study of the natural history of Beckwith-Wiedemann syndrome in a series of adult patients and the genotype-phenotype correlations in the recently described *NBAS*-associated disease. Finally, one of the first therapeutic attempts with MEK inhibitors in a patient with RASopathy, treated at the Regina Margherita Children's Hospital in 2019, will be presented.

2 Introduction

Children with syndromic diseases and medical complexity are a challenge for diagnosis, treatment, and research. Advances in next-generation sequencing (NGS) technologies have led to unprecedented discoveries of new disease-associated genes that have led to the definition of the pathogenesis of numerous rare diseases and paved the way for deep phenotyping and personalized therapeutic approaches [1, 2]. NGS approaches include targeted sequencing, such as clinical exome sequencing (CES), sequencing of approximately 6000 genes associated with Mendelian diseases, whole exome sequencing (WES), and whole genome sequencing (WGS). WES analyzes the complete set of protein-coding regions, which constitutes approximately 3% of the entire genome that is over 90 million bases and WGS provides analyzes of the whole human genome that is about 3 billion bases [3]. It is estimated that the use of these technologies allows considerable savings for the National Health Service (NHS), as it would allow to obtain a diagnosis in a significant percentage of patients, avoiding the unnecessary numerous and inconclusive instrumental and laboratory analysis [1, 2]. Achieving an etiological diagnosis ends the diagnostic odyssey of rare patients but represents rather than a point of arrival, a starting point for the care and cure of these children often burdened by poor knowledge, lack of guidelines and shared therapeutic care pathways [4]. In this context, clinical research on the natural history of the disease and basic research on the pathogenetic mechanisms are of fundamental importance. The increase in this knowledge allows to structure shared care pathways and guidelines for follow-up and potentially to develop innovative and etiological therapies aimed at correcting the genetic defect underlying the phenotype [2]. For some pathologies with an older clinical and etiological definition, a lot of knowledge is available today that prompted the first therapeutic approaches aimed at patients [5, 6]. For example, RASopathies, first clinically described in 1883 [7] and caused by genetic defects discovered in 2001 [8] exploited the relative frequency of the disease, approximately 1 in 2000 [9], and the extensive biological research on the molecular

pathway shared with cancer [10]; therefore specific biological drugs are now available and, in recent years, the first in vivo therapeutic approaches have been tested on patients [6, 11].

3 Aims

The aim of this study is to provide an overview of the various aspects of clinical genetics from laboratory to patient's bed, from the basic and clinical research to personalized therapy. The results of a series of complex pediatric patients studied with exome sequencing will be presented, focusing on the challenge represented by the discovery of new disease-associates genes, namely *H3F3A* and *H3F3B* [12]. Two examples of deep phenotyping will then be discussed, one aimed at studying the evolution over time and the natural history of a rare disease, the Beckwith Wiedemann spectrum [13] and one aimed at discovering new genotype-phenotype correlations of a recently defined syndrome, the *NBAS*-associated disease [14]. Finally, one of the first therapeutic approaches aimed at patients with rare diseases will be presented, reporting the experience of treatment with MEK inhibitors in a patient with RASopathy [15].

4 Molecular Diagnosis of Rare Diseases in Children

In this chapter a cohort of patients with suspected genetic disease analyzed with exome sequencing at the Regina Margherita Children's Hospital of Torino in the years 2015-2020, will be reported. Two children in this cohort were found to carry pathogenic variants in the *H3F3A* and *H3F3B* genes that, at the time of the analysis, were not associated with a phenotype. An international collaborative work allowed to confirm the association of this genes with the disease and will be reported as example of new gene discovery [12].

4.1 Exome Sequencing in a cohort of Pediatric Patients with Medical Complexity

4.1.1 Introduction

Congenital anomalies and intellectual disability are the most common indications for genetic analysis in the pediatric population and include a several conditions. Identification of an underlying diagnosis ends the diagnostic odyssey of these patients and lead to better management [2]. Diagnostic yield of exome sequencing in the literature varies from 25% [16–21] to 57% [22–25] mainly depending on patients' selection and clinical characteristic of the studied cohorts.

4.1.2 Patients and Methods

4.1.2.1 Patients

One hundred twenty-three patients followed at the Pediatric Clinical Genetics Service of the Regina Margherita Children's Hospital from January 2015 to January 2020 were included in the study and analyzed with CES, WES or WGS analysis. Patients with a complex clinical picture suggestive of genetic origin with previous negative genetic and metabolic analyses were included.

4.1.2.2 Genetic analyses

4.1.2.2.1 Clinical exome sequencing (CES)

The clinical exome sequencing kit used (SOPHIA GENETICS) consists of over 100,000 probes and spans 12 Megabases which correspond to the coding part of approximately 4,900 genes, the variants of which are known to cause hereditary diseases. The Sophia DDM® platform was used for biocomputerized data analysis and variant prioritization with annotations and preclassifications of SNV, Indels and CNV in all genes under analysis. Variant validation and segregation was attained by Sanger sequencing.

4.1.2.2.2 Whole exome sequencing (WES)

Targeted enrichment and massively parallel sequencing experiments were performed on genomic DNA extracted from circulating leukocytes for the affected subjects and their parents, by means of Illumina NextSeq 500 instrument. Exome capture was carried out using SureSelect Clinical Research Exome V2 kit (Agilent), obtaining more than 100 million paired-end reads per sample. Data analysis was performed using a bioinformatics approach that mainly exploits the Genome Analysis Toolkit (GATKV.3.7) [26]. Mapping of reads was done by BWA V.0.7.12 [27], and GATK tools were used for basic quality recalibration and variant calling. SNPs and small INDELs were identified using the GATK HaplotypeCaller used in gVCF mode, followed by genotyping, phasing, and filtering of variants based on the latest GATK "best practices". High-quality variants were then filtered out against public databases (dbSNP150 and gnomAD V.2.0) to preserve private variants associated with a clinical phenotype, variants noted with unknown frequency or with MAF <0.1% and occurring with a frequency <2% in an internal database that includes frequency data of approximately 900 Whole Exome Sequencing matched to the population. SnpEff toolbox (V.4.3) [28] was used to predict the functional impact of variants, which were filtered to preserve only those located in exons with any effect on the coding sequence and in the splice-site regions site (variants from -3 to +8 from exon-intron junction). Furthermore, functional annotation of variants was performed using SnpEff and dbNSFP (V.3.5) [26, 29, 30]. The functional impact of the variants was analyzed by Combined Annotation Dependent Depletion (CADD) V.1.3, Mendelian Clinically Applicable Pathogenicity (M-CAP) V.1.0 [31, 32] and InterVar V.0.1 .6, to obtain the clinical interpretation according to the 2015 ACMG/AMP guidelines [33]. Variant validation and segregation were carried out by Sanger sequencing.

4.1.2.2.3 Whole genome sequencing (WGS)

Whole genome sequencing was performed on extracted DNA using sequencing-by-synthesis (SBS) NGS. The data were processed via the laboratory's proprietary pipeline v8.10.11 and aligned and reported according to build 37.1 of the Human Reference Genome

(http://www.ncbi.nlm.nih.gov/projects/genome/assembly/grc/human/). The genome was sequenced to a minimum of 40-fold coverage. Over 99% of the genome was covered at 10-fold coverage or more and at least 97% of the genome was callable (passes all quality filters). Based on the quality filters and through the analysis of an extended, multi-generation family set [34], SNV sensitivity is 99.1% and analytical Positive Predictive Value (PPV), i.e. true positive/[true positive + false positive] is 99.9%. Small insertion and deletion events were detected and reported for this assay. Insertions up to 35 bases and deletions up to 28 bases have a sensitivity and analytical PPV of approximately 80-85%. This assay has the capability to detect copy number events greater than 10 kb, however sensitivity was only assessed for events greater than 20 kb and was found to be approximately 85%. Boundaries of the CNVs reported cannot be assessed with complete accuracy, and the boundaries are estimated to lie within +/- 1 kb of the event, unless otherwise noted. For SNVs and small insertion and deletion events, interpretation is limited to variant positions that overlap an exon and its 15 base pair flanking sequence. For CNVs, interpretation is limited to events that either overlap an exon or have a boundary 1 kb upstream or downstream of an exon. Mitochondrial SNVs detected at an allele fraction greater than or equal to three percent are assessed for pathogenicity. Heteroplasmy will be reported for clinically significant variants. Mitochondrial CNVs and small insertion and deletions are not reported.

4.1.2.2.4 Variant interpretation

Variants were classified following the standards and guidelines recommended by the American College of Medical Genetics and Genomics [35].

4.1.3 Results

The cohort included 123 patients, 58 (47.2%) females and 72 (52.8%) males (Table 1), aged 4 months – 48 years; 92.6% (112/121) of the patients had 0-18 years. Clinical Exome Sequencing (CES) was performed in 45.5% of the cases (56/123), Whole Exome Sequencing (WES) in 17.1% (21/123) and Whole Genome Sequencing (WGS) in 37.4% (46/123).

Patients' detailed description is reported in Table 1 and overall results of the analyses are reported in Table 2. Details of the positive results are reported in Table 3.

Table 1. Cohort description.

Patient	Gender	Age (Years)	Short Phenotype	Pregnancy	Family History	Analysis		Result
1	M	4,8	Hypotonia, Atrial Defect, Rhizomelia, Delayed Bone Age, Facial Dysmorphisms	Uneventful	Negative	WGS	Trio	Negative
2	F	11,8	Muscular Dystrophy	Uneventful	Negative	WGS	Trio	Positive
3	M	3,2	Developmental Delay, Hypotonia, patent ductus arteriosus, Cryptorchidism, Nephrocalcinosis, Short Stature, Bone Marrow Failure, Facial Dysmorphisms	Intra Uterine Growth Restriction, Polyhydramnios	Negative	CES	Solo	Positive
4	F	7,8	Developmental Delay, Intellectual Disability, Bilateral Deafness	Polyhydramnios, assisted reproductive technology	Negative	WGS	Trio	VUS
5	M	15,1	Intellectual Disability, Aortic Stenosis, Left Cryptorchidism, Right Congenital Clubfoot	Uneventful	Negative	WGS	Trio	Negative
6	M	5,2	Developmental Delay, Hypotonia, Deafness, Brain Abnormalities	Uneventful	Negative	WGS	Trio	VUS
7	M	0,8	Macrosomia, Hypotonia, Unilateral Postaxial Polydactyly, Camptodactyly, Atrial septal defect, Epilepsy, Brain Atrophy	Increased Nuchal Translucency	Negative	WGS	Trio	Positive
8	F	4,6	Developmental Delay, Spastic Diplegia, Facial Dysmorphism	Uneventful	Negative	CES	Solo	VUS
9	M	6,9	Beckwith Wiedemann Syndrome with Extra Symptoms: Macrocephaly, Developmental Delay	Uneventful	Negative	CES	Solo	Negative
10	F	Fetus	Renal Pelvis Dilatation, Ectrodactyly	Renal and Hand Anomalies	Negative	CES	Solo	Positive
11	M	2,2	Hypotonia, Neonatal Macrosomia, Facial Dysmorphisms	Uneventful	Negative	CES	Solo	Positive
12	M	4,3	Developmental Delay, Sensorineural Deafness, Delayed Bone Age Delay, Dysmorphisms	Uneventful	Positive	WGS	Trio	Positive

13	M	5,4	Developmental Delay, Intellectual Disability, Brain Anomalies, Facial Dysmorphisms	Uneventful	Positive	WGS	Trio	VUS
14	M	9,2	Developmental Delay, Autism, Tall Stature, Facial Dysmorphism	Uneventful	Negative	CES	Solo	Positive
15	F	4,5	Global developmental delay, Macrocephaly, Strabismus, IperCKemia, Ataxia and extrapyramidal signs, Ptosis, Mild dysmorphic features	Uneventful	Negative	WGS	Trio	Positive
16	F	0,9	Bilateral Congenital Cataract, Nasal Bone Hypoplasia, Short Stature, Facial Dysmorphisms	Bilateral Cataract	Negative	WGS	Trio	Negative
17	F	3,7	Hypotonia, Developmental Delay, Joint Hypermobility, Skeletal Anomalies, Facial Dysmorphisms	Uneventful	Negative	WGS	Trio	Positive
18	M	7,4	Brain Malformations, Multiple Arthrogryposis	Anhydramnios	Negative	CES	Solo	Negative
19	F	14,0	Intellectual Disability, Ventricular Defect, Facial Dysmorphisms	Uneventful	Negative	CES	Solo	Negative
20	F	1,0	Brain Abnormalities, Distal Arthrogryposis, Microretrognathy	Uneventful	Negative	CES	Trio	Negative
21	F	9,7	Hypotonia, Developmental Delay, Intellectual Disability, Epilepsy, Arnold-Chiari Malformation Type 1, Facial Dysmorphisms	Uneventful	Negative	WGS	Trio	Positive
22	M	4,0	Klippel-Feil anomaly, Cheilognatopalatoschisis	Uneventful	Positive	CES	Solo	Negative
23	M	10,1	Developmental Delay, Intellectual Disability, Hypoacusis, Hypothyroidism, Obesity	Intra Uterine Growth Restriction, Preeclampsia	Negative	CES	Solo	Negative
24	M	5,9	Developmental Delay, Intellectual Disability, Facial Dysmorphisms	Intra Uterine Growth Restriction, Cytomegalovirus Infection	Negative	CES	Solo	Negative
25	F	13,0	Intellectual Disability, Deafness, Microcephaly, Tubular Acidosis	Uneventful	Negative	WGS	Trio	Negative
26	M	5,3	Bilateral Deafness, Macrosomia	Uneventful	Negative	WGS	Trio	VUS

27	F	5,6	Developmental Delay, Congenital Central Hypothyroidism, Obesity, Cutaneous Angiomatosis	Uneventful	Positive	CES	Solo	Positive
28	F	10,6	Developmental Delay, Intellectual Disability, Facial Dysmorphisms	Uneventful	Negative	WGS	Trio	Positive
29	F	1,7	Brain Abnormalities, Macrocephaly, Dysmorphisms	Polyhydramnios, Gestational Diabetes	Negative	CES	Solo	Positive
30	F	6,9	Intellectual Disability, Brain Anomalies, Strabismus, Microcephaly, Facial Dysmorphisms	Uneventful	Negative	WGS	Trio	Negative
31	M	3,8	Leukoencephalopathy	Uneventful	Negative	WGS	Trio	Negative
32	F	5,9	Developmental Delay, Intellectual Disability, Hydrocephalus, Atrial and Ventricular Defect, Facial Dysmorphisms	Twin Pregnancy	Positive	WES	Trio	New Candidate Gene
33	F	16,6	Aortic Valvular Heart Disease, Short Stature, Cholestatic Liver Disease, Facial Dysmorphisms	Uneventful	Negative	WES	Trio	New Candidate Gene
34	F	11,2	Intellectual Disability, Developmental Regression, Facial Dysmorphisms	Uneventful	Negative	WGS	Trio	Positive
35	M	29,0	Left Transverse Hemimelia, Right Longitudinal Hemimelia, Congenital Clubfoot	Uneventful	Negative	CES	Solo	Positive
36	F	14,9	Intellectual Disability, Tetralogy of Fallot, Growth Retardation, Facial Dysmorphisms	Cardiomyopathy	Negative	WGS	Trio	Positive
37	F	12,4	Epileptic Encephalopathy, Scoliosis	Uneventful	Negative	CES	Solo	Positive
38	F	10,0	Pulmonary Stenosis, Facial Dysmorphisms	Uneventful	Negative	WES	Trio	Positive
39	M	0,8	Developmental Delay, Macrosomia, Biliary Tract Ectasia, Facial Dysmorphisms	Uneventful	Negative	CES	Solo	Positive
40	M	11,0	Mild Intellectual Disability, Tethered Cord, Mitral Valve Disease, Macrocephaly	Macrosomia, Polyhydramnios	Negative	CES	Solo	Positive

41	M	5,8	Developmental Delay, Intellectual Disability, Strabismus, Microcephaly	Uneventful	Negative	WGS	Trio	Negative
42	M	4,5	Dextrocardia, Neurodevelopmental Delay	Uneventful	Negative	CES	Solo	Negative
43	M	16,7	Learning Difficulties, Chorioretinal Dystrophy, Short Stature, Facial Dysmorphisms	Uneventful	Negative	WES	Trio	New Phenotype
44	F	11,6	Developmental Delay, Intellectual Disability, Cleft Palate, Bilateral Varus Metatarsus, Facial Dysmorphism	Uneventful	Negative	WGS	Trio	Positive
45	F	5,7	Congenital Heart Disease, Facial Dysmorphisms	Cardiomyopathy	Negative	CES	Solo	Negative
46	M	11,1	Intellectual Disability, Facial Dysmorphisms	Uneventful	Negative	CES	Solo	Negative
47	F	11,3	Blepharophimosis, Double Left Renal District, Facial Dysmorphisms	Uneventful	Positive	CES	Solo	Negative
48	M	3,6	Dextrocardia, Ventricular defect, Right Pulmonary Hypoplasia	Cardiomyopathy	Negative	WES	Trio	VUS
49	F	3,2	Developmental Delay, Epilepsy, Microcephaly,	Art, Uneventful	Negative	CES	Solo	Negative
50	M	7,1	Developmental Delay, Intellectual Disability Mild Hypotonia, Microcephaly, Facial Dysmorphisms	Uneventful	Negative	WGS	Trio	Positive
51	M	15,6	Developmental Delay, Intellectual Disability, Epileptic Encephalopathy, Hirschprung's Disease, Skeletal Abnormalities, Facial Dysmorphisms	Uneventful	Negative	WGS	Trio	Positive
52	M	1,3	Hypotonia, Facial Dysmorphisms	Uneventful	Negative	WGS	Trio	Positive
53	F	2,8	Developmental Delay, Hypoacusis, Congenital Heart Disease, Left Polyothia	Uneventful	Positive	CES	Solo	Positive
54	M	0,6	Hypotonia, Brain Abnormalities, Distal Arthrogryposis, Microcephaly	Uneventful	Negative	WGS	Trio	VUS

55	M	9,3	Mild Intellectual Disability, Bilateral Cryptorchidism, Hyperopia, Facial Dysmorphisms	Uneventful	Negative	CES	Solo	Positive
56	F	5,5	Developmental Delay, Heart Disease, Short Stature, Facial Dysmorphisms	Cardiomyopathy	Negative	WES	Trio	Negative
57	M	9,8	Developmental Delay, Intellectual Disability, Bilateral Cryptorchidism, Developmental Abnormality of the Spine, Scoliosis	Uneventful	Negative	WGS	Trio	Positive
58	F	9,1	Intellectual Disability, Facial Dysmorphisms	Uneventful	Negative	CES	Solo	Negative
59	M	4,0	Hypotonia, Epilepsy, Cryptorchidism, Unilateral Postaxial Hexadactyly, Macrosomia	Macrosomia, Polyhydramnios.	Negative	WES	Trio	New Candidate Gene
60	M	8,9	Pulmonary Stenosis, Short Stature and Facial Dysmorphisms	Uneventful	Negative	WES	Trio	New Candidate Gene
61	M	10,0	Multiple Exostoses	Uneventful	Negative	CES	Solo	Negative
62	M	7,5	Situs Viscerum Inversus, Klippel-Feil Anomaly	Uneventful	Negative	CES	Solo	Negative
63	F	Fetus	Multiple Malformations	Multiple malformations	Negative	CES	Solo	Negative
64	M	11,0	Intellectual Disability, Heart Disease, Distal Arthrogryposis, Short Stature, Facial Dysmorphisms	Uneventful	Negative	CES	Solo	Positive
65	F	0,8	Skeletal Abnormalities, Bone Marrow Failure	Gestational Diabetes	Negative	CES	Trio	New Phenotype
66	M	15,9	Intellectual Disability, Short Stature, Facial Dysmorphisms	Uneventful	Negative	CES	Solo	Negative
67	F	3,1	Developmental Delay, Dandy-Walker Malformation, Cleft Soft Palate, Scoliosis, Congenital Clubfoot, Facial Dysmorphisms	Intra Uterine Growth Restriction. Dandy-Walker Malformation, Club Feet	Negative	WGS	Trio	Positive
68	M	2,0	Generalized Hypertonus, Congenital Clubfoot	Uneventful	Negative	CES	Solo	Negative

69	M	1,8	Severe Hypotonia, Brain Abnormalities, Blindness, Facial Dysmorphisms	Uneventful	Negative	WGS	Trio	Positive
70	M	1,6	Hypotonia, Ventriculomegaly, Hypocalcemia, Immunodeficiency	Uneventful	Negative	WGS	Trio	Negative
71	F	0,5	Muscular Dystrophy	Uneventful	Negative	WGS	Trio	Positive
72	F	11,5	Developmental Delay, Intellectual Disability, Epilepsy, Microcephaly	Uneventful	Negative	WGS	Trio	Positive
73	M	4,9	Developmental Delay, Intellectual Disability, Strabismus, Microcephaly, Facial Dysmorphisms	Uneventful	Negative	CES	Solo	Positive
74	F	10,5	Developmental Delay, Intellectual Disability, Epilepsy, Vitreous Hyperplasia	Uneventful	Negative	CES	Solo	Positive
75	F	6,9	Tethered Cord, Ventriculomegaly, Visual Impairment, Hyposomatism, Chronic Liver Disease, Hypogammaglobulinemia	Uneventful	Negative	WES	Trio	Positive
76	F	11,8	LACHT Syndrome (Pulmonary Agenesis, Congenital Heart Defect And Thumb Hypoplasia), Skeletal Abnormalities	Uneventful	Negative	WES	Trio	New Candidate Gene
77	M	4,9	Bilateral Congenital Cataract, Patellar Agenesis, Skeletal Dysplasia	Uneventful	Negative	CES	Solo	VUS
78	F	3,7	Bilateral Hearing Loss, Right Aortic Arch, Microglossia, Microstomy, Facial Dysmorphisms	Intra Uterine Growth Restriction, Cardiomyopathy, Polyhydramnios	Negative	WES	Trio	Negative
79	M	45,6	Cerebellar Hypoplasia, Retinitis Pigmentosa, Glaucoma, Growth Hormone Deficiency, Hypogonadotropic Hypogonadism	Uneventful	Negative	CES	Solo	Positive
80	F	7,5	Developmental Delay, Intellectual Disability, Hypotonia, Facial Dysmorphisms	Uneventful	Negative	CES	Solo	Negative
81	M	0,3	Mild Intellectual Disability, Ventricular and Renal Asymmetry, Cryptorchidism, Microcephaly, Facial Dysmorphisms	Intra Uterine Growth Restriction, Gestational Diabetes	Negative	WGS	Trio	Positive

82	M	12,4	Intellectual Disability, Hyperopia, Hyperlordosis, Onychodystrophy	Uneventful	Negative	WGS	Solo	Negative
83	F	0,7	Auriculo-Condylar Syndrome	Uneventful	Positive	CES	Solo	Negative
84	F	14,2	Mild Intellectual Disability, Scoliosis, Short Stature	Uneventful	Negative	CES	Solo	Negative
85	M	2,1	Hypotonia, Epilepsy, Brain Abnormalities	Uneventful	Negative	WGS	Trio	Positive
86	M	6,6	Developmental Delay, Intellectual Disability, Hypotonia, Brain Abnormalities, Congenital Heart Disease	Uneventful	Negative	WES	Trio	Positive
87	F	4,4	Brain Anomalies, Ventricular Defect, Short Stature, Facial Dysmorphisms	Uneventful	Positive	WES	Trio	Negative
88	M	8,2	Developmental Delay, Intellectual Disability, Pituitary Hypoplasia, Visual Impairment, Urogenital Malformation, Hyposomatism, Facial Dysmorphisms	Multiple Malformations	Negative	CES	Solo	VUS
89	M	19,7	Developmental Delay, Intellectual Disability, Mixed Bilateral Hearing Loss, Cleft Lip And Palate, Growth Hormone Deficiency, Short Stature, Hypogonadotropic Hypogonadism	Uneventful	Negative	CES	Solo	Positive
90	M	34,7	Thumb Hypoplasia, Renal Agenesis, Klippel-Feil Anomaly, Right Lung Hypoplasia	Uneventful	Negative	WES	Trio	Negative
91	M	13,5	Developmental Delay, Intellectual Disability, Tetralogy of fallot, Bilateral Cryptorchidism, Short Stature, Facial Dysmorphisms	Uneventful	Negative	WGS	Trio	Positive
92	M	13,0	Developmental Delay, Intellectual Disability, Bilateral Cryptorchidism, Facial Dysmorphisms	Uneventful	Negative	WGS	Trio	Positive
93	M	1,2	Cervical Syringomyelia, Congenital Clubfoot, Facial Dysmorphisms	Bilateral Club Feet	Negative	WGS	Trio	Negative
94	F	9,2	Developmental Delay, Intellectual Disability, Facial Dysmorphism	Uneventful	Negative	WGS	Trio	Negative
95	M	6,0	Developmental Delay, Recurrent Rhabdomyolysis, Primary Hypothyroidism	Uneventful, Assisted Reproductive Technology	Negative	WES	Trio	Positive

96	M	9,5	Intellectual Disability, Bilateral Cryptorchidism, Severe Microcephaly, Facial Dysmorphisms	Uneventful,	Negative	WGS	Trio	Negative
97	M	47,4	Developmental Delay, Intellectual Disability , Hyperopia, Dwarfism, Hypothyroidism, Tympanosclerosis, Periodontal Disease, Chronic Renal Failure	Uneventful,	Negative	WGS	Trio	Negative
98	M	13,9	Retinopathy, Hip Dysplasia, Growth Retardation	Uneventful,	Negative	WGS	Trio	Negative
99	M	12,8	Intellectual Disability, Aortic Arch Dilation, Poor Weight Gain, Gingival Hyperplasia, Facial Dysmorphisms	Uneventful	Negative	CES	Solo	Negative
100	F	10,5	Developmental Delay, Bilateral Ptosis, Short Stature	Toxoplasma Infection	Negative	WES	Trio	Positive
101	M	12,6	Congenital Glaucoma, Short Stature, Chronic Liver Disease, Hypogammaglobulinemia	Uneventful	Negative	WES	Trio	Positive
102	F	6,7	Intellectual Disability, Macrostomy, Connatal Tooth, Facial Dysmorphisms	Uneventful, Assisted Reproductive Technology	Negative	WES	Trio	New phenotype
103	F	3,8	Developmental Delay, Cerebellar Vermis Hypoplasia	Uneventful	Negative	WES	Trio	Positive
104	F	10,8	Mild Intellectual Disability, Tethered Cord, Atrioventricular Canal Defect, Short Stature, Facial Dysmorphisms	Uneventful	Negative	CES	Solo	Negative
105	M	3,9	Moebius-Like Phenotype	Uneventful	Negative	WGS	Duo	Positive
106	F	5,8	Developmental Delay, Congenital Heart Disease, Strabismus	Oligoidroamnios	Negative	CES	Solo	Negative
107	M	16,6	Epilepsy, Mild Ataxia, Strabismus, Cryptorchidism, Facial Dysmorphisms	Oligohydroamnios	Negative	WGS	Trio	Positive
108	M	3,4	Pulmonary Stenosis, Short Stature, Facial Dysmorphisms	Cardiomyopathy	Positive	WES	Trio	New Phenotype
109	M	0,9	Multiple Bone Fractures, Pulmonary Hypertension	Uneventful	Negative	CES	Solo	Positive

110	F	5,6	Developmental Delay, Intellectual Disability, Bilateral Coloboma, Facial Dysmorphisms	Uneventful	Negative	WES	Solo	Positive
111	F	10,6	Intellectual Disability, Microcephaly, Facial Dysmorphisms	Uneventful	Negative	CES	Solo	Positive
112	F	8,4	Mild Intellectual Disability, Facial Dysmorphisms	Uneventful	Negative	CES	Solo	Negative
113	F	0,9	Systemic Vascular Disease with Hypertension and Stroke	Uneventful	Positive	WGS	Trio	New Candidate Gene
114	F	10,1	Intellectual Disability, Duodenal Atresia, Facial Dysmorphisms	Uneventful	Positive	CES	Solo	VUS
115	M	6,6	Developmental Delay, Intellectual Disability, Bilateral Coloboma, Facial Dysmorphisms	Uneventful	Negative	CES	Solo	Negative
116	M	3,8	Developmental Delay, Congenital Heart Disease, Facial Dysmorphisms	Uneventful	Negative	CES	Solo	VUS
117	M	17,0	Keratoconus, Short Stature	Uneventful	Negative	CES	Solo	Positive
118	F	7,4	Developmental Delay, Intellectual Disability, Macrocephaly, Wilms Tumor	Polyhydramnios	Negative	CES	Solo	Positive
119	F	3,4	Developmental Delay, Muscular Dystrophy	Uneventful	Negative	WGS	Trio	Positive
120	F	Fetus	Multiple Malformations With Severe Hydrocephalus	Multiple Malformations	Positive	CES	Solo	Negative
121	F	1,5	Developmental Delay, Hypotonia, Microcephaly	Uneventful	Negative	WGS	Trio	Positive
122	F	3,9	Developmental Delay, Cleft Palate, Congenital Heart Disease, Growth Retardation, Facial Dysmorphisms	Uneventful	Negative	CES	Solo	Negative
123	F	1,2	Developmental Delay, Hypotonia, Arnold Chiari Malformation Type 1, Bilateral Ptosis	Uneventful	Negative	CES	Trio	Positive

VUS – variant of unknown significance

Table 2. Overall results.

	Type of Analysis			
Result	*CES (n=56)*	*WES (n=21)*	*WGS (n=46)*	***Total***
Positive	39.3% (n=22)	38.1% (n=8)	56.5% (n=26)	45.5% (n=56)
Negative	50% (n=28)	19% (n=4)	30.4% (n=14)	37.4% (n=46)
VUS	8.9% (n=5)	4.8% (n=1)	10.9% (n=5)	8.9% (n=11)
New Candidate Gene	-	23.8% (n=5)	2.2% (n=1)	4.9% (n=6)
New Phenotype	1.8% (n=1)	14.3% (n=3)	-	3.3% (n=4)
Total	56	21	46	123

VUS – variant of unknown significance

Table 3. Positive results.

Patient	Gene	Variant	Variant classification	Associated phenotype	Inheritance	Zigosity	Segregation Analysis
2	*COL6A3*	NM_004369.3: c.6156 G>A; p.Lys1052	Likely Pathogenic	Bethlem Myopathy 1	AD	Heterozygous	*De Novo*
3	*KAT6A*	NM_006766.5: c.4626_4627del, p.Gln1543Alafs*9	Pathogenic	Mental retardation, autosomal dominant 32 (KAT6A syndrome)	AD	Heterozygous	*De Novo*
7	*H3F3A*	ENST00000366813.1:c.377A>G, p.Gln126Arg	Pathogenic	New gene	AD	Heterozygous	*De Novo*
10	*NIPBL*	NM_133433.4: c.4791dupT; p.Asn1598fs*1	Pathogenic	Cornelia de Lange syndrome 1	AD	Heterozygous	*De Novo*
11	*FKBP14*	NM_017946.3: c.362dupC; p.Glu122Argfs*7	Uncertain Significance	Ehlers-Danlos syndrome, kyphoscoliotic type, 2	AR	Homozygous	Biallelic
12	*ANKRD11*	p.Asp1854Argfs*96	Likely pathogenic	KBG syndrome	AD	Heterozygous	Maternally Inherited
14	*NFIX*	NM_001271043.2: c.412G>T; p.Asp138Tyr	Likely Pathogenic	Sotos syndrome 2/ Marshall-Smith syndrome	AD	Heterozygous	*De Novo*
15	*H3F3B*	ENST00000254810.8):c.377A>G; p.Gln126Arg	Pathogenic	New gene	AD	Heterozygous	*De Novo*
17	*SETBP1*	NM_015559.3: c.2561C>A; p.Ser854Tyr	Likely Pathogenic	Schinzel-Giedion midface retraction syndrome	AD	Heterozygous	*De Novo*

Patient	Gene	Variant	Variant classification	Associated phenotype	Inheritance	Zigosity	Segregation Analysis
21	*ASLX1*	NM_015338.5: c.2789G>A, (p.Trp930*)	Pathogenic	Bohring-Opitz Syndrome	AD	Heterozygous	*De Novo*
27	*GNAS*	NM_000516.6: c.728 C>T; p.Ala243Va	Likely pathogenic	Pseudohypoparathyroidism	AD	Heterozygous	Inherited from Affected Parent
28	*PDE4D*	NM_001104631.2: c.2051A>G (p.Glu684Gly)	Pathogenic	Acrodysostosis-2	AD	Heterozygous	*De Novo*
29	*PIK3CA*	NM_006218.4: c.1356_1358delAGA, p.Glu453del	Pathogenic	Cowden syndrome 5	AD	Heterozygous	*De Novo*
34	*SHANK3*	c.3679dupG; p.Ala1227Gly*56	Pathogenic	Phelan-McDermid syndrome	AD	Heterozygous	*De Novo*
35	*FLNB*	NM_001164317.2: c.5274+1G>A	Pathogenic	Spondylocarpotarsal synostosis syndrome	AD	Heterozygous	*De Novo*
36	*SRCAP*	NM_006662.2: c.7330C>T, p.Arg2444Ter	Pathogenic	Floating-Harbor syndrome	AD	Heterozygous	*De Novo*
37	*SMC1A*	NM_001281463.1: c.1276_1282del; p.Ser426Lysfs*6	Pathogenic	Cornelia de Lange syndrome 2	X-linked D	Heterozygous	Unknown
38	*PTPN11*	NM_002834.5:c.417G>C (p.Glu139Asp) *False negative at previous Sanger sequencing analysis*	Pathogenic	Noonan syndrome 1	AD	Heterozygous	*De Novo*

Patient	Gene	Variant	Variant classification	Associated phenotype	Inheritance	Zigosity	Segregation Analysis
39	*IFT122*	NM_018262.3: c.512G>A, p.Arg171Gln - c.2474-3C>G	Uncertain Significance; Uncertain Significance	Cranioectodermal dysplasia 1	AR	Compound Heterozygous	Biallelic
40	*PIK3CA*	NM_006218: c.3074C>A, p.Thr1025Asn	Pathogenic	Cowden syndrome 5	AD	Heterozygous	*De Novo*
44	*SATB2*	NM_001172517.1: c.1979_1981delTCA, p.Ile660del	Pathogenic	Glass syndrome	AD	Heterozygous	*De Novo*
	DPM1	NM_003859.2: c.779C>T; p.Thr260Ile	Uncertain Significance	Congenital disorder of glycosylation, type Ie	AR	Homozygous	Biallelic
50	*DYRK1A*	NM_001396.4: c.787C>T, p.Arg263*	Pathogenic	Mental retardation, autosomal dominant 7	AD	Heterozygous	*De Novo*
51	*PIGO*	NM_032634.4: c.2854+1G>A; c.79G>A, p.Gly27Ser	Pathogenic; Uncertain significance	Hyperphosphatasia with mental retardation syndrome 2	AR	Compound Heterozygous	Biallelic
52	*LRPPRC*	NM_133259.4: c.2056A>G, p.Ile686Val (pat); c.1921-7A>G (materna).	Uncertain Significance; Uncertain Significance	Leigh syndrome, French-Canadian Type	AR	Compound Heterozygous	Biallelic
53	*SMAD4*	NM_005359.5: c.1499 T>C, p.Ile500Thr	Likely Pathogenic	sy Myhre	AD	Heterozygous	Unknown
55	*PACS1*	NM_018026.4: c.607 C>T; p.Arg203Trp	Pathogenic	sindrome PACS1-correlata (sindrome di Schuurs-Hoeijmakers)	AD	Heterozygous	*De Novo*

Patient	Gene	Variant	Variant classification	Associated phenotype	Inheritance	Zigosity	Segregation Analysis
57	*Chromosme 9 mosaic trisomy*	CNV	Pathogenic	Mosaic trisomy 9	-	-	*De Novo*
64	*SH3PXD2B*	NM_001017995.3: c.400 G>T, p.Glu134*	Pathogenic	Frank-ter Haar syndrome.	AR	Homozygous	Biallelic
67	*PIEZO2*	NM_022068.3: c.8045G>T, p.Gly2682Val	Likely pathogenic	Sindrome di Marden-Walker	AD	Heterozygous	*De Novo*
69	*RYR1*	NM_000540.2: c.11314C>T, p.Arg3772Trp (pat); 4.4Kb loss (mat)	Likely pathogenic; Likely pathogenic	Central Core Disease	AR	Compound Heterozygous	Biallelic
71	*CAPN3*	NM_000070.3: c.1524G>A;p-Glu508= (mat), c.1194-2A>G (de novo)	Likely Pathogenic; Pathogenic	CAPN3 muscular dystrophy	AR	Compound Heterozygous	Maternally Inherited; *De Novo*
72	*ASXL3*	NM_030632.3: c.3349 C>T; p.Arg1117*	Pathogenic	Bainbridge-Ropers syndrome	AD	Heterozygous	*De Novo*
73	*SOX5*	NM_001261414.3: c.1309C>T; p.Arg437Cys	Likely Pathogenic	Lamb-Shaffer syndrome	AD	Heterozygous	*De Novo*
74	*CREBBP*	NM_001079846.1: c.5243G>A, p.Arg1748His	Likely Pathogenic	Menke-Hennekam syndrome 1 Rubinstein-Taybi syndrome 1	AD	Heterozygous	*De Novo*
75	*NBAS*	NM_015909.4: c.686_687insT, p.Ser230Glnsf*4 (pat) - c.6840 G>A, p.Gly2238_Thr2280del (mat)	Pathogenic; Likely Pathogenic	SOPH syndrome Infantile liver failure syndrome 2	AR	Compound Heterozygous	Biallelic

Patient	Gene	Variant	Variant classification	Associated phenotype	Inheritance	Zigosity	Segregation Analysis
79	*PNPLA6*	NM_001166111.2: c.2431G>A, p.Gly811Ser - c.3296G>A, p.Arg1099Gln	Likely Pathogenic; Likely Pathogenic	Sindrome di Boucher-Neuhauser	AR	Compound Heterozygous	Biallelic
81	*NSD2*	NM_001042424.3: c.2523delG; p.Ser842AlafsTer17	Pathogenic	*NSD2*- neurodevelopmental disorder	AD	Heterozygous	*De Novo*
	BRWD3	NM_153252.5: c.4384A>G; p.Ser1462Gly	Uncertain Significance	Mental retardation, X-linked 93	X-linked R	Emizigosi	Maternally Inherited
85	*RRM2B*	p.Ala158Thr and p.Glu194Gly	Likely pathogenic; Pathogenic	Mitochondrial DNA depletion syndrome	AR	Compound Heterozygous	Biallelic
86	*HUWE1*	NM_031407.7: c.7029 G>A, p.Gln2343=	Pathogenic	Mental retardation, X-linked syndromic, Turner type	X-linked	Emizigosi	*De Novo*
89	*CHD7*	NM_017780.4: c.3082 A>G; p.Val44Met	Pathogenic	CHARGE sy	AD	Heterozygous	*De Novo*
91	*PACS1*	NM_018026.4: c.607 C>T; p.Arg203Trp	Pathogenic	sindrome PACS1-correlata (sindrome di Schuurs-Hoeijmakers)	AD	Heterozygous	*De Novo*
92	*NFIX*	NM_001271043.2:c.167T>A; p.Met56Lys	Likely pathogenic	Sotos syndrome 2	AD	Heterozygous	*De Novo*
95	*TANGO2*	NM_001283106.2: c.262C>T, p.Arg88*(mat) - c.338del, p.Gly113Alafs*10 (pat)	Likely Pathogenic; Likely Pathogenic	Metabolic encephalomyopathic crises, recurrent rhabdomyolysis, cardiac arrhythmias, and neurodegeneration	AR	Compound Heterozygous	Biallelic

Patient	Gene	Variant	Variant classification	Associated phenotype	Inheritance	Zigosity	Segregation Analysis
100	*CTCF*	NM_006565.3; c.293T>C, p.Leu98Ser	Likely Pathogenic	Mental retardation, autosomal dominant 21	AD	Heterozygous	*De Novo*
	ATP7B	NM_000053.3: c.2605G>A, p.Gly869Arg	Pathogenic	Wilson disease	AR	Hompzygous	Biallelic
101	*NBAS*	NM_015909.4: c.1501C>T, p.Arg501*(pat) c.6840G>A, p.Gly2238_Thr2280del (mat)	Pathogenic; Likely Pathogenic	SOPH syndrome Infantile liver failure syndrome 2	AR	Compound Heterozygous	Biallelic
103	*VLDLR*	NM_003383.5: c.154T>C, p.Cys52Arg	Uncertain Significance	Cerebellar hypoplasia and mental retardation with or without quadrupedal locomotion 1	AR	Homozygous	Biallelic
105	*TUBB3*	NM_006086.4: c.785G>A; p.ARg262His	Likely pathogenic	Fibrosis of extraocular muscles, congenital, 3A	AD	Heterozygous	*De Novo*
	CREBBP	NM_004380.3: c.2417T>C; p.Met806Thr	Uncertain Significance	Rubistein taybi syndrome	AD	Heterozygous	Unknown
107	*PACS1*	NM_018026.4: c.607 C>T; p.Arg203Trp	Pathogenic	sindrome PACS1-correlata (sindrome di Schuurs-Hoeijmakers)	AD	Heterozygous	*De Novo*
	PRKCG	NM_002739.5: c.529+2 T>C	Pathogenic	Spinocerebellar ataxia 14	AD	Heterozygous	*De Novo*
109	*EFEMP2*	NM_016938: c.1043T>G; p.Met348Arg	Uncertain Significance	Cutis laxa, autosomal recessive, type IB	AR	Homozygous	Biallelic

Patient	Gene	Variant	Variant classification	Associated phenotype	Inheritance	Zigosity	Segregation Analysis
110	*PACS1*	NM_018026.4: c.607 C>T; p.Arg203Trp	Pathogenic	sindrome PACS1-correlata (sindrome di Schuurs-Hoeijmakers)	AD	Heterozygous	*De Novo*
101	*TCF4*	NM_003199.3: c.1512del; p.Ser505Valfs*30	Pathogenic	Pitt-Hopkins syndrome	AD	Heterozygous	*De Novo*
107	*OBSL1*	NM_015311.3: c.1940_1946del; p.Trp647Leufs*24	Pathogenic	3-M syndrome 2	AR	Homozygous	Biallelic
108	*AMER1*	NM_152424.4: c.1072C>T; p.Arg358*	Pathogenic	Osteopathia striata with cranial sclerosis	X-linked D	Heterozygous	*De Novo*
109	*LMNA*	NM_170707.4: c.745C>T; p.Arg249Trp	Pathogenic	Muscular dystrophy, congenital	AD	Heterozygous	*De Novo*
121	*PDHA1*	NM_000284.3: c.1142_1145dupATCA ; p.Trp383SerfsTer6	Pathogenic	Pyruvate Dehydrogenase Deficiency	X-linked D	Heterozygous	*De Novo*
123	*TRAF7*	NM_032271.2: c.1964G>A; p.Arg655Gln	Pathogenic	Cardiac, facial, and digital anomalies with developmental delay	AD	Heterozygous	*De Novo*

4.1.4 Discussion

Molecular diagnosis was achieved in 56/123 patients (45.5%). CES analysis allowed the diagnosis in 39.3% of the cases studied, WES in 38.1% and WGS in 56.5%. The diagnostic rate of CES and WES, is consistent with the yield reported in the literature which varies from 25% to 52% [16–21]. The considerable diagnostic success rate of WGS is likely related to the sensitivity and specificity of the analysis and to the better coverage of the exonic regions. Furthermore, this analysis was reserved for patients with particularly severe clinical pictures, in which the probability of identifying a genetic etiology was particularly high. The 56.5% diagnostic rate obtained by WGS in our cohort is among the highest among those reported in the literature which range from 34% to 57% [22–25]. These findings confirm that exome sequencing is a powerful diagnostic tool for pediatric patients with complex rare disease.

4.2 Histone H3.3 beyond cancer: Germline mutations in Histone 3 Family 3A and 3B cause a previously unidentified neurodegenerative disorder in 46 patients

4.2.1 Introduction

The study of histones and their role in epigenetics is a rapidly expanding field. Histones are nuclear proteins that associate with DNA to facilitate packaging into condensed chromatin. Histones are dynamically decorated with posttranslational modifications (PTMs), which regulate these processes as DNA repair, gene expression, mitosis, and meiosis. Dysregulation of PTMs leads to cancer, neurodevelopmental syndromes, psychiatric disorders, and even cardiovascular disease [36–39]. The vast array of diseases that stem from histone dysregulation makes understanding histone biology vital to understanding the pathophysiology of many diseases and developing treatments. Histones are highly evolutionarily conserved, and only a few germline disease-causing variants in the histones themselves have been found [40]. Rather, most disease-causing variants affecting histone regulation are found in histone-modifying proteins or histone chaperones. Somatic mutations in histone H3.3 (H3.3), encoded by both *H3F3A* and *H3F3B*, have recently been identified in pediatric glia and other tumors. This discovery revolutionized the field of epigenetic changes in tumors and how they lead to cancer progression [41]. There has been one case report suggesting a relationship between a neurodevelopmental syndrome and *H3F3A*, but no additional patients or functional data have been published previously [42]. Studying how histone mutations cause disease can provide the key to understanding how mutations in the histone network lead to disease.

Histone 3 family 3 (H3F3) histones (H3.3) mark active genes, maintain epigenetic memory, and maintain heterochromatin and telomeric integrity. Every nucleosome contains a version of H3. H3.1 and H3.2 are canonical histones that are replication dependent and, therefore, added to chromatin only during DNA replication. H3.3, however, is a replication-independent variant, which differs from the canonical H3.1 and H3.2 by only five and four amino acids, respectively

[43]. *H3F3A* and *H3F3B* code for an identical protein product, H3.3, a 135–amino acid protein (after cleavage of the first methionine) with a histone tail, four α helices, and two loop domains. These genes, however, contain different regulatory and coding sequences, which lead to different expression patterns and levels for *H3F3A* and *H3F3B*. Both *H3F3B* and *H3F3A* are expressed ubiquitously, during development and throughout life, with relatively high levels of expression in the brain, testes, ovaries, and uterus [44].

Because of the biologic importance of *H3F3A* and *H3F3B*, their orthologs have been studied extensively in multiple model organisms. When both *H3f3a* and *H3f3b* are knocked out in mice, it causes embryonic lethality at embryonic day 6.5, and reduced expression leads to sterility, growth retardation, and increased neonatal lethality [45]. Disrupting either *His3.3A* or *His3.3B* in *Drosophila* is tolerated; however, disrupting both leads to sterility and increased lethality [46]. While knockout models have been studied in mice and *Drosophila*, germline missense mutations have not. There have been many studies in yeast that show the lethality of various missense mutations, but it is difficult to infer whether that means missense mutations in humans would also have a profound effect [47].

In this work, we have identified a cohort of 46 unrelated patients bearing *de novo* heterozygous germline missense mutations in *H3F3A* or *H3F3B* with a core phenotype of progressive neurologic dysfunction and congenital anomalies. Notably, although all known H3.3 mutations in humans cause cancer, none of the patients in our cohort have cancer. These mutations are distinct and appear to be acting, although it is a completely different pathogenic mechanism than the cancer-causing mutations. The mutations are spread throughout the coding sequence, and neither the location of the mutation nor whether the mutation is in *H3F3A* or *H3F3B* appears to affect the phenotype. The breadth of these previously unidentified disease-causing mutations in *H3F3A* and *H3F3B* provides evidence for how sensitive the neural-related functions of H3.3 are to small variation.

4.2.2 Materials and Methods

The Institutional Review Boards of Columbia University, the University of Michigan, Children's Hospital of Eastern Ontario, University Medical Center Hamburg-Eppendorf, and the Children's Hospital of Philadelphia approved this study. Informed consent was obtained from all individual participants included in the study. Additional informed consent was obtained from all individual participants for whom identifying information is included in this article.

4.2.2.1 Exome and genome sequencing

Genomic DNA was extracted from whole blood from the affected children and their parents. Exome or genome sequencing was performed with a variety of standard capture kits and the general assertion criteria for variant classification following ACMGG/AMP (American College of Medical Genetics and Genomics/Association for Molecular Pathology) guidelines [35]. There were no other variants in these patients that survived filtration and analysis using either dominant or recessive models and could explain the phenotypes.

4.2.2.2 Patient and control fibroblast cell lines

Six healthy control cells lines that were matched to available patient cells for passage number, age, and sex were obtained from the Coriell Institute for Medical Research tissue bank. All these fibroblast samples were derived from skin biopsies performed either on the arm or on the leg of the patient. Only a portion of the patients who participated in our study agreed to donate cellular material, and the patient mutations that were analyzed reflect the sum of the viable donations.

4.2.2.3 Histone derivatization and PTM analysis by nano–LC-MS

Histones were purified in acid as previously described by Karch *et al.* [48]. Acid-extracted histones (15 to 25 μg) were resuspended in 100 mM ammonium bicarbonate (pH 8), derivatized using propionic anhydride, and digested with trypsin as previously described [48]. The resulting histone

peptides were desalted using the C18 Stage Tips, dried using a centrifugal evaporator, and reconstituted using 0.1% formic acid in preparation for nano–LC-MS analysis.

Nano-LC was performed using the Thermo Fisher Scientific Easy nLC 1000 System equipped with a 75 μm by 20 cm in-house packed column using Reprosil-Pur C18-AQ (3 μm; Maisch GmbH, Germany). Buffer A was 0.1% formic acid, and buffer B was 0.1% formic acid in 100% acetonitrile. Peptides were resolved using a two-step gradient from 0 to 26% B over 45 min and then from 26 to 98% B over 10 min at a flow rate of 300 nl/min. The high-performance LC was coupled online to an Orbitrap Elite mass spectrometer operating in the positive mode using a Nanospray Flex ion source (Thermo Fisher Scientific) at 2.40 kV. MS was performed using data-independent acquisition (DIA) as previously described with slight modifications [48]. Briefly, two full MS scans [mass/charge ratio (*m*/*z*), 300 to 100) were acquired in the Orbitrap with a resolution of 120,000 (at 200 *m*/*z*) every eight DIA MS/MS events using isolation windows of 50 *m*/*z* each (e.g., 300 to 350, 350 to 400… 650 to 700). The full MS scan is performed twice within the same duty cycle to allow for a more resolved definition of the precursor peak profile. MS/MS events were acquired in the ion trap operating in normal mode. Fragmentation was performed using collision-induced dissociation in the ion trap mass analyzer with a normalized collision energy of 35. Automatic gain control (AGC) target and maximum injection time were 10×10^6 and 50 ms for the full MS scan and 10×10^4 and 150 ms for the MS/MS scan, respectively.

Data were searched using EpiProfile. The peptide relative ratio was calculated using the total area under the extracted ion chromatograms of all peptides with the same amino acid sequence (including all of its modified forms) as 100%. For isobaric peptides, the relative ratio of two isobaric forms was estimated by averaging the ratio for each fragment ion with different mass between the two species. Two to three biological replicates were analyzed per condition, and the relative abundance of each peptide modification was averaged across the runs.

4.2.2.4 Western blot validations

Isolated histones were separated on a 4 to 12% NuPAGE bis-tris gel and transferred to a 0.2-µm nitrocellulose blotting membrane. Membranes were blocked in TBS-T [50 mM tris-HCl (pH 7.5), 150 mM NaCl, and 0.1% Tween 20] containing 5% milk powder and probed for H3.3 (Thermo Fisher Scientific, MA5-24667; 1:5000), H3 (Abcam, ab1791; 1:5000), and H4 (Abcam, ab7311; 1:5000) primary antibodies diluted in TBS-T containing 5% milk powder. This was followed by anti-rabbit horseradish peroxidase (Abcam, ab99697; 1:10,000) and visualized using enhanced chemiluminesence prime Western blotting detection chemiluminescent reagent.

4.2.2.5 RNA-seq expression analysis

RNA was extracted using the RNeasy Mini Kit (QIAGEN) on the six samples at the same time. Extracted RNA samples underwent quality control assessment using Bioanalyzer (Agilent, Santa Clara, CA, USA) and were quantified using NanoDrop from NanoDrop Technologies (Wilmington, DE, USA). RNA libraries were prepared using the Illumina TruSeq RNA sample prep V2 with ribosomal RNA depletion and were sequenced using HiSeq 2500 sequencer (Illumina Inc., San Diego, CA, USA) at the Center for Applied Genomics at the Children's Hospital of Philadelphia per standard protocols (paired-end 100 base pairs). The RNA-seq data were aligned on the hg19 reference genome using STAR (www.encodeproject.org/software/star/) and processed using Cufflinks (http://cole-trapnell-lab.github.io/cufflinks/). For each gene, we compared the expression levels between cases and controls. A gene was considered differentially expressed if the *P* value is less than 0.05 and fragments per kilobase of transcript per million mapped reads has at least twofold change. To identify overrepresented functional categories among genes that are differentially expressed, we performed annotation analysis using the David Functional Annotation Resource (https://david.ncifcrf.gov/). Multiple testing was adjusted using the Benjamini-Hochberg approach, and enrichment was declared if the adjusted *P* value is less than 0.05.

4.2.2.6 Cellular analysis

Cellular proliferation was assayed with five patients and six control fibroblast cell lines; they were plated at 3×10^4 cells per well and then were manually counted at baseline, 24, 48, 72, and 96 hours. Then, the means ± SEM of three biological replicates using three technical replicates each were analyzed. Cell viability was analyzed with three patients and three control fibroblast cell lines; the cells were plated and grown until ~80% confluent. Then, they were stained for annexin V/propidium iodide (PI), and fluorescence-activated cell sorting (FACS) was performed on Accuri C6 (BD Biosciences). Then, the means ± SEM of four biological replicates using two technical replicates each were analyzed. Cell cycle analysis was performed with three patients and three control fibroblast cell lines; the cells were plated and grown until ~80% confluent. They were then stained for PI, and FACS was performed on Calibur and analyzed by FlowJo. Then, the means ± SEM of four biological replicates using two technical replicates each were analyzed.

4.2.2.7 Zebrafish analysis

All zebrafish experiments were approved by the University of Southern California Institutional Animal Care and Use Committee (protocol #20258). *h3f3a*^{db1092} mutants were genotyped, and control mCherry or dominant-negative D123N H3f3a mRNAs were prepared and injected at 900 ng/μl into one-cell stage embryos as described [12]. Acid-free cartilage staining with Alcian Blue was performed as described [49]. In situ hybridization was performed with the probes and procedures described in [12]. Images were captured on a Leica DM2500 compound microscope.

4.2.2.8 Computational analysis of structural location of the variants

For each H3.3 variant location, we analyzed its pattern of interatomic contacts (see below) using experimental structural information. The list of known structures was retrieved from the UniProt record of H3.3 (P84243). In all cases, the structure of H3.3 was incomplete, that is, only a fragment in complex with other proteins is described. For each variant, we identified the Protein Data Bank (PDB) entries that provided information about its location.

4.2.2.9 Computing interactions at the native locus

For each variant, we computed the network of interatomic interactions of the native residue. This network was obtained following a simple protocol: (i) retrieve the corresponding PDB, (ii) compute the network of interactions for all the protein residues using Ring, (iii) extract the interaction data corresponding to the native residue, and (iv) organize these interaction data into three groups [intramonomer (within the same H3.3 monomer), intermonomer (between H3.3 monomer and other proteins), and H3.3-DNA] [50]. Intramonomer interactions were only kept when the atoms involved came from residue pairs (i,j) separated by more than two residues in sequence, i.e., $|i - j| > 2$. Ring computations were executed with default parameters, except for "interaction type," which was set to "all." H3.3-DNA contacts were only included if their distance was lower than 5.5 Å.

4.2.3 Results

4.2.3.1 Patient mutations and phenotype

Our patient cohort consists of 46 unrelated patients bearing *de novo* germline missense mutations in *H3F3A* or *H3F3B* (Figure 1). Both *H3F3A* and *H3F3B* code for H3.3. Therefore, a heterozygous mutation in either gene would affect only about 25% of the total H3.3 in the cell, depending on different expression levels from the two genes. None of the patients have malignancies, but they share a phenotype of developmental delay, usually severe and often progressive, with mostly minor congenital anomalies (Table 4). These patients were identified through exome or genome sequencing performed for the indication of neurodevelopmental delays and/or congenital anomalies (Table 4, Figure 2). There is substantial phenotypic heterogeneity in the patients, and future individuals are likely to be identified using unbiased molecular testing. Notably, 9 of the 46 patients (21%) have demonstrated clinical neurologic degeneration, which suggests that this may be a progressive disorder. Multiple patients (26% of the cohort) have cortical atrophy on brain magnetic resonance imaging (MRI), even without intractable epilepsy. For example, the oldest patient in this cohort (32 years) developed seizures at the age of 14 years and a progressive spastic paraparesis starting at the age of 29 years.

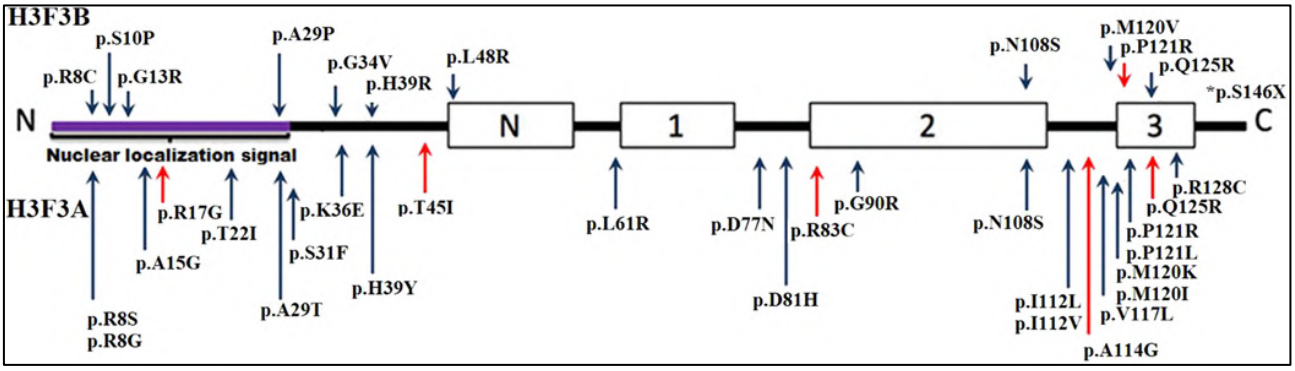

Figure 1. *H3F3A* mutations (NM_002107.4) and *H3F3B* mutations (NM_005324.4). N, 1, 2, and 3 refer to the N-Helix, Helix-1, Helix-2, and Helix-3 of H3.3, respectively. Upper mutations are encoded by *H3F3B*, and lower mutations are encoded by *H3F3A*. Red arrows indicate mutations found in two or more unrelated patients. A few variants, p.N108S, p.P121R, and p.Q125R, were

found in the same position in both H3F3A and H3F3B. *p.S146X is only present in an *H3F3B* alternate transcript not shown here.

Table 4. Clinical findings of affected patients. Developmental delay was seen in varying degrees in the majority of patients; hypotonia, poor growth, oculomotor abnormalities, seizures, abnormal skull shape, and microcephaly were also commonly seen in the patients.

33 *H3F3A*/13 *H3F3B*	
25 unique *H3F3A*/12 unique *H3F3B* variants	
3 variants in both *H3F3A* and B	
27 males/19 females	
Ages: 2 months to 32 years; 3 deceased at 2, 10 months, and 2.5 years	
Growth	
Height undergrowth	15/46 (33%)
Height overgrowth	5/46 (11%)
Weight undergrowth	4/37 (11%)
Weight overgrowth	9/37 (27%)
Microcephaly	12/46 (26%)
Development/neurologic	
Achieved independent sitting (range: 6 months to 7 years)	33/45 (73%)
Achieved independent walking (range: 15 months to 8 years)	25/41 (61%)
Spoke at least one word (range: 12 months to 6 years)	16/43 (37%)
Progression of neurologic disease	9/46 (20%)
Brain anomalies on imaging	30/41 (73%)
Cortical atrophy	10/41 (24%)
Seizures	23/46 (50%)
Hypotonia	31/46 (67%)
Spasticity	10/46 (22%)
Contractures	12/46 (22%)
Oculomotor abnormalities	25/46 (54%)
Craniofacial	
High/prominent forehead	14/46 (30%)
Hypertelorism	11/46 (24%)
Craniosynostosis/abnormal head shape (excluding plagiocephaly)	14/46 (30%)
Other	
Atrial septal defect	8/46 (18%)
Skeletal abnormalities	16/46 (35%)
Genital abnormalities	Males 12/27 (44%)
	Females 0/19 (0%)
Chronic constipation	11/45 (24%)

Figure 2. Patient facial features: Although the patients are not strikingly dysmorphic, they share some features that include a broad forehead, high insertion of the columella, and deep-set almondshaped eyes with short palpebral fissures. Photo Credits: Amy Pizzino, Children's Hospital of Philadelphia; Sarah Joy Dean, University of Alabama; Davor Lessel, University Medical Center Hamburg-Eppendorf; Constance T.R.M. Stumpel, Maastricht University Medical Center; Claudia Catarino, Ludwig-Maximilians University; Sandra Mercier, CHU Nantes; Michael J. Lyons, Greenwood Genetics Center; Julian A. Martinez-Agosto, David Geffen School of Medicine, UCLA; Elliott Sherr, UCSF; Elly Brokamp, Vanderbilt University; Katrin Õunap, Tartu University Hospital; Francesca Clementina Radio, Ospedale Pediatrico Bambino Gesù; Nina Powell-Hamilton, Alfred I. duPont Hospital for Children; K.E. Stuurman, Erasmus University Medical Center; Theresa Grebe, Phoenix Children's Hospital.

The severity of the phenotype does not correlate with the location of the mutation or whether the mutation is in *H3F3A* or *H3F3B*. Four unrelated patients have the p.T45I mutation and exhibit the full range of the phenotype severity. The age at sitting for patients with the p.T45I mutation ranges from 8 months to not achieved within 4.5 years. The age at walking was 21 months, 2 years, and 3 years and not achieved at 4.5 years. One exhibited developmental regression, while the other three did not, and only one has seizures. Even the tone abnormalities are inconsistent with three exhibiting hypotonia, while one has hypertonia. This strongly suggests that the variation in phenotype is not due to the location of the mutation but rather due to either modifying alleles or environmental factors.

Five mutations [*H3F3A* (NM_002107.4) p.R17G, p.T45I, p.A114G, p.Q125R, and *H3F3B* (NM_005324.4) p.P121R] were detected in two or more unrelated patients. p.Q125R was found in *H3F3A* in three individuals and in a different individual in *H3F3B*, while p.P121R was found in *H3F3A* in one individual and in *H3F3B* in two other individuals. Notably, in two patients,

the mutations (*H3F3A* p.Q125R and p.V117L) were identified only by trio genome sequencing after negative exome sequencing, as the last exon of *H3F3A* is currently not covered by some exome capture kits. We speculate that similar mutations in *H3F3A* may be underdiagnosed in current exome studies. It should be noted for nomenclature consistency purposes that, historically, many publications on H3.3 exclude the initiator methionine in the residue count. In this publication, we will use the traditional histone nomenclature and exclude the first methionine.

One mutation in *H3F3B* (p.S146X) is only present in the alternate transcript. It is p.V117V in the canonical transcript. Although the mutation is only in the alternate transcript, the patient phenotype is consistent with the rest of the cohort, and the patient cells have the same phenotype as the other patient cells analyzed. The role of the alternate transcript is currently unknown and requires additional study.

These 37 unique missense mutations in 46 patients are all *de novo* and, with one exception (*H3F3A* c.362 T > A; p.M120K, 1 incidence), are not found in a large database of 138,632 controls, the Genome Aggregation Database (gnomAD) [51]. Upon closer view of the raw data for this p.M120K variant, it may be a technical mapping error, as it is only present on one strand and did not meet the previous Exome Aggregation Consortium (ExAC) quality control criteria for reporting. In the general population, both genes have a very low rate of missense variants; the gnomAD missense *Z* score is 3.21 for *H3F3A* and 2.95 for *H3F3B* (>2 is significant) [51].

4.2.3.2 Computational modeling of patient mutations

It is likely that these variants are pathogenic through various different mechanisms, as they are found throughout the entire coding sequence in different domains. To explore these mechanisms further, we used molecular modeling of all 37 of the variants reported here. These 37 variants were mapped to a total of 25 loci distributed over several experimental structures. Eleven locations were in the structure of H3.3 in the nucleosome; at the sequence level, they spread from central positions

to near the C-terminal end of H3.3. The remaining 14 locations (as well as H39, which was also present in the nucleosome) were mapped to different complexes between H3.3 and epigenetic regulators. At the sequence level, they concentrated in the N-terminal tail of H3.3.

In Figure 3 (top), we show the location of the variants in the H3.3 structure (for clarity, they are shown only in one H3.3 monomer) and (Figure 3, bottom) a summary of the amount and type of interatomic contacts at each mutation locus. Together, these data suggest three broad scenarios for the variants' impact. In the first one, variants are likely to disrupt the H3.3-DNA interaction because the native residue is involved in a large number of contacts with the DNA. For instance, this would be the case of p.R83C because the arginine residue penetrates the DNA minor groove. In the second scenario, variants are more likely to disrupt the histone octamer, either because they affect the intramonomer contacts of H3.3 (e.g., p.Q125R) or because they may alter the interaction of H3.3 with other nucleosomal histones (e.g., p.L48R). In the third scenario, the variants disrupt histone-protein binding such as the p.G90R mutation disrupting chaperone binding. In summary, through different mechanisms, the variants in this section are likely to affect the formation, the deposition, or the stability of the nucleosomes containing H3.3 or of the nucleosome pairing. This may result in a generalized loosening of chromatin structure in those processes requiring the incorporation of H3.3 to the nucleosome.

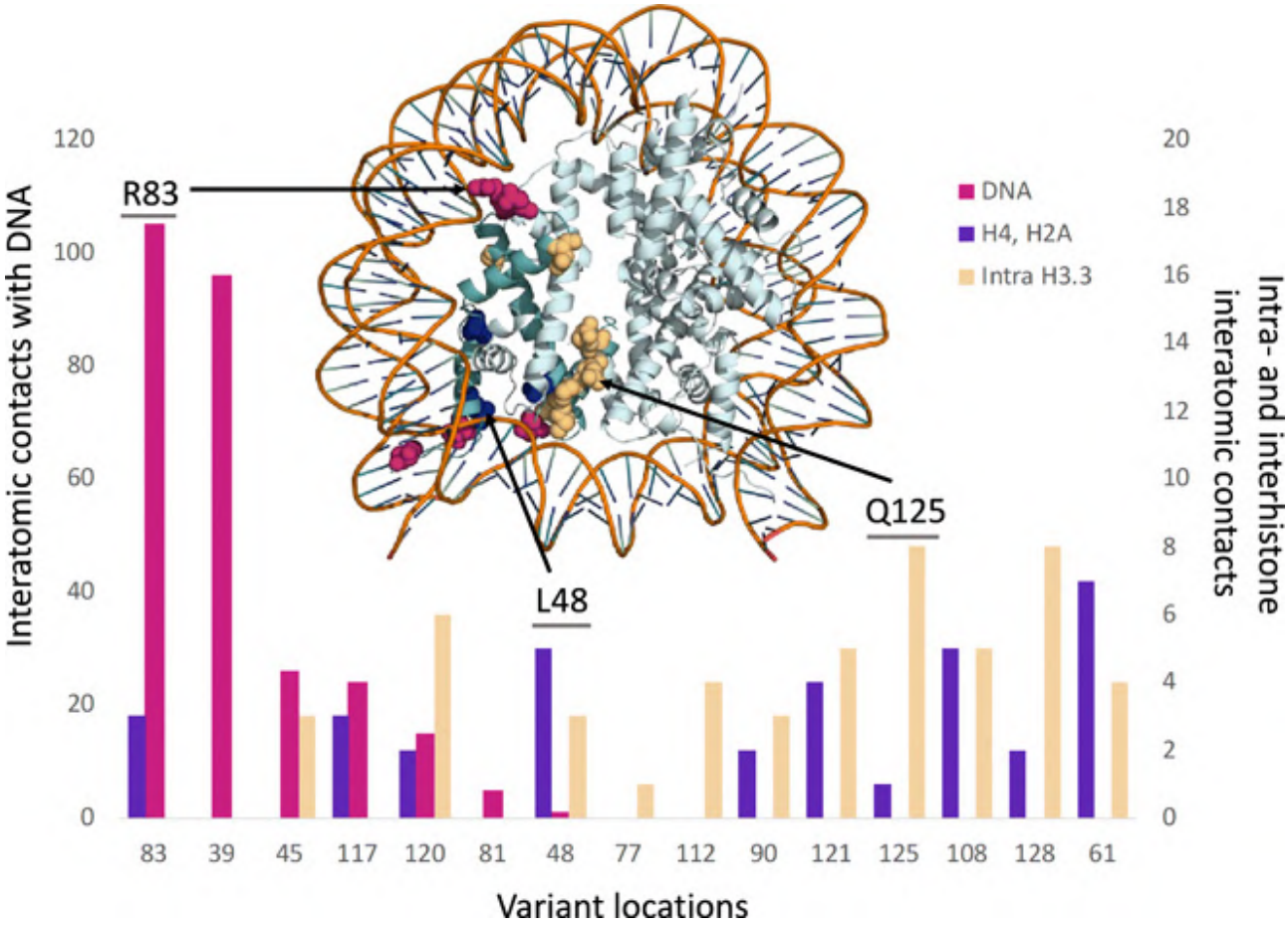

Figure 3. Variant locations in the nucleosome. At the top of the figure, we show the structure of the nucleosome with the H3.3 variants identified with spheres; the H3.3 monomer carrying them is colored in dark emerald green. The coloring of the variants reflects the predominating interactions at each location: DNA binding (magenta), intramonomer contacts (light orange), and contacts with other histones (dark blue). The same color code is used in the histogram below the structure, where we show the amount of the three interaction types at each location. Note that we use different y axis for these interactions: The y axis to the left corresponds to the H3.3-DNA binding contacts (magenta bars), and the y axis to the right corresponds to the intramonomer (light orange bars) and intermonomer contacts (dark blue bars).

The available complexes between H3.3 and epigenetic regulators (Figure 4A) involve short stretches of the H3.3 tail bound to sites of different shapes (Figure 4B). The number of interprotein contacts at the variant locus may vary substantially. For example, p.H39 has 33 and 4 contacts with SETD2 (SET Domain Containing 2, Histone Lysine Methyltransferase) and ZMYND11 (Zinc Finger MYND-Type Containing 11) domains, respectively. We find that residues p.R8, p.S31, p.K36, and p.H39 are involved in more than 10 contacts across epigenetic regulators, suggesting that their mutation may disrupt one or more biologically relevant interactions. For the remaining residues, the

number of interprotein contacts decreases rapidly, limiting our ability to interpret mutation impact. For example, visual analysis of the H3.3-BRD4 (Bromodomain-containing protein 4) complex shows that p.A15 barely participates in the complex between both proteins; contact analysis shows that p.A15 has only one interatomic contact with Brd4. Consequently, we conclude that destabilization of the H3.3-Brd4 complex is an unlikely explanation for pathogenic variants. A general mechanism that may also be valid for variants in the histone tail is that they may disrupt the internucleosome packing, an important interaction in which H3 tails are involved [52]. In summary, most of the variants in this section are likely to affect the interaction between H3.3 and epigenetic regulators with consequences that will depend on the biological role of each complex, or they may loosen chromatin structure by disrupting internucleosome packing.

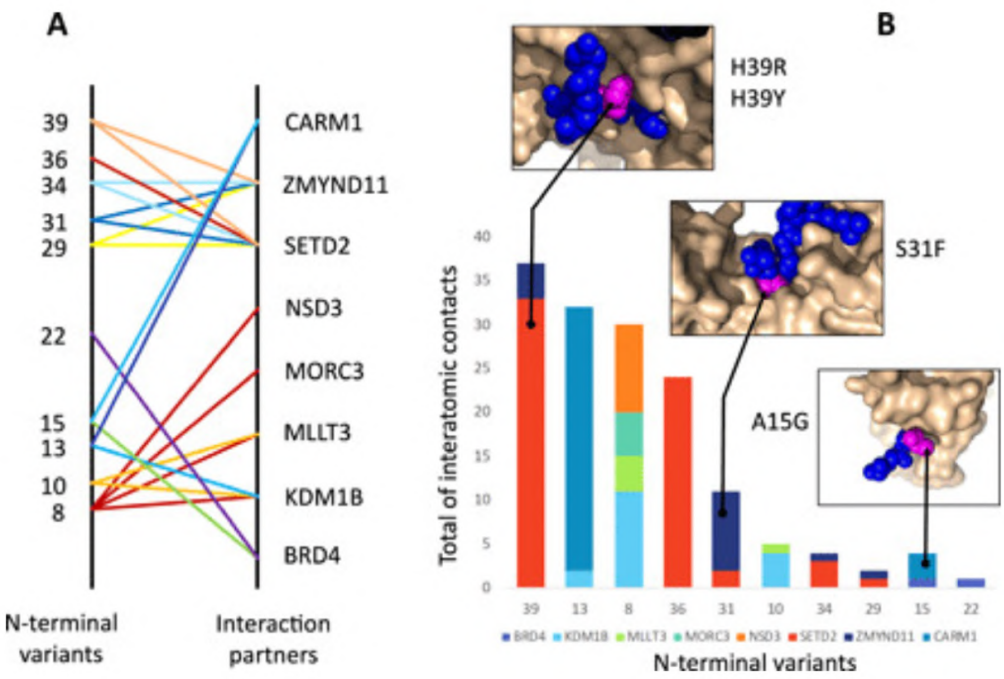

Figure 4. Variant locations in H3.3-epigenetic regulator complexes. Variant locations could be mapped to the experimental structure of different complexes involving H3.3. In (A), we show the variants mapped and the gene names of the H3.3 partners in the corresponding complex. The same color is used for the lines originating in the same variant These complexes include CARM1 (Coactivator Associated Arginine Methyltransferase 1), ZMYND11, SETD2, NSD3 (Histone-lysine N-methyltransferase NSD3), MORC3 (MORC Family CW-Type Zinc Finger 3), MLLT3 (MLLT3 Super Elongation Complex Subunit), KDM1B (Lysine Demethylase 1B), and BRD4. In (B), we show the total

amount of interatomic interactions at each location, for each H3.3-epigenetic regulator complex. To help interpretation, we give three examples where we can see the histone tail (blue spheres) interacting with its partner (continuous surface in light orange); the histone residue at the variant location is shown in magenta.

4.2.3.3 Dysregulation of PTMs is distinct for each mutation

To quantify this histone PTM dysregulation, patients' Epstein-Barr virus–transformed lymphoblasts (*H3F3A* p.A15G, *H3F3A* p.R17G, *H3F3A* p.T45I, *H3F3B* p.A29P, and *H3F3B* p.P121R) and primary fibroblasts (*H3F3A* p.R17G, *H3F3A* p.G90R, and *H3F3A* p.T45I) were obtained from patients and age- and ethnicity-matched controls. Histones were extracted and analyzed by nano–liquid chromatography–tandem mass spectrometry (LC-MS/MS) as previously described [53]. This allowed for a rigorous and robust quantification of histone PTM levels, providing insight into the global epigenetic state in each cell type. For reference, the average of the control lymphoblasts is depicted in Figure 5A. Notably, analysis of coefficients of variation both within and across patients and controls revealed that the distribution of histone PTM abundances was very similar (Figure 5B). Although these data show modest changes compared to cells that express p.K27M- or p.K36M-mutant H3.3, which display a near complete loss of di- and trimethylation at K27 or K36, a dominant negative effect cannot be ruled out [54].

It was also observed that the overall histone PTM variation was slightly greater in healthy donors than in patients. Nonetheless, some histone PTMs were reproducibly altered when comparing patients to controls (Figure 5D). Although all patients share a common phenotype of developmental delay, only some of them developed major congenital malformations (i.e., cardiac and cranial anomalies). Further study of the specific local dysregulation during development may lead to insights into the transcriptional control in these processes (i.e., cardiac and cranial development). In general, the magnitude of the changes was modest and may reflect the cell types studied and developmental timing.

The tails of H3.3 and the other H3 histones (1 to 89 amino acids) are identical except for residue 31, where they contain alanine and serine, respectively. Because peptides are generated by cleavage

at arginine residues, it is technically impossible to assign PTMs to a specific H3 histone, except in the case of p.A29P. For this case, two PTM abundances (K27 and K36) were compared between (i) protein transcribed from the mutant p.A29P allele from patient cells, (ii) protein transcript from the wild-type (WT) allele from the same patient cells, and (iii) protein transcribed from the two WT alleles from a control (Figure 5E). These data show notable local deregulation of PTMs on the mutant protein, while the WT protein from the affected patient shows fewer differences from the control. This is a more minor effect than that of published somatic oncogenic mutations; however, the difference neither confirms nor refutes a dominant negative effect [55].

Together, these data suggest that the mutant histones can be incorporated into the nucleosome, cause marked local deregulation of chromatin state, and modestly alter the global control of histone modifications. Of greatest interest are the local chromatin changes induced by mutant histone deposition: H3.3 is known to have roles in diverse functions, including gene expression and repression, chromatin stability, DNA damage repair, and differentiation. These mutant proteins and their aberrant PTM states could disrupt any of these processes to lead to the observed phenotype.

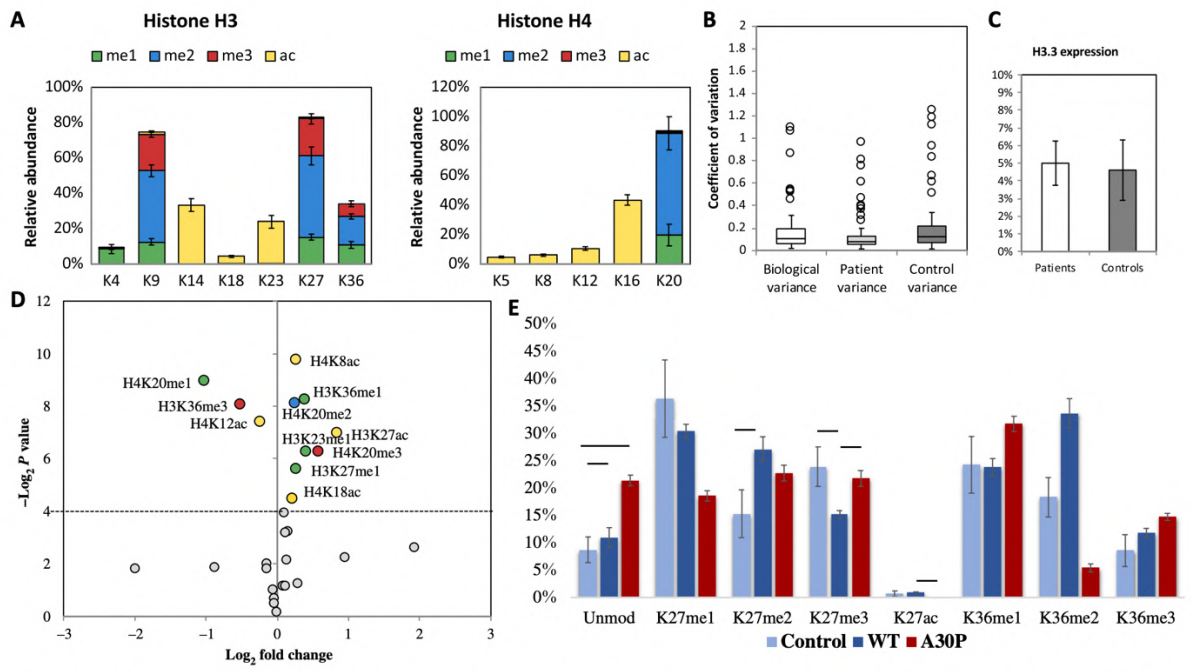

Figure 5. qMS analysis of patient samples. (A) Average profile of PTMs on canonical histones H3 and H4 across control lymphoblasts. Error bars represent SD (n = 9 donors; 3 biological replicates each). (B) Tukey boxplot depicting the coefficients of variation of 73 modified histone H3 and H4 peptides detected by nano–LC-MS/MS (biological variance: across all 14 donors; patient variance: across five patients; control variance: across nine controls). (C) Average histone H3.3 protein abundance (relative to total histone H3) in patient and control lymphoblasts. Error bars represent SD. (D) Volcano plot demonstrating significantly altered histone PTMs in patients versus controls. Dotted line represents P < 0.05 significance threshold. (E) K9 and K14 PTM abundances were compared between (i) protein transcribed from the mutant p.A15G allele from patient cells, (ii) protein transcript from the wild-type (WT) allele from the same patient cells, and (iii) protein transcribed from the WT alleles from a control. Note that the peptide from amino acids 9 to 17 is indistinguishable between canonical H3 and H3.3, so the WT peptide encompasses both. (F) A29P is the only mutation occurring on the same peptide that distinguishes H3.3 from H3. PTMs that fall on this peptide are compared across the mutant peptide, the WT peptide from the mutant sample, and the average profile of the peptide from control samples. *P < 0.05, **P < 0.01, and ***P < 0.001. This shows notable local deregulation of PTMs on the mutant peptide. qMS, quantitative mass spectrometry.

4.2.3.4 Dysregulation of transcripts associated with proliferation and mitosis

To evaluate which biological pathways were differentially perturbed in the patients, we performed RNA sequencing (RNA-seq) on fibroblast cells derived from patients and age- and ethnic-matched controls. All reads were aligned with the STAR (Spliced Transcript Alignment to a Reference) aligner, and Cufflinks was used for performing differential expression analysis. In fibroblast cells (three mutations listed above versus three controls), the H3.3 transcripts (*H3F3A* and *H3F3B*) contribution to total histone H3 expression ranged from 45.1 to 72.6% in cases and 64.1 to 81.7% in controls. We found 323 genes to be differentially expressed with at least two-fold changes in fibroblast cells ($P < 0.05$). Of these 323 genes, 166 were up-regulated, and 157 were down-regulated in cases. Differentially expressed genes were analyzed through David Functional Annotation Resource, and we found no significant biological signal in the genes with lower expression in cases but showed significant enrichment for up-regulated genes important in mitotic cell cycle process [Benjamini-Hochberg–corrected P ($P_{\text{BH-corrected}}$) = 7.8×10^{-14}], mitotic nuclear division ($P_{\text{BH-corrected}} = 5.8 \times 10^{-10}$), cell division ($P_{\text{BH-corrected}} = 7.5 \times 10^{-10}$), and many other mitosis-related processes.

To assess whether up-regulation of mitosis-related genes alters cells proliferation, we quantified the cellular proliferation capacity of five patient fibroblast lines compared to six age- and sex-matched control fibroblast lines. Patient lines had increased cell proliferation, notably at 72 and 96 hours (Figure 6A). Furthermore, all five patient lines shared similar viability to the six control lines (Figure 6B). Cell cycle analyses showed that *H3F3A* p.G90R and *H3F3A* p.T45I had a similar cell cycle profile to the control lines, while *H3F3A* p.R17G showed a decrease in cells in G_1 phase and an increase in cells in S phase compared to all three control lines (Figure 6C).

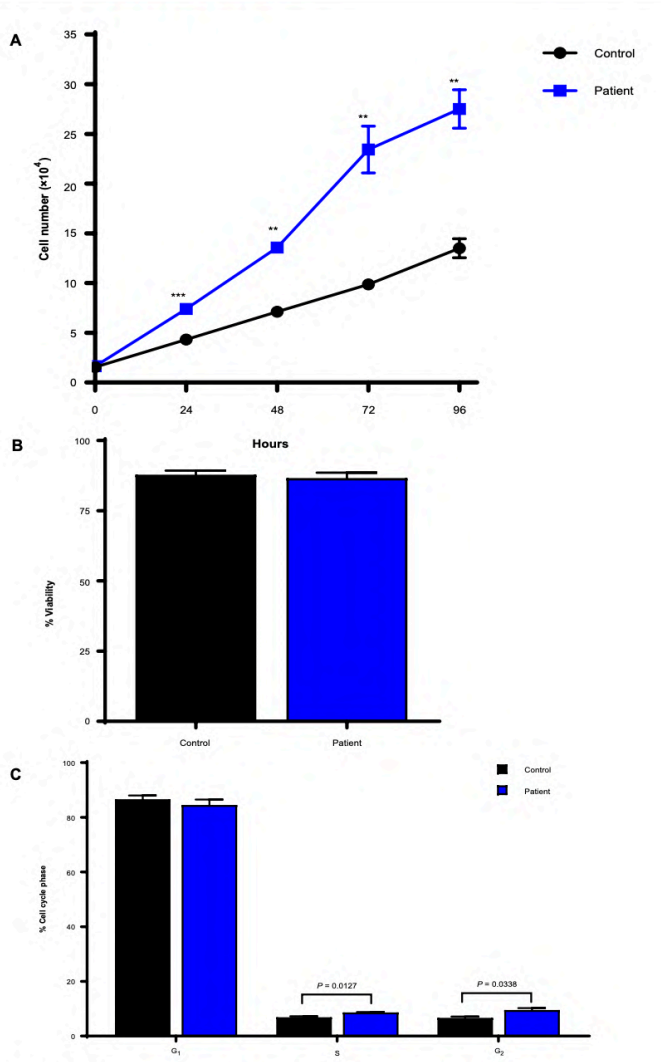

Figure 6. Cellular dynamics of patient fibroblasts. (A) Five *H3F3A/B* patient fibroblast lines (*H3F3B*: p.G34V; *H3F3A*: p.R17G; *H3F3A*: p.G90R; *H3F3A*: p.T45I; and *H3F3B*: p.V117V or p.S146X in alternate

transcript) demonstrated increased proliferation over six matched controls. **P < 0.005 and ***P < 0.0005. Data represent means ± SEM of three biological replicates using three technical replicates each. (B) The same five *H3F3A/B* patient fibroblasts and six controls show no major differences in cell viability. The data represent the means ± SEM of four biological replicates using two technical replicates each. (C) Cell cycle analysis showed differences in the S (P = 0.0127) and G2 (P = 0.0338) phase in the same five patient cell line compared to the six control fibroblast lines. Data represent the means ± SEM of four biological replicates using two technical replicates each.

4.2.3.5 Deficit in neural crest–derived cells in a zebrafish model

A dominant zebrafish model (p.D123N) derived from a forward genetic screen has been previously reported with craniofacial abnormalities, which were replicated in our patient cohort (Figure 7A) [56]. This heterozygous missense variant replicates the dominant inheritance observed in humans and is only two amino acids away from a mutation identified in an affected patient (p.Q125R). Further investigation of this model also reveals a defect in foxd3-positive neural crest–derived glia, as well as melanocytes and xanthophores (Figure 7, B to D) The loss of glial cells may relate to the hypomyelination phenotype that is noted on the brain MRIs of over one-third of the H3.3 cohort as glial cells are the cell type responsible for myelination.

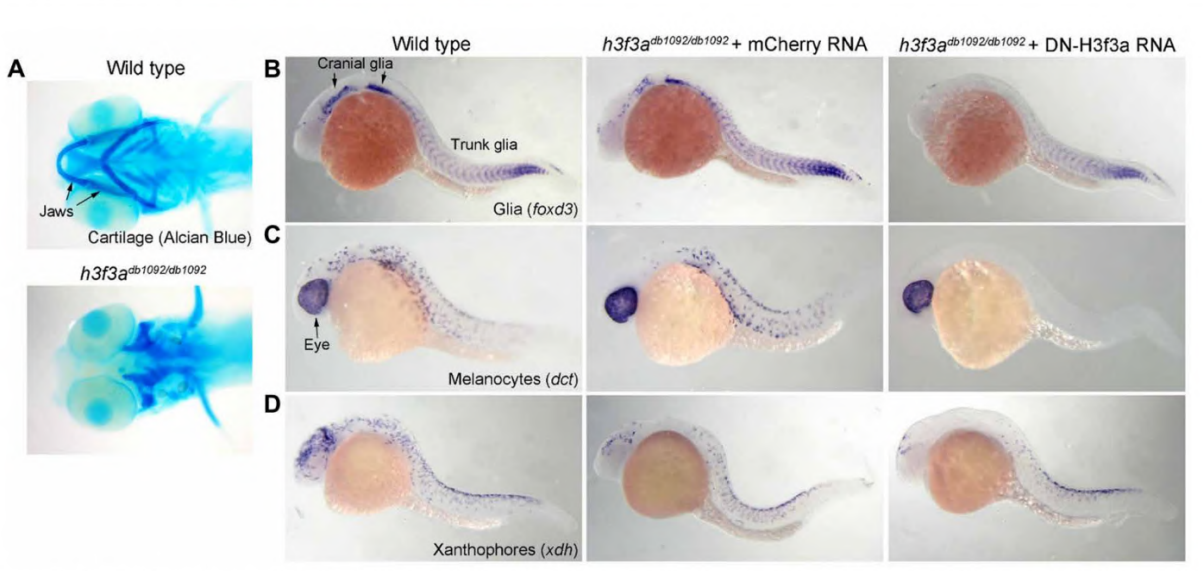

Figure 7. Requirement of H3.3A for neural crest–derived glia and pigment cells. (A) Ventral whole-mount views of larval zebrafish heads at 5 dpf stained with Alcian Blue. Homozygous h3f3adb1092 mutants display complete loss of neural crest–derived jaw cartilages (n = 10/10). (B to D) In situ hybridization of zebrafish embryos for markers of glia (foxd3; 24 hpf), melanocytes (dct; 27 hpf),

and xanthophores (xdh; 27 hpf). Homozygous h3f3adb1092 mutants injected at the one-cell stage with a control mCherry RNA show partial reductions in cranial glia (n = 5), melanocytes (n = 4), and xanthophores (n = 3), while those injected with dominant-negative H3f3a RNA to further reduced H3.3A function show complete loss of melanocytes (n = 5) and severe reductions of glia (n = 6) and xanthophores (n = 4) throughout cranial and trunk regions.

4.2.4 Discussion

The discovery of missense mutations in H3.3 that cause a neurodevelopmental disorder, but not cancer, has profound implications for future research in histone biology. Until now, H3.3 mutations have only been directly linked to cancer [41]. These specific mutations that cause a neurodevelopmental phenotype are distinct from the ones that cause cancer. The cancer mutations are mostly in lysines in the histone tail, while the only lysine mutation in our cohort is p.K36E. When this lysine-36 is mutated in cancer, it is mutated to methionine and not glutamate [57]. The patient with the p.K36E mutation was 32 years old when he was last evaluated and still had no signs of cancer, suggesting that the p.K36E mutation does not lead to a strongly increased risk of malignancy. The only other variant in our cohort that is similar to a cancer-linked variant is the p.G34V mutation in *H3F3B*. This p.G34V variant in *H3F3A* has been shown to cause cancer only when combined with mutations in *ATRX/DAXX* (ATRX Chromatin Remodeler/Death Domain Associated Protein) and *TP53* (TAR-DNA binding protein-43) [57]. Understanding why the somatic p.G34V variant causes cancer, but germline variants cause a neurodevelopmental phenotype, is currently unknown and requires further study.

Notably, although the mutations are spread throughout the coding sequence, they all converge on a similar phenotype. Each mutation affects different specific interactions but converge on the same phenotype. This suggests that the phenotype is due to dysregulation of H3.3 in general and not limited to a single mechanism. Molecular modeling revealed that mutations in the histone core likely affect nucleosome stability, while the mutations in the tail affect various protein-protein interactions. In addition to molecular modeling data, previous work in other species such as yeast can provide insights

into the pathogenic mechanism of these variants. Of particular interest, two of the five amino acids that differentiate H3.3 from canonical H3 (p.S31 and p.G90) are mutated in our patient cohort. Both p.S31 and p.G90 are essential for proper recognition of H3.3 by other proteins. Mutagenic analysis in yeast shows that mutations at p.G90 prevent H3.3-specific chaperones DAXX and UBN1 (Ubinuclein 1) from binding [58]. The serine at position 31 is required for recognition of H3.3 by ZMYND11 [59]. Mutations in *ZMYND11* cause an autosomal dominant neurodevelopmental phenotype similar to that seen in our patient cohort, including hypotonia, seizures, dysmorphic facial features, and developmental delay [60]. A second mutation in our patient cohort, p.G34V, has also been shown to disrupt ZMYND11 binding to H3.3 [59]. Other variants may disrupt histone octamer formation, nucleosome sliding, and chaperone binding based on mutagenic analysis of both H3 and H3.3 in model organisms [61–63]. We hypothesized that additional missense mutations in our cohort induce epigenetic dysregulation of histone PTMs. These histones' PTMs within the nucleosome affect chromatin state, mitotic initiation, protein-chromatin interactions, and gene expression [64–68]. Specific PTMs of unincorporated histones also mediate chaperone recognition before incorporation into the nucleosome [69].

The fact that all of these mutations are heterozygous is particularly noteworthy. Since there are two genes that produce H3.3, a heterozygous mutation in one of them means that 75% of the alleles are WT. A missense mutation in only 25% of the alleles is sufficient to cause global developmental delay, hypomyelination, cortical atrophy, and craniofacial anomalies. *H3F3A* and *H3F3B* are not expressed at the same levels so the amount of mutant protein could be more or less than 25% in any individual patient or tissue at any particular time; however, we observe the same phenotype regardless of whether the mutation is in *H3F3A* or *H3F3B* so a higher expression level from one of the genes cannot explain the severity of the phenotype. The fact that a single missense mutation in one allele causes such a severe phenotype strongly supports the importance of tight regulation of histones and histone PTMs. Furthermore, since our studies showed that the changes in the PTMs are in cis on the

mutant H3.3 and not in trans on the WT H3.3 in the same nucleosome as is observed in the cancer causing mutations, the severity of the phenotype cannot be explained by a global dysregulation of PTMs.

Although the exact mechanism of the cellular pathology in these patients is unclear, H3.3 is vital for normal neurologic functioning. A recent study showed that H3.3 begins to replace H3.1 and H3.2 in postnatal mouse and human brains in a time-dependent manner and displaces these canonical H3 variants almost completely in adulthood. The important role of H3.3 over time may explain the unique neurodegenerative phenotype, as mice with decreased H3.3 expression in the hippocampus have impaired long-term memory [70]. Humans with major depressive disorder have increased percentages of H3.3 in the nucleus accumbens, which is modulated by antidepressant therapy [71]. This suggests that H3.3 modulators may represent potential targeted therapies for H3.3-related disorders and perhaps associated neuropsychiatric conditions in the general population. Future studies in patient-derived induced pluripotent stem cell neural cell types may further elucidate the underlying pathology.

Although these are the first germline variants associated with histone H3, germline variants in histones H1 and H4 with similar features have been reported. The overgrowth and neurodevelopmental delay associated with Rahman syndrome (MIM 617537) are caused by truncating variants in H1 Histone Family, Member E (*HIST1H1E*) [72]. Recently, two specific germline variants in histone H4, which caused delayed growth and neurodevelopment, have been described in two families [73]. In addition, there are many neurodevelopmental disorders associated with the histone lysine methylases and demethylases. These histone-related disorders provide a unique window into the role of histones in the control of development and growth.

In conclusion, we show here that heterozygous de novo missense variants in *H3F3A* and *H3F3B*, coding for H3.3, are associated with a previously undescribed phenotype of developmental delay, neurodegeneration, epilepsy, facial dysmorphism, and congenital anomalies. The functional effects

of these mutations appear to be different from those that are well-studied in cancer and may offer a target for therapy for these and other patients.

5 Deep phenotyping

The diagnosis of a rare disease is the starting point for studying disease clinical features and choosing the best treatment options [2]. Patients with ultra-rare and newly discovered diseases, often face the lack of specific guidelines and the lack of knowledge on the possible complications and prognosis [74]. Moreover, clinical research on rare disease often requires international collaborations to reach enough patients to be described and studied. In this chapter two examples of clinical research through deep phenotyping on rare disease will be discussed: natural history of Beckwith Wiedemann spectrum [13] and genotype-phenotype correlation of NBAS-associated disease [14].

5.1 Phenotype evolution and health issues of adults with Beckwith-Wiedemann Syndrome

5.1.1 Introduction

With a prevalence of approximately 1 in 10,000 overall live births [75] and 1:1,000 in children conceived through assisted reproductive techniques [76], Beckwith–Wiedemann syndrome (BWS, OMIM #130650) is the commonest overgrowth condition and the paradigm of genomic imprinting disorders. Phenotype ranges within a wide spectrum of anomalies including overgrowth, macroglossia, abdominal wall defects, nephrourological malformations, hyperinsulinemic hypoglycemia, lateralized overgrowth, ear lobe creases or helical pits, hemangiomas and facial naevus flammeus, organomegaly [77–80] and increased risk of embryonal tumors in early childhood [81, 82]. The wide range of clinical presentations is partially explained by the complex heterogeneous molecular physiopathology and by the mosaic distribution of the epigenetic anomalies of the 11p15.5 chromosomal region, found in more than 80% of the clinically diagnosed patients [83]. The variable clinical presentation and the complex molecular bases have recently been highlighted, consistent with adoption of more appropriate terminology — *BWS spectrum* (BWSp) — and introduction of a new scoring system for the clinical diagnosis [83]. Generally, mild presentations do not require treatment, while the severe ones deeply impact patients' health condition and quality of life [84]. Some features (e.g. macroglossia, umbilical hernia) frequently mitigate throughout childhood making the syndrome less recognizable and impactful. Conversely, other features (e.g. limb length discrepancy) can persist through adulthood or even worsen [83] potentially easing complications (e.g. scoliosis as a consequence of uncorrected lower limb length discrepancy or anterior open bite consequent to severe macroglossia) [83, 84].

As tumor risk and overall clinical surveillance are limited to childhood, scientific reports and medical knowledge concerning BWSp is mostly limited to the first decade of life. Very few is currently known on BWSp natural history and presentation in adulthood: information on BWSp impact later in life is limited and rarely reported [85]. However, this issue appears to be of paramount importance in clinical practice as parents and young adult patients themselves have a variety of questions about possible medical problems arising in adulthood and later consequences of childhood health issues. Adolescents and adults frequently ask about fertility, pregnancy, tumor risk and later health status. Anecdotal experiences allow physicians to provide only unsatisfactory information. With these premises and prompted by patients' associations (Italian Association of Patients with BWSp, Associazione Italiana Sindrome di Beckwith-Wiedemann, AIBWS, www.aibws.org), here we investigated these issues.

5.1.2 Methods

Patients - We recruited patients with BWSp aged > or = 18 years with a search conducted through the BWS Registry of the Pediatric Genetics of our Institution and information gathered through AIBWS, data were acquired after obtaining the informed consent. BWSp diagnosis was assessed clinically and/or molecularly according to recent diagnostic criteria [83].

Data collection – Data collection was conducted through 1) administration of a standard questionnaire and 2) revision of clinical documentation, including recent medical visits or, when unavailable, conducting a physical exam. Telephone interviews, e-mail communication, contacts with the general practitioners and personal examination of the available clinical documentation including pictures were used to obtain the data. Data acquisition was divided in the following sections and items: *1) BWSp diagnosis*. Information about BWSp phenotype and genotype, including ages at diagnosis, molecular tests, specific procedures, and timing of follow up and tumor surveillance were acquired; *2) Correction of BWSp related anomalies.* Each BWSp clinical feature were investigated, with the specific medical or surgical strategy adopted, as well as the evolution of the defect, and the

impact on the overall health status at the time of the study. Information about macroglossia and associated orthodontic, swallowing and speech anomalies, the need for reductive glossectomy or orthodontic intervention were obtained. Regarding lateralized overgrowth, attention was focused on the affected body part and, in case of lower limb involvement, the orthopedical surgery or orthoses correction needed. For patients affected by abdominal wall defects information about surgery required and aesthetical revision were acquired. In-depth details were also recorded for neonatal hypoglycemia and nephrourological conditions; 3*) Follow up and cancer surveillance procedures.* Attention was focused on specific procedures and timing of follow up and medical checks concerning tumoral aspect of BWSp (i.e. abdominal ultrasound, alpha-fetoprotein measurement, etcetera); *4) Growth.* Current stature, weight and cranial circumference were acquired. Standard Deviations (SDS) was calculated for each patient based on local standards [86] and definitive stature was compared with parental height if known; *5) Qualification, functioning and physical activity.* Educational level, current and previous jobs, sport activities were obtained; *6) Prenatal findings, pregnancy and delivery data and psychomotor development*. In this section we collected information about prenatal findings, pregnancy and delivery complications, as well as data about development milestones, learning difficulties and eventual intellectual disability *7) Adult health condition.* Data about current and through-adulthood health status diseases or medical issues arose in adulthood were investigated. To each subject was primarily asked in general terms if since 18 years of age he/she had met relevant health issues requiring a significant medical intervention *8) Tumor data* were collected, focusing on histology, age of diagnosis, methods of diagnosis (accidental diagnosis, related symptoms or tumoral screening) and therapeutic strategies. *9) Reproduction and procreation.* We surveyed data about fertility (attempts to conceive, fertility exams and tests), pregnancy, delivery, and health status of the patients' offspring.

5.1.3 Results

Forty-two patients were contacted and 34 (aged 18 to 58 years, mean age 28.5±9.9, 18 females and 16 males) agreed to participate in the study. Thirty patients had a clinical diagnosis with a BWSp score ≥ 4 and four patients with a clinical score of 3 points had a positive molecular test confirming the diagnosis. Molecular tests were performed in 31 subjects, at mean age of 19.1±15.0 years: 14 patients presented 11p15.5 Imprinting Center 2 Loss of Methylation (IC2-LoM, 41.2%), 2 *KCNQ1* microduplication [87] and 1 microdeletion [88] associated with IC2-LoM, (8,8%), 2 Imprinting Center 1 Gain of Methylation (IC1-GoM, 5,9%), 1 microdeletion of the IC1 associated with IC1GoM (2,9%), 5 had 11p15.5 Paternal Uniparental Disomy (UPD(11)pat, 14.7%), 1 *CDKN1C* mutation (2.9%). Five out of the 31 patients analyzed resulted negative at the molecular tests (16.1%), while molecular analysis was not performed in 3 patients out of 34 (8.8 %). Age at diagnosis ranged from birth to 41 years (mean 5.0±9.9 years), in 17 cases (50.0%) diagnosis was formulated at birth due to easily recognizable features, in other three cases (8.8%) in the first year of life.

1) **BWSp features and correction of BWSp-related malformations** — *Table* 5 shows the clinical features and the related treatment. *Figure* 8 shows facial characteristics and macroglossia of adult patients. Overall, 52.9% (18/34), 14.7% (5/34) and 17.6% (6/34) patients underwent one, two or more surgical interventions, respectively, and five patients never underwent surgery. Surgical treatment was required for tongue reduction, cryptorchidism, lower limb length discrepancy correction, mandibular advancement, abdominal wall defects correction (all surgically corrected at birth in case of omphalocele), surgical removal of tumors, penis surgery due to recurvation and labia minora reduction due to asymmetry.

Table 5. BWSp features in the study group.

Feature	Cases/Sample †
Macroglossia	**31/32 (96.9%)**
Hemi-macroglossia	6/31 (19.4%)
Surgery	14/31 (45.2%)
Surgical tongue reduction	11/31 (35.5%)
Maxillary advancement/mandibular retraction	5/31 (16.1%)
Multiple maxillofacial surgical corrections	3/31 (9.7%)
Orthodontic and Speech anomalies	15/31 (48.4%)
Orthodontic therapy	18/29 (62.1%)
Speech therapy	9/29 (31.0%)
Birth weight > +2 SDS	13/23 (56.5%)
Final height > +2 SDS	15/34 (44.1%)
Lateralized overgrowth	**22/33 (66.7%)**
Lower limb length discrepancy	20/33 (60.6%)
Surgically corrected	6/20 (30.0%)
Treated with orthoses only	4/20 (20.0%)
Upper limb overgrowth	8/22 (36.4%)
Facial asymmetry/overgrowth	7/22 (31.8%)
Abdominal wall defect	**24/31 (77.4%)**
Omphalocele	12/24 (50.0%)
Umbilical hernia (1 surgically reduced)	7/24 (29.2%)
Inguinal hernia (1 surgically reduced)	6/24 (25.0%)
Diastasis recti	3/24 (12,5%)
Neonatal hypoglycemia	**12/31(38.7%)**
Persisting through infancy	5/12 (41.7%)
Treated with diazoxide	3/5 (60.0%)
Pancreatectomy	1/12 (8.3%)
Urinary anomalies	**12/32 (37.5%)**
Cystic kidney	6/12 (50.0%)
Renal agenesia	1/12 (8.3%)
Ureteral malformation	1/12 (8.3%)
Nephrolithiasis	5/12 (41.7%)
Recurrent urinary tract infections	2/12 (16.7%)
Cryptorchidism	**7/16 (43.8%)**
Bilateral cryptorchidism	4/7 (57.1%)
Malignant tumors	**8/34 (23.5%)**
Wilms' tumor	4/34 (11.8%)
Hepatoblastoma	1/34 (2.9%)
Early-T acute lymphoblastic leukemia	1/34 (2.9%)
Intratubular germ cell neoplasia	1/34 (2.9%)
Testicular Sertoli-cell tumor	1/34 (2.9%)
Benign tumors	**4‡/34 (11.8%)**
Mammary fibroepithelioma	2/34 (5.9%)
Non-functional adrenal adenoma	1/34 (2.9%)
Hepatic angioma	1/34 (2.9%)
Uterine myoma	1/34 (2.9%)

† Sample included cases from the whole cohort with information available. ‡ One patient with a malignant tumor had also a benign one (ID #*22*).

Figure 8. Facial characteristics of adult patients with BWSp showing mild (a,c), moderate (h,i) or severe (d,e) prognathism consistent with mild (b) hemimacroglossia or severe one, operated in infancy (g, j), and typical ear creases (f).

2) ***Follow up and cancer surveillance*** —Twenty-six patients (76%) underwent cancer surveillance in infancy undergoing quarterly abdominal ultrasound (up to 8 years of age) and, all but three of them, with serum alpha-fetoprotein measurement (up to 4 years of age). Three patients still undergo abdominal ultrasound for nephrourological conditions, while further five by individual

initiative. Eight patients never performed cancer surveillance in childhood, 7 because of a late diagnosis, made at 8, 11, 15, 16, 23, 28, 41 years, respectively.

3) ***Growth —*** Final height was > +2 SDS in 15 patients (44%). Mean height SDS was +1.33 ±1.50, range from -2.32 to +3.80. In 26 subject parents' anthropometric data were available so it was possible to compare final height to the genetic target: 15 (57.7%) showed height above their genetic target.

4) ***Educational level, social inclusion and physical activity —*** Educational level in the cohort is quite heterogeneous: four patients achieved university degree and five are successfully performing university studies, while 19 patients obtained or are obtaining a secondary school graduation. Four subjects obtained primary school graduation. Four patients failed and had to repeat the same grade. Fourteen (66.7%) of the 21 adult patients with available information, were gainfully employed. Regular physical activity was performed by 22 subjects, seven on a competitive level, although lower limb length discrepancy was present in six of them.

5) ***Prenatal findings, pregnancy, delivery and developmental milestones*** — Prenatal tests detected fetal anomalies consistent with BWSp (such as macrosomia and/or placentomegaly, increased abdominal circumference, omphalocele, elevated nuchal translucency) or elevated alphafetoprotein levels in mother's serum in 12 patients out of 22 for whom this information was available. In six cases (17.6%) spontaneous delivery was complicate by obstructed labour and in 12 cases (35.3%) caesarean section was necessary because of omphalocele, long/thick umbilical cord with loops, failing of fetal presentation during labor, breech presentation or suspected fetal hypoxia. Developmental delay or mild cognitive impairment was reported in nine (26.4%) out of 34 patients. In most cases the developmental delay was classified as mild, mostly consistent with speech delay, allowing the successfully achievement of secondary instruction, although special school was required in two cases. Neurodevelopmental outcome was more severely impaired in patient #15, probably related to the chromosomal anomaly [88] and patients #8 and #14, likely as

a consequence of neonatal hypoxic ischemic encephalopathy or recurrent hyperinsulinemic hypoglycemia. Patient #8, suffered by neonatal asphyxia consistent with prolonged obstructed transvaginal delivery and macrosomia. He suffered from severe neonatal hypoglycemia and recurrent hypoglycemic episodes during infancy up to 12 years of age, requiring diazoxide treatment, complicated by drug resistant epilepsy. He was unable to work but achieved first level secondary school education. Patient #14 suffered perinatal hypoxia consistent with delivery complication. Neurodevelopmental delay was diagnosed in the first year of age, associated to absence seizure. Speech was delayed (started at 3 years of age), autonomous walking was fully achieved at 7 years and full sphincteric control was only partially achieved. Stuttering and pronunciation deficit improved with speech therapy but was persisting at time of visit. He was able to achieve secondary school diploma with special program.

6) ***Adult health condition*** —*Table 6* shows relevant clinical conditions besides BWSp features. *Table 7* lists adult conditions which are allegedly consequent of pediatric phenotype.

Table 6. List of health issues and medical conditions in childhood and adulthood.

ID	Age (years)	Genotype	BWSp phenotype	Sex	Relevant † health issues	
					In infancy and adolescence	**In adulthood**
1	30	LoM IC2	MG, UH	F		
2	18	Negative	LO, MG, MS, NTH	M		Scoliosis and recurrent back pain
3	35	LoM IC2	LO, bilateral C, IH, OM, NTH, renal cysts	M		Azoospermia
4	58	Negative	MG, O, NTH	F	Recurrent severe urinary tract infections	Uterine myoma. Maculopathy, two episodes of transitory ischemic attack at 42 y and a third at 45 y resulting in left ear central hypoacusis
5	18	Negative	LO, emi-MG, O, UH, MS, OM, left kidney agenesia, right kidney malformation	F	Brain Chiari malformation (occasional finding at MRI for recurrent lipothymias)	Mammary gland fibroadenoma, scoliosis, atopic dermatitis, labia minora overgrowth with asymmetry (surgical reduction)
6	23	UPD(11)pat	LO, MG, UH, IH NPH, renal cysts	M	Perinatal Hypoxic-Ischemic Encephalopathy, hyperinsulinemic hypoglycemia recurrent through infancy until 9 y, mild intellectual disability	Drug-resistant epilepsy
7	19	GoM IC1	LO, MG, OM, WT	F		
8	45	GoM IC1	LO, MG, IH, NPH, OM, MS, left C, unilateral renal agenesis	M	Perinatal Hypoxic-Ischemic Encephalopathy, hyperinsulinemic hypoglycemia recurrent through infancy, severe intellectual disability	Drug-resistant epilepsy
9	43	LoM IC2	MG, O, NTH, MS	F	Volvulus at 50 days	
10	18	LoM IC2	LO, MG, O	M		
11	25	LoM IC2	LO, MG	F		

12	18	LoM IC2	LO, MG, MS	F	Recurrent syncopal episodes (vasovagal)	
13	20	UPD(11)pat	LO, MG, urolithiasis	F		Recurrent urinary tract infections
14	24	Not tested	LO, MG, UH, NPH, urolithiasis, C	M	Perinatal hypoxic-ischemic encephalopathy, hyperinsulinemic hypoglycemia recurrent through infancy, severe intellectual disability	Nasal polyposis, absence seizure, right ear neurosensorial deafness, psychiatric intermittent explosive disorder requiring involuntary commitment
15	-	LoM IC2, IC2 deletion [88]	MG, MS, UH, OM, NTH	F	Essential Thrombocythemia JAK2 V617F positive, mild psychomotor delay, facial dysmorphisms [88]	Early-T acute lymphoblastic leukemia
16	30	Negative	MG, UH, OM, bilateral C	M		Azoospermia
17	25	LoM IC2	LO, MG, UH, GNP, MS	F	Type 1 diabetes mellitus	
18	42	UPD(11)pat	LO, UH, WT, renal cysts	M		Infertility, genital surgery for *recurvatio penis*, recurrent urolithiasis
19	22	LoM IC2	LO, O, UH, OM, renal cysts, severe MG, glabellar nevus flammeus	M	Corpus callosum dysplasia and congenital abnormalities of the dural venous sinuses, severe macroglossia requiring intubation at birth, bronchiolitis (respiratory support, tracheostomy at 1,5 year of life), left vocal cord paralysis and dysphonia, Patent Ductus Arteriosus surgically corrected (1 y)	Scoliosis, recurrent back pain
20	18	GoM IC1, IC1 microdeletion	LO, MG, OM, ureteral malformation, WT, left ureteral malformation, left C, MS	M	Recurrent otitis (myringoplasty)	Mild mitral valve insufficiency, inflammatory bowel disease, obesity (class III), obstructive sleep apnea, primary hypertension

21	41	LoM IC2	LO, MG, MV, MS, sponge kidney, nephrocalcinosis, bilateral C, auricular pits	M		Adrenal adenoma, Sertoli-cell testicular tumor, primary hypertension, atrial fibrillation, azoospermia, recurrent urolithiasis
22	18	Negative	LO, emi-MG, O, NPH, MS	F	Brain Chiari type I malformation, total pancreatectomy for persistent intractable hyperinsulinism	Scheduled abdominal plastic surgery for multiple abdominal laparotomies, iatrogenic diabetes mellitus
23	-	LoM IC2	LO, MG, O, OM, renal cysts, MS	M		Hepatoblastoma
24	19	LoM IC2	LO, MG, O, MS	F		
25	20	LoM IC2	LO, MG, UH	F		Chronic autoimmune thyroiditis
26	29	Not tested	LO, MG	F		
27	30	LoM IC2	MG, O, urolithiasis, MS, NTH	F	Abdominal debridement due to adhesion	Aesthetic abdominal wall surgery for scars
28	41	UPD(11)pat	LO, MG, NTH, OM	F		Scoliosis and recurrent back pain
29	31	*CDKN1C* mut	MG, O, IH, left C	M		Left testicle IGCNU ‡, facial epidermal nevus removal, azoospermia, tibial varism
30	25	Not tested	LO, emi-MG, MS	F		Recurrent migraine, alopecia
31	37	microdup KCNQ1 - LoM IC2	O, MS	F		Long QT Syndrome type 1
32	38	microdup KCNQ1 - LoM IC2	MG	M		Long QT Syndrome type 1, asthma
33	19	UPD(11)pat	LO, MG, WT	M		
34	28	LoM IC2	LO, MG, O, NPH, OM, auricular pits	M	recurrent through infancy hyperinsulinemic hypoglycemia	Chronic non-specific colitis, intestinal resection due to obstruction, asthma

†*: BWS features not likely related with adulthood medical status were omitted.* ‡: *Intratubular Germ Cell Neoplasia*, *Unclassified* (IGCNU). Abbreviations: Cryptorchidism, C; Macroglossia, MG; Macrosomia, MS; Lateralized Overgrowth, LO; Umbilical Hernia, UH; Inguinal Hernia, IH; Omphalocele, O; Neonatal Transient Hyperinsulinism, NTH; Neonatal Persisting Hyperinsulinism, NPH; Organomegaly, OM; Wilms' Tumor, WT.

Table 7. Incidence of adulthood medical issues and correlation with pediatric BWSp-related features.

BWS features		**Frequency**	**Adulthood sequelae allegedly connected**	**Frequency**
Macroglossia		31/32 (96.9%)	Persisting speech, pronunciation or swallow difficulties	9/31 (29.0%)
Lateralized overgrowth	Presence of lower limb length discrepancy	20/33 (60.6%)	Scoliosis, back pain	3/22 (13.6%)
	Absence of lower limb length discrepancy	2/33 (6.1%)		1/22 (4.5%)
Abdominal surgery		13/33 (39.4%)	Aesthetic surgery for abdominal scars	1/13 (7.7%)
Urinary anomalies †		12/32 (37.5%)	Recurrent episodes of urolithiasis	4/12 (33.3%)
			Recurrent urinary tract infections	2/12 (17.7%)
Neonatal macrosomia		13/23 (56.5%)		
	Obstructed labour	6/23 (26.1%)‡		
	Neonatal hypoxic-ischemic encephalopathy	3/13 (23.1%)	Drug-resistant epilepsy or absence seizure right ear neurosensory deafness, psychiatric intermittent explosive disorder §	3/34 (8.8%)
Neonatal hypoglycemia		12/31 (38.7%)		
			Iatrogenic diabetes mellitus secondary to pancreatectomy	1/12 (8.3%)
Cryptorchidism	Bilateral	4/16 (25.0%)	Azoospermia	3/4¶ (75.0%)
	Monolateral	3/16 (18.9%)	Azoospermia	1/3¶ (33.3%)

†: nephrocalcinosis, multicystic kidney, solitary kidney. ‡: Five of the 6 patients born by obstructed labour were macrosomic fetus. §: Of the 12 patients affected by neonatal hyperinsulinism, 2 had drug resistant epilepsy and 1 had absence seizure, right ear neurosensory deafness and psychiatric intermittent explosive disorder. These three patients also suffered from perinatal hypoxic-ischemic encephalopathy therefore neurological disorders listed above could be consequences either of neonatal hypoglycemia or neonatal hypoxic-ischemic encephalopathy as well. ¶: three males were never tested for fertility nor tried to conceive.

7) ***Neoplasm*** (*Figure 9*) — Wilms' tumor (WT) has been diagnosed in four patients, at 2, 3, 5 and 10 years of age, respectively: in three cases WT was detected by abdominal ultrasound, either during cancer screening (*n*=2) or in the context of an intercurrent illness at 3 years of age, with subsequent diagnosis of BWSp (*n*=1). In one case WT was diagnosed at 5 years of age after the finding of hematuria. Adult-onset malignancies occurred in four patients. Patient #23 developed hepatoblastoma at the age of 22 years, requiring liver transplantation, duodeno-cephalo-pancreatectomy, multiple cycles of chemotherapy and surgical removal of pulmonary metastasis. In spite of intensive treatment, he died five years after diagnosis. Patient #15 developed a T-Acute Lymphoblastic Leukemia (ALL) at 21 years of age. The girl was diagnosed with V617F JAK2 positive essential thrombocythemia at the age of 6 years. She was treated with AEIOP-BFM 2009 protocol and underwent allogenic bone marrow transplantation from HLA identical sibling, with a graft failure two months after and deceased after relapse at 23 years of age. Patient #21 developed a non-functional adrenal adenoma at the age of 22 years and testicular Sertoli-cell tumor at 24 years, successfully removed and patient #29 developed testicular *Intratubular Germ Cell Neoplasia*, *Unclassified* (IGCNU) at 27 years of age. *Figure* 10 shows Kaplan-Meier curve of the tumor-free probability in BWS up to 30 years of life. Benign adulthood-onset tumors occurred in further three patients with two mammary gland fibroma, one uterine myoma and one hepatic angioma (*Table* 8).

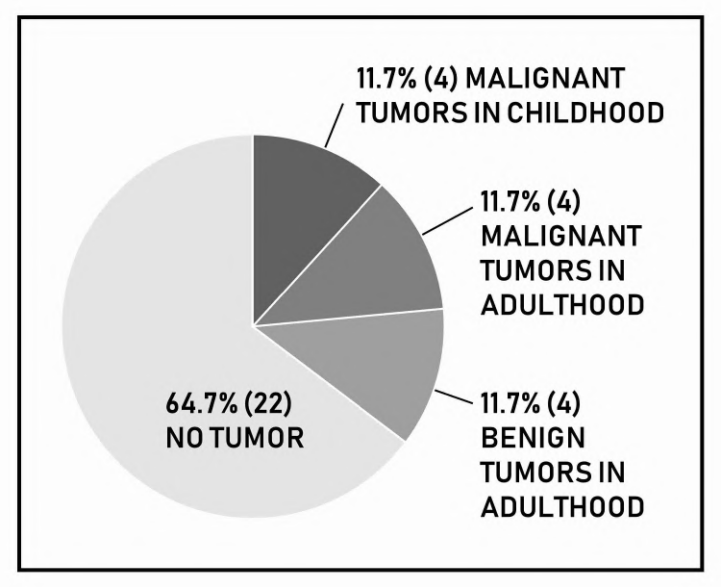

Figure 9. Tumor rate in the cohort

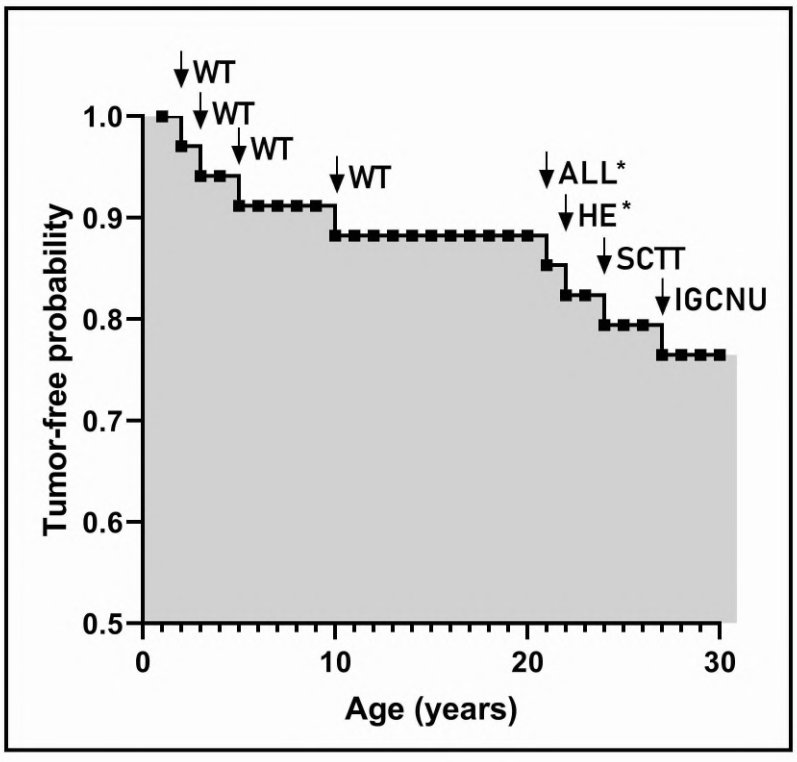

Figure 10. Kaplan–Meier curve of the tumor-free probability in BWS up to 30 years of life: Four patients developed Wilms' tumor (WT), one T-acute lymphoblastic leukemia (ALL), one hepatoblastoma (HE), one testicular Sertoli-cell tumor (SCTT), and one Intratubular germ cell neoplasia, unclassified (IGCNU).

Table 8. Data of patients with tumors.

Patient ID	Tumor type	Malignant (M) or benign (B)	Genotype	Age at tumor diagnosis	Diagnosis modalities	Surgery	Medical Therapy	Current age
#7	Wilms' tumor	M	GoM IC1	10 y	US Abdominal screening	Nephrectomy	-	19 y
#15	Early T- acute lymphoblastic leukemia	M	LoM-IC2, IC2 deletion	21 y	Hematological screening in myelodysplasia	Splenectomy due to graft failure	AEIOP- BFM ALL 2009 protocol, Allogeneic Bone Marrow Transplantation	Died at 23 y after relapses
#18	Wilms' tumor	M	UPD(11)pat	2 y	US Abdominal screening	Nephrectomy	-	42 y
#20	Wilms' tumor	M	GoM IC1 (microdeletion) [89]	5 y	Hematuria	Nephrectomy	AIEOP TW 2003 protocol	18 y
#23	Hepatoblastoma, cholangioblastic variant	M	LoM-IC2	22 y	Abdominal mass	Orthotopic liver transplant + pancreatic-duodenectomy	Adjuvant chemotherapy	Died at 27 y after relapses
#29	Intratubular Germ Cell Neoplasia, Unclassified	M	*CDKN1C* mut	27 y	Testicular mass	Orchidectomy	-	31 y
#33	Wilms' tumor	M	UPD(11)pat	3 y	Abdominal US due to intercurrent pathology	Renal Lobectomy	Adjuvant chemotherapy	18 y

#21	Testicular Sertoli-cell tumor	M	Not performed	24 y	Testicular mass	Orchidectomy	-	41 y
	Non-functional adrenal adenoma	B with uncertain malignant potential		22 y	Incidentaloma at US	Laparoscopic adrenalectomy	-	
#4	Uterine myoma	B	Negative	40 y	Menorrhagia	Myomectomy	-	58 y
#5	Mammary fibroepithelioma	B	Negative	16 y	Tenderness, self-examination	Tumorectomy	-	18 y
#22	Hepatic angioma	B	Negative	6y	US abdominal screening	-	-	19 y
	Mammary fibroepithelioma	B		18 y	Tenderness, self-examination	-	-	19 y

8) ***Reproduction issues and procreation —*** Four patients, two females and two males, successfully procreated, three physiologically and one through artificial reproductive techniques. Patient #9 (female, IC2-LoM) conceived a male at the age of 31 and a female at the age of 33 years, both from uncomplicated pregnancy with normal prenatal screening tests. Delivery was spontaneous for the male and by caesarean section for the female due to transverse fetal position during labor. Both children were in good health, had normal psychomotor development and no BWSp features. Patient #31 (female) and #32 (male) were siblings. In their family segregates an intragenic inverted microduplication of 160-kB within *KCNQ1* exons 10 responsible for both Long QT syndrome type 1 (LQTS1) [90] and IC2-LoM [87]. They physiologically conceived and had children with unrelated partners. Patient #31 (female) had a miscarriage and two daughters; the younger was born with omphalocele, macroglossia, facial nevus flammeus, post-axial hexadactyly and auricular pits consistent with BWSp. Molecular tests showed that she inherited the intragenic inverted microduplication of *KCNQ1* segregating in the family, while her older sister was in good health and did not inherit the molecular anomaly: the mother was diagnosed with BWSp after the daughter. Patient #32 (male) had two children, a female at 34 years of age and a male at 35, both born after uneventful pregnancies and showing normal psychomotor and physical development. The female was affected by absence seizure controlled with valproate and didn't carried the intragenic inverted *KCNQ1* microduplication segregating in the family. Conversely, the male was diagnosed with LQTS1 by electrocardiography and by the presence of the intragenic inverted microduplication of *KCNQ1*: he undergoes cardiologic follow-up without any complication. Patient #18 (male) was infertile (oligozoospermia and teratozoospermia) and underwent a cycle of homologous In Vitro Fertilization (IVF) to conceive a female child. The latter was diagnosed with isolate right renal agenesis during pregnancy. The patient had no cryptorchidism: no specific cause of infertility was detected, and sperm analysis was normal.

Overall, seven of the 16 males (43.8%) were affected by cryptorchidism, bilateral in four cases. Four of them presented azoospermia or infertility. In three cases fertility tests were not performed. Patient #3 had bilateral orchidopexy at 4 years and had azoospermia. Patient #8 was affected by unilateral cryptorchidism and had his left testicle removed: no further investigation on his fertility status was performed nor he tried to conceive. Patient #14 received bilateral orchidopexy at 5 years of age and never attempted to conceive nor was tested for fertility. Patient #16 received bilateral orchidopexy at 6 years, was diagnosed with azoospermia at 19 years, consistent with left testicle atrophy and hypotrophy of the right one. Patient #20 had left cryptorchidism corrected at the age of 2 years; his subsequent fertility status was undetermined. Patient #21 underwent bilateral orchidopexy at the age of 8 years and showed azoospermia: at 24 years of age he was diagnosed with testicular Sertoli-cell tumor and underwent orchifunicolectomy. Patient #29 had left cryptorchidism surgically treated (age data was not available) and was subsequently diagnosed with azoospermia: he had testicle biopsy showing right testicle atrophy and an *Intratubular Germ Cell Neoplasia*, *Unclassified* (IGCNU) of the left gonad, which was removed.

The eight remaining male patients without cryptorchidism never attempted to conceive and none was ever tested for seminal anomalies. As concerns females, except for patient #9 and #31, none of the 16 remaining women attempted to conceive or referred gynecological or hormonal issues implicated in fertility, with the exception of mild common menstrual disorders and benign tumors showed in *Table* 8.

5.1.4 Discussion

Despite adulthood health status represents a relevant concern for patients affected by BWSp and their parents, information on these issues are barely mentioned in literature. Greer KJ Et al [85] described a pedigree with *CDKN1C* mutation responsible for familial BWSp with four adults having fertility issues (azoospermia, low count and motility, abnormal morphology) and hearth anomalies,

suggesting echocardiographic follow-up and semen analysis in adulthood. Other authors reported adults with BWSp and renal anomalies with recurrent urinary tract infections and kidney stones [91], severe renal function impairment following diffuse nephroblastomatosis and Wilms tumor [92] hearing deficiency as a consequence of stapedial fixation [93], genital anomalies [91, 94], partial bowel malrotation [91], pituitary adenoma [95], long-QT syndrome [96], psoriasis [97], hypothyroidism and thyroid adenoma [98].

In this study a consistent number of adults with BWSp are described providing an initial view on the natural history of the condition. Most of medical issues in adulthood are conceivably evolution of BWSp infant features or consequences of their surgical correction. The majority of patients with BWSp undergo at least one surgical intervention. It is interesting to note that, in spite of the surgery performed (overall 50 in 29 patients), only few of them obtained full correction of the defect: indeed, such interventions were rarely judged fully satisfactory by the patients themselves. Although, surgery usually ameliorates the health status, often the features which required intervention persist in adulthood, resulting in compromised function or leading to esthetical concerns. This observation is not trivial, especially from the patients' point of view and underlines the need for specific research and improvement in this setting.

Macroglossia is well known to be the most common feature in patients affected by BWSp. Orthodontic anomalies, speech disturbances and swallow difficulties persisting in adulthood were reported by nine patients. These findings were present in both patients treated by orthodontic devices and those surgically treated, confirming that patients affected by macroglossia, even after surgical reduction, may not achieve complete normal function [99], in spite of the absence of sensory losses after tongue reduction [100].

Lateralized overgrowth with or without lower limb length discrepancy was the plausible cause of scoliosis and recurrent back pain described by four patients. Three of them were affected by lower

limb length discrepancy (two surgically corrected, one functionally compensated by orthoses). Two of them performed competitive and two of them amateur sport activity.

Pancreatectomy for persistent hyperinsulinism was the cause of iatrogenic diabetes mellitus in one patient. Also nephrourological health issues during adulthood were reported: 70% of patients with nephrourological anomalies had frequent recurrent urolithiasis or urinary tract infections in adulthood [101].

Obstructed labour secondary to fetal macrosomia and the possibly related neonatal hypoxic-ischemic encephalopathy are described in medical literature as a possible cause of intellectual disability in BWSp [102, 103]. Morbidity related this issue appears to be confirmed in our cohort: the three patients with hypoxic-ischemic encephalopathy showed a mild to severe degree of intellectual disability and seizures. However, all these cases also were affected by persistent hyperinsulinemic hypoglycemia at birth and through infancy, that could have played a role in the neurodevelopmental defect.

Thirty-one percent (5 out of 16) of the male patients in the cohort were infertile and 25% (4 out of 16) showed azoospermia in sperm analysis. Azoospermia was present in 4 adults: three had bilateral cryptorchidism and one unilateral. Overall, half of the males were affected by cryptorchidism and underwent a not timely surgical correction of cryptorchidism. As an early orchidopexy has been shown to be key for a proper testicular reproductive function [104, 105], a late correction was a plausible explanation for the high rate of infertility encountered. This further underlines that, as in nonsyndromic children, a timely orchidopexy is of paramount importance in patients with syndromic presentation [106] and surgery should not be postponed during the first years of life although a definite diagnosis has been made or other medical interventions are required. However, the finding of azoospermia in an adult with *CDKN1C* mutation and unilateral cryptorchidism is relevant. Four similar cases have been described by Greer KJ et al. [85] in a family with the same molecular defect: three had documented severe abnormalities of spermatogenesis (only one with cryptorchidism) and

the other had infertility and testicular atrophy by clinical examination. As discussed, a mutation in *CDKN1C* might affect the expression of ZNF215, a zinc-finger protein located within the IC2 domain and important for a regular spermatogenesis [107]. Indeed, male BWSp subfertility appears a potentially relevant issue for BWSp adult patients, either as a consequence of cryptorchidism or a primary dysfunction of the testes, and further studies are therefore warranted in order to manage and preserve the reproductive function of male BWSp patients. As far as it concerns females, except for two patients, none of the remaining reported attempt to conceive, therefore we are unable to offer further information about female fertility.

The most relevant issue concerning health in adulthood is tumor predisposition. Literature is scattered of anecdotal reports on adult-onset tumors including adrenal adenoma [108], bilateral pheochromocytoma [109], astrocytoma [94], acute myeloid leukemia [110], ACTH-secreting pituitary adenoma [95], virilizing adrenocortical tumors [111, 112], thyroid adenoma [98], breast cancer [113] and fibroadenoma [111]. However, general clinical experience denies specific increase of tumor risk in adults with BWSp and it is a common convincement that it approaches that observed in the general population after the first decade of life, but no study that specifically evaluated this issue on a large cohort has been performed. In this study we have observed a tumor risk of 11.7% during childhood consistent with that reported in literature. Surprisingly, we observed in adults the same number of malignant tumors we documented in childhood. This observation doubles the overall risk previously estimated in BWSp raising tumor rate to 23.5%. Likely, this data is overestimated due to the study design. First, a collection bias is plausible, as more than half of the cohort described has been gathered though a search among the associates of AIBWS, with an over representation of adult with relevant health issues. Second, one of the testicular tumors observed is notably associated with delayed intervention for cryptorchidism. It is anyhow interesting the observation in young adulthood of three tumors usually observed in childhood (ALL, hepatoblastoma and Sertoli-cell testicular

tumor), two of them leading to patients' death. Finally, it should be noted that one case of WT was diagnosed at the age of 10 years, beyond the end of the ultrasound screening recommended in infancy.

In conclusion, in this study it is described the first large cohort of adults with BWSp. Although no novel specific aspect of BWSp emerged, adult patients present several medical issues related to complications of developmental defects characterizing the pediatric phenotype. These observations underlie the preventive role of follow-up strategies in childhood and evidence the need for an improvement in treating the medical problems connected with BWSp in the first years of life. With the limitation discussed, our data show that tumor rate in BWSp cumulatively raises 23.5% including young adulthood, but the small number of patients and tumors described do not allow to provide a precise estimate of cancer risk in adulthood and mostly do not imply any revision of the proposed tumor screening protocols. However, this issue deserves undoubtedly further investigation.

5.2 NBAS pathogenic variants: Defining the associated clinical and facial phenotype and genotype-phenotype correlations

5.2.1 Introduction

Three phenotypes have been associated with biallelic inactivating/hypomorphic variants in the neuroblastoma-amplified sequence (NBAS; MIM# 608025): (a) infantile liver failure syndrome 2 (ILF2; MIM# 616483), an autosomal recessive condition characterized by isolated hepatic involvement with recurrent episodes of acute liver failure during intercurrent febrile illness [114]; (b) short stature, optic nerve atrophy, Pelger-Huët anomaly (SOPH; hyposegmented neutrophil nucleus; MIM# 614800) [115], which involves skeletal, ocular, and immune system in the absence of frank hepatic involvement; (c) a severe skeletal, ocular, and neurological phenotype consistent with the clinical diagnosis of acrofrontofacionasal dysostosis type 1, in the absence of both liver and immunological involvement [116, 117].

A wide spectrum of pathogenic variants throughout the coding sequence of *NBAS* have been associated with ILF2, whereas SOPH has been linked to the recurrent homozygous c.5741G>A missense change (p.Arg1914His). This genotype has been frequently reported in an isolated Russian Yakut population due to a founder effect [115]. In addition, acrofrontofacionasal dysostosis type 1 has been described in a single consanguineous family segregating a splice-site change (c.6237−3C>G) affecting transcript processing (skipping of exon 48), and resulting in a truncated protein [116].

Over the time, ILF2 patients with more complex phenotypes have been reported, presenting with diverse involvement of hepatic, skeletal, ocular, and immune systems [118–122]. In majority of cases, psychomotor development and cognitive development are normal. However, in some cases, neurological involvement has been reported, varying from mild developmental delay to severe intellectual disability [118, 120–124].

NBAS encodes a component of an endoplasmic reticulum (ER) tethering complex involved in Golgi-to-ER retrograde transport [114]. NBAS interacts with SNARE proteins that are known to participate in intracellular vesicular trafficking. The specific mechanism by which defective NBAS function contributes to liver disease is, however, unknown, along with its pathophysiologic link to the observed skeletal, immune, ocular, and neurological involvement. Although the heterogeneous phenotypes associated with biallelic inactivating/hypomorphic *NBAS* variants are suggestive of a pleiotropic effect, genotype–phenotype correlations have not been systematically explored.

Here, we report on two unrelated cases, whose clinical features included short stature, hypogammaglobinemia, ocular involvement, and elevated liver transaminases with no episodes of acute liver failure; these patients carried two novel *NBAS* variants, one of which was a recurrent synonymous change (i.e., no predicted change at the specific codon) affecting transcript processing. We systematically reviewed the clinical and molecular features of the reported cases, defined a consensus for facial features associated with *NBAS* pathogenic variants, and explored the occurrence of genotype–phenotype correlations.

5.2.2 Patients description

Patient 1 was a 7-year-old male born from healthy nonconsanguineous parents of Italian origin; the pregnancy was uneventful. Due to a previous fetal loss and maternal constitutional thrombophilic disorder, the mother was treated with heparin during pregnancy. Fetal karyotype on amniocytes was normal (46,XY). The patient was born at 38 weeks by spontaneous delivery, with an Apgar score of 9/10. Parameters at birth included reduced length: 42 cm, −3.16 standard deviation (*SD*) and weight, 1.87 kg, −2.86 *SD*. In the first months of life, the patient developed congenital bilateral glaucoma that was surgically treated by trabeculectomy. Hypogammaglobulinemia was observed at the age of 7 months during hospital admission for gastroenteritis (IgG: 28 mg/dl, reference range 218–907; IgA: 5 mg/dl, reference range 10–85; IgM: 6 mg/dl, reference range 31–116). At 18 months, the patient started subcutaneous immunoglobulin replacement therapy (0.4 $g \cdot kg^{-1} \cdot month^{-1}$) due to persistent low

levels of IgG. At 6 years of age, despite optimal immunoglobulin G (IgG) levels, he had developed *Listeria encephalomeningitis* with subsequent hydrocephalus that required ventriculoperitoneal shunting. Peripheral blood smear examination carried out after the molecular diagnosis disclosed a Pelger-Huët anomaly. He presented with persistently elevated liver AST and ALT (with ALT > AST, ALT zenit 652 U/L, nadir 76 U/L, reference range 8–40 U/L). The patient never showed signs of portal hypertension; transient hepatic elastography, as well as albumin and coagulation factors, as markers of the liver's biosynthetic capacity, were all within a normal range. At 7-years of age, the patient developed iron deficiency. As part of the diagnostic work-up, a duodenal biopsy showed severe villous atrophy, which suggested celiac disease. From his first years of life, he presented hypothyroidism (TSH: 10.3 mIU/L, reference range 0.4–4.4; fT4: 1.11 mg/dL, reference range 8.8–16.5 mIU/L) in the absence of autoantibodies. He was treated with l-thyroxine. He showed delayed growth with a proportionate short stature. At 6 years of age, he weighed 12.0 kg (−3.8 *SD*), his height was 92.3 cm (−4.6 *SD*), and he displayed skeletal anomalies. At 1 year of age, whole-body X-ray disclosed short diaphyseal plates at long bones, diaphyseal radial bowing, and short metacarpophalangeal bones. Developmental milestones were slightly delayed, and he presented mild dysmorphic features (Figure 11), including closely spaced eyes, anteverted nares, smooth philtrum, narrow mouth, small hands with fifth finger clinodactyly, and sandal gap.

Patient 2 was a 4-year-old female born from nonconsanguineous, ealthy, Italian parents; the pregnancy was uneventful. Due to constitutional thrombophilic disorder, the mother was treated with heparin during pregnancy. Prenatal first trimester screening using maternal blood biochemical markers showed increased α-fetoprotein, 2.76 multiple of median (MoM), decreased pregnancy-associated plasma protein A (0.06 MoM), and increased human chorionic gonadotropin levels (6.74 MoM). At 16 weeks, intrauterine growth restriction was detected. Fetal karyotype on amniocytes was normal (46,XX). The patient was born after cesarean section at 28 weeks of gestation due to maternal HELLP (hemolysis, elevated liver enzymes, and low platelets) syndrome; her Apgar

score was 5/7. Assessment at birth documented a reduced length (29.6 cm, −2.45 SD), weight (550 g, −1.93 *SD*), and head circumference (21.6 cm, −2.3 *SD*). Since birth, the patient had persistently elevated liver AST and ALT levels (with ALT > AST, ALT zenit 428 U/L, nadir 101 U/L, reference range 8–40), without signs of portal hypertension. Transient hepatic elastography and tests of the biosynthetic capacity of the liver were normal. She also presented a sacral cleft at S1 with a tethered spinal cord. At 18 months, the patient was hospitalized for gastroenteritis and severe hypogammaglobulinemia (IgG: 93 mg/dl, normal range: 442–1,139) with decreased IgA and IgM (5 and 15 mg/dl, respectively; normal ranges: 21–150 and 43–184). At 24 months, due to persistent low IgG levels, she started subcutaneous immunoglobulin replacement therapy (0.27 $g \cdot kg^{-1} \cdot month^{-1}$). Peripheral blood smear examination carried out after the molecular diagnosis disclosed a Pelger-Huët anomaly. At 4 years of age, she presented delayed growth with a proportionate short stature (weight 10.8 kg, height 87.8 cm, respectively −3.0 and −3.1 *SD*), and mild developmental delay. Facial features included a broad forehead, midface retrusion with mandibular prognathism, closely spaced eyes, upslanting palpebral fissures, simplified ears with underfolded helix and small lobes, smooth

philtrum, and a narrow mouth with thin lips (Figure 11). She presented retinopathy of prematurity and severe myopia with −11.50 and −12.50 diopters in the right and left eye, respectively.

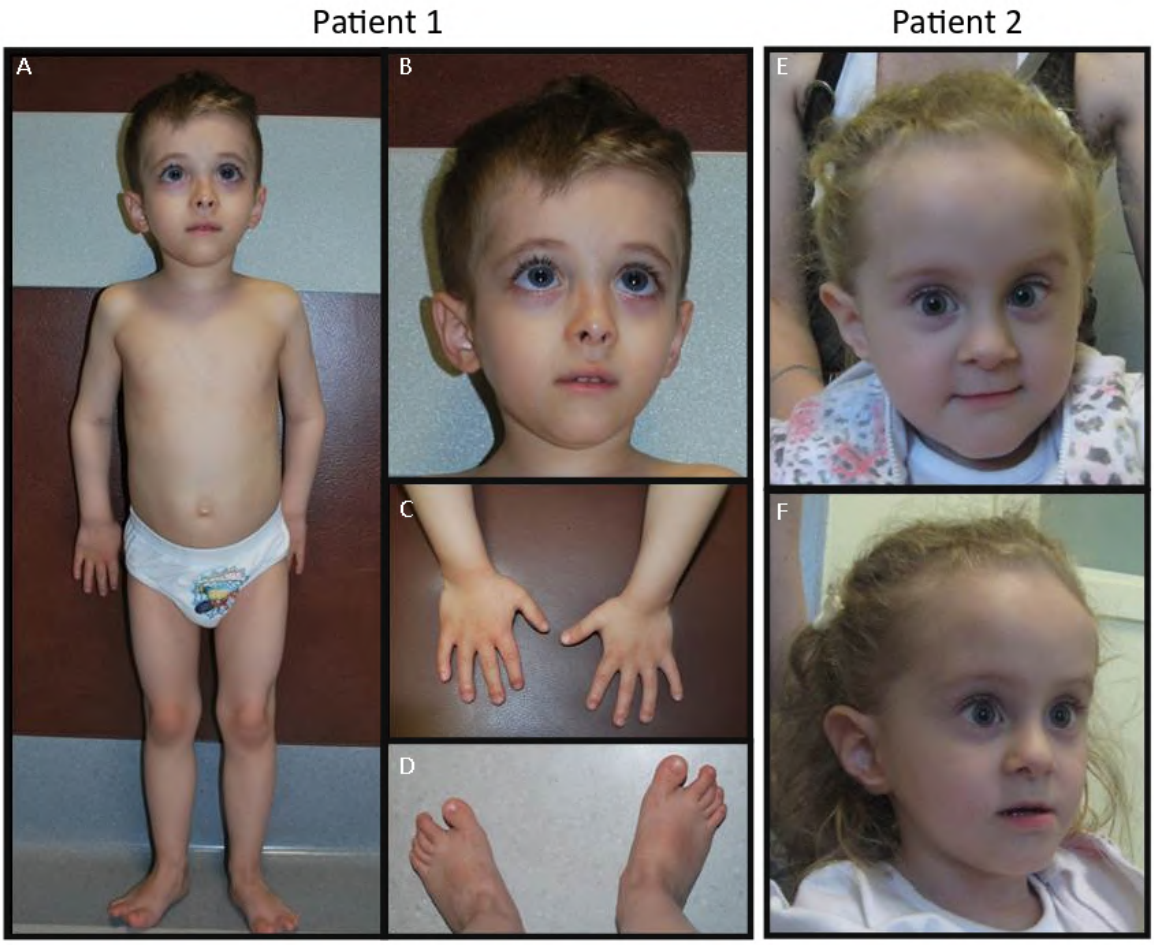

Figure 11. Panel A and B show full body and face pictures of the studied affected subject (II-2) from family 1. Note closely spaced eyes, anteverted nares, smooth philtrum, and narrow mouth. Panels C and D display the small hands with clinodactily of the fifth finger, and the sandal gap, respectively. In panels E and F, facial features of patient II-2 from family 2 are reported. She had broad forehead, midface retrusion with mandibular prognathism, closely spaced eyes with upslanting palpebral fissures, simplified ears with underfolded helix and small lobe, smooth philtrum, narrow mouth with thin lips.

5.2.3 Results

5.2.3.1 Molecular analysis

In 2016, due to their complex phenotypes, the two subjects were enrolled in the "Undiagnosed Patients Program", Ospedale Pediatrico Bambino Gesù, Rome, Italy. Informed consents for the

molecular analyses were obtained from the legal tutors of the two participating subjects. The study adhered to the Declaration of Helsinki standards and was approved by the internal Ethics Committee of the Department of Medical Sciences, University of Torino, Italy. Targeted enrichment (SureSelect Clinical Research Exome V2 kit; Agilent, Santa Clara, CA) and massively parallel sequencing (NextSeq 500; Illumina, San Diego, CA) were performed on genomic DNA extracted from circulating leukocytes of the affected subjects and their parents. Data analysis was performed using an in-house implemented pipeline, which mainly takes advantage of the Genome Analysis Toolkit (GATK V.3.7) framework, as previously reported [125–127]. High-quality variants with an effect on the coding sequence or affecting splice-site regions were filtered against public databases (dbSNP150 and gnomAD V.2.0) to retain (a) private and clinically associated variants, (b) annotated variants with an unknown frequency or having MAF < 0.1%, and occurring with a frequency <2% in an in-house database including frequency data from >1,000 population-matched whole-exome sequencing (WES). The functional impact of variants was analyzed by Combined Annotation Dependent Depletion V.1.3, Mendelian Clinically Applicable Pathogenicity V.1.0 [31, 32], and using InterVar V.0.1.6 to obtain clinical interpretation according to the American College of Medical Genetics and Genomics-Association for Molecular Pathology 2015 guidelines [33]. Among the high-quality variants found in patient 1 (11,978) and patient 2 (14,859) predicted to have a functional impact, six genes (patient 1) and four genes (patient 2) with variants compatible with either a recessive or dominant transmission model that passed the public and in-house database filters were used for further analyses. These genes were prioritized taking into account both the predicted impact on protein function and biological relevance of the relative genes allowed to identify compound heterozygosity for two variants in *NBAS* in both subjects. Specifically, each subject carried a heterozygous truncating variant (subject 1: NM_015909.3: c.1501C>T, p.Arg501*; subject 2: NM_015909.3: c.686dupT, p.Ser230Glnfs*4), which was found to occur in trans with a concomitant rare synonymous substitution (c.6840G>A, p.Thr2280Thr; 1/245,982; gnomad.broadinstitute.org) [51] affecting the last nucleotide of exon 51. Splicing-site score analysis predicted disruption of the

adjacent splice-site donor. Variant validation and segregation were attained by Sanger sequencing, confirming the recessive pattern of inheritance (Figure 12 a–d). The synonymous variant did not occur in >1,000 population-matched exomes. Visual inspection of flanking informative markers did not allow tracking back of any ancestral relationship between the two families, suggesting either they were distantly related or the mutation arose independently. The three variants were submitted to the ClinVar database (variation ID: 204581; 617878; 617879).

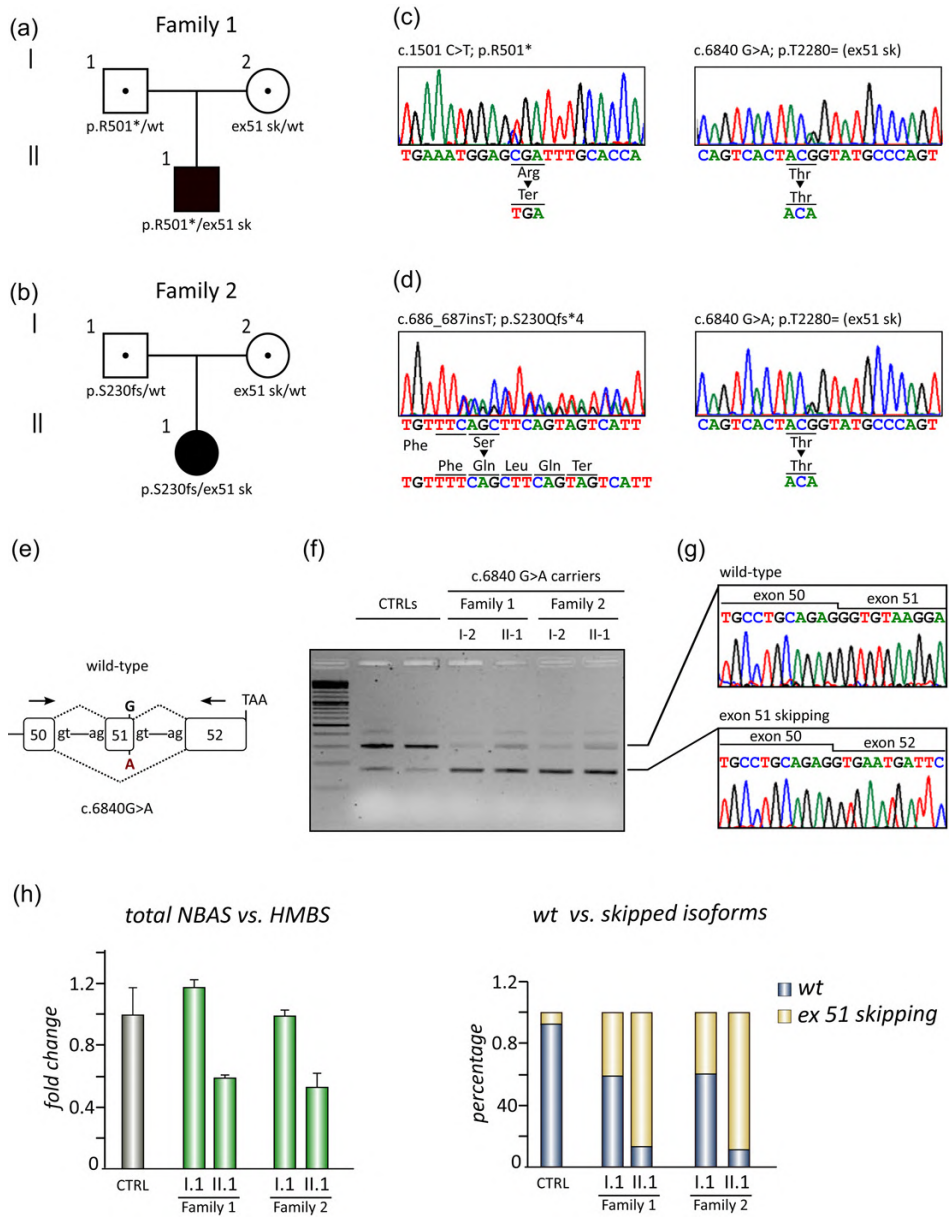

Figure 12. Pedigrees and molecular data. (a,b) Pedigrees of the two probands and variant segregation analysis. Sanger sequence electropherograms are reported in panels (c,d). (e) A schematic representation of exon 50–52 genomic region of the *NBAS* gene. The c.6840G>A variant

affects the last base of exon 51, and it is predicted to alter the intron 51 donor splice site (intron-splicing consensus sites are shown). Arrows above the exons indicate the primers used for exon 51 skipping analysis. (f) Gel electrophoresis analysis of the complementary DNA between exons 50 and 52. Skipping of exon 51 is also present in control subjects, but it is clearly enhanced in subjects carrying the pathogenic variant. The two bands were gel-purified and Sanger sequenced. (g) Electropherograms show the wild-type exon 50–51 junction (above) and the aberrant exon 50–52 junction (below). CTRLs: healthy controls. (h) Total NBAS mRNA levels (left) and relative amounts of WT vs. exon 51 skipped isoforms (right), analyzed by RT-PCR. Both probands showed a reduced expression of total *NBAS*, compatible with NMD, associated with the nonsense variants inherited from the fathers. In the mothers, carriers of the c.6840G>A variant, approximately 40% of *NBAS* transcript lacks exon 51. In probands, this transcript is over 90% of the total *NBAS*. A small amount of exon 51 skipping is also present in controls. CTRL: control; mRNA: messenger RNA; NBAS: neuroblastoma-amplified sequence; NMD: nonsense-mediated decay; RT-PCR: reverse transcription-polymerase chain reaction; WT: wild-type; HMBS: hydroxymethylbilane synthase.

5.2.3.2 Gene expression studies

To verify the predicted disruptive effect of c.6840G>A, total RNA was extracted from peripheral blood mononuclear cells obtained from the two probands and their heterozygous parents and DNAse digested (Direct-Zol RNA MiniPrep system, Zymo Research, Irvine, CA); complementary DNA (cDNA) was then obtained from 1 µg RNA (M-MLV Reverse Transcriptase kit; Applied Biosystem, Wilmington, DE). The effect of the c.6840G>A substitution on transcript processing was assessed by direct sequencing of the relevant portion of the *NBAS* cDNA. As shown, the variant altered *NBAS* transcript splicing leading to skipping of exon 51 and, in turn, to a mature messenger RNA (mRNA) variant encoding for a protein that lacked an in-frame portion of 43 amino acid residues within the C-terminal region (p.Gly2238_Thr2280del; Figure 12 e–g). Real-time reverse transcription polymerase chain reaction analysis using the Universal Probe Library system (Roche diagnostics, Risch-Rotkreuz, Switzerland) showed that both probands had a reduced expression of the *NBAS* gene compared to their mothers or an healthy control, likely due to the degradation of alleles carrying the truncating variants by nonsense-mediated decay (NMD). Moreover, we evaluated the relative amount of the wild-type (WT) allele versus the exon 51 skipped allele, using assays spanning the exon 51–52 junction (WT) or the exon 50–52 junction (allele with exon 51 skipping),

respectively. As expected, the c.6840G>A substitution caused skipping of exon 51 in ~40% and in ~90% of total *NBAS* mRNA level from mothers (carriers) and probands, respectively.

5.2.3.3 Gestalt analysis

Nonspecific dysmorphic features have been previously reported in patients with biallelic pathogenic *NBAS* variants [121]. To explore this issue systematically, we compared 28 frontal facial images collected from 16 patients (published and present cases; cohort including 10 females and 6 males, age range: 0.6–37 years, median age: 9 years, ethnicity: 14 Europeans and 2 Arabs) and unaffected controls using the Face2Gene research application (version 18.1.8; **www.face2gene.com**), with the facial recognition technology called DeepGestalt (FDNA Inc, Boston, MA), which has been described by Gurovich et al. [128]. Controls included a total of 16 unrelated age- and gender-matched individuals. There was a difference in profiling between patients with biallelic *NBAS* pathogenic variants and controls. The most characteristic facial features emerging in *NBAS* patients' composite photo included hypotelorism, thin upper lip, pointed chin, and reduced subcutaneous fat conferring a "progeroid" appearance. These traits were more evident when the comparisons were performed in children versus those observed when all cases were included (Figure 13 a–f). This may explain why previous observations did not identify a recognizable facial gestalt in subjects with biallelic *NBAS* pathogenic variants.

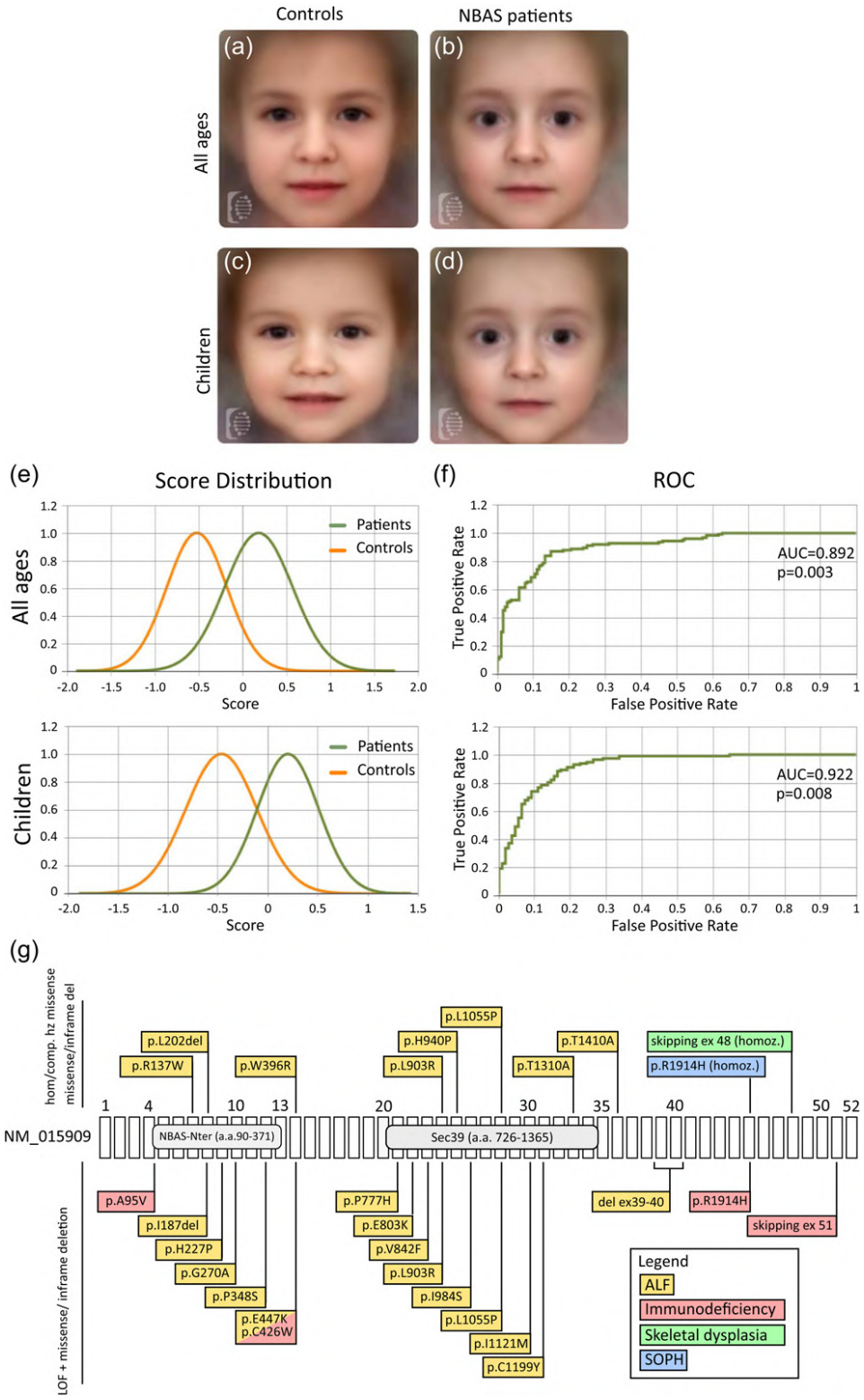

Figure 13. *NBAS*-associated facial phenotype and genotype–phenotype correlations. (a–d) Composite photos obtained from patients [115, 118, 120, 121, 123, 124] and age-/gender-matched controls. Facial features of subjects with biallelic inactivating/hypomorphic *NBAS* variants include hypotelorism, thin upper lip, pointed chin, and a progeroid appearance. These traits are more evident in children (panels [c d]) than in the group that includes all cases (panels [a, b]). The software used loaded images to generate a score distribution reported for all cases (panel [e], above) and

children (panel [e], below). Statistical evaluation was performed measuring the area under the curve (AUC) of the receiver operating characteristic (ROC) curve and calculating the p value (p = 0.003 for all, and p = 0.008 for children, panel [f]). (g) Distribution of the known disease-causing *NBAS* pathogenic variants. Cartoon showing the 52 coding exons of the *NBAS* gene (reference sequence NM_015909). The two known protein domains NBAS-Nter (amino acids 90–371) and Sec39 (amino acids 726–1,365) are also represented. We reported only missense/in-frame deletions/splicing variants leading to an in-frame deletion. Top: pathogenic variants found in homozygous or compound heterozygous state. Bottom: pathogenic variants reported in compound heterozygosity concomitantly with a nonsense variant. Variant p.Arg1914His is associated with SOPH when in homozygosis (in blue). The c.6237−3C>G change (skipping of exon 48) is associated with a specific skeletal phenotype when occurring in homozygosity (in green;[116, 117]). Variants in yellow are associated with acute liver failure and are mostly missense in the functional domains. Variants in pink are associated with immunodeficiency and are located at the edges of the protein. Only two variants, p.Glu447Lys and p.Cys426Trp, are both associated with liver involvement and immunodeficiency. *NBAS*: neuroblastoma-amplified sequence; SOPH: short stature, optic nerve atrophy, Pelger-Huët anomaly.

5.2.4 Discussion

So far, 47 different pathogenic *NBAS* variants have been reported in 71 individuals. To explore possible genotype–phenotype correlations, the available clinical data were collected (Table 9) [115, 118, 120, 121, 123, 124, 129–134].

Table 9. Genotypes and phenotypes of NBAS reported cases (update 23 August 2018).

Mutations				Clinical features							References
Allele 1	**Exon/ Intron**	**Allele2**	**Exon/ intron**	**Hepatic**	**Immuno**	**Ocular**	**Skeletal**	**Neurologic**	**Other**	**n. cases**	
c.850A>T; p.Lys284*	10	c.284C>T; p.Ala95Val	4	ELT, hepatomegaly	PHA, hypogammaglobulinemia, reduced natural killer cells, no response to vaccinations	Optic atrophy, retinal dystrophy	Short stature, skeletal dysplasia, reduced bone density	Normal psychomotor and development, normal intelligence	Cervical instability, hypoglicemia, hyperammoniemia, metabolic abnormalities during crises (hypoketosis, dicarboxylic aciduria, and epoxy-acid excretion), reduced subcutaneous fat, recurrent vomiting	1	[121] patient 15; [130] patient 1
c.409C>T; p.Arg137Trp	7	c.409C>T; p.Arg137Trp	7	ALF, hepatosplenomegaly	no PHA	no	Large fontanels with delayed closure, neonatal spontaneous fractures, reduced bone density, delayed bone age. NO short stature	Axial hypotonia, developmental delay	Hirsutism,abnormal thoracic configuration, wrinkled skin	3	[123, 124]
c.686dupT; p.230Qfs*4	9	c.558_560del; p.Ile187del	8	ALF	no PHA	Optic atrophy	Short stature	Normal psychomotor and development, normal intelligence		1	[121] patient 1
c.1749G>A; p.Trp583*	17	c.680A>C; p.His227Pro	9	ALF, hepatomegaly	Urticaria and angioedema, low numbers of CD8+ T cells and high CD4+/CD8+ T cell-ratios, high IgE. PHA not assesed.	no	Short stature, delayed bone age,	Normal psychomotor development	Anorexia, recurrent vomiting, reduced subcutaneous fat, troncular obesity, metabolic	2	[129]

							reduced bone density		abnormalities during crises (urinary ketosis, AA in plasmas)		
c.2926del; p.Ser976Profs*16	25	c.809G > C; p.Gly270Ala	10	ALF	PHA not assesed	no	NO short stature	Normal psychomotor development, normal intelligence		1	[131]
c.2203-3C>G; skipping exon 21	IVS 20	c.1042C>T; p.Pro348Ser	12	ALF	PHA not assesed	no	NO short stature	Normal psychomotor development, normal intelligence		1	[121] patient 7
c.2203-3C>G; skipping exon 21	IVS 20	c.1042C>T; p.Pro348Ser	12	ALF	PHA, erythema nodosum, Crohn's disease	no	short stature			1	[121] patient 8
c.409C>T; p.Arg137Trp	7	c.1186T>A; p.Trp396Arg	14	ALF, hepatomegaly	PHA, reduced natural killer cells	NO optic atrophy, myopia, astigmatism	Short stature, skeletal dysplasia, fractures	Mild developmental delay with subsequent normal intelligence	Cervical instability, redundant skin, reduced subcutaneous fat, recurrent vomiting	1	[121] patient 16; [130] patient 2
c.5454_5455delTT; p.Leu1818fs*16	44	c.1339G>A; p.Glu447Lys	14	ALF	hypogammaglobulinemia, no PHA	Pale disc, vascular attenuation and narrowing, and occlusive appearance in the fundus of both eyes	Large anterior fontanelle, short stature, skeletal dysplasia, reduced bone density, fractures	marked hypotonia, severe developmental delay, thin corpus callosum, enlarged ventricles	Recurrent vomiting, contractures	2	[122]
deletion exons 49-50; p.Val1528Glyfs*2	49	c.1278T>G; p.Cys426Trp	14	ALF	PHA, hypogammaglobulinemia	no	Short stature	Normal psychomotor and development, normal intelligence		1	[121] patient 13
c.1187G>A; p.Trp396*	14	c.2330C>A; p.Pro777His	21	ALF	PHA not assesed	no	NO short stature	Normal psychomotor and development, normal intelligence		1	[121] patient 9
c.5389+1G>T; skipping exon 43	IVS 44	c.2407G>A; p.Glu803Lys	22	ALF, hepatosplenomegaly	PHA not assesed	no	NO short stature	Normal psychomotor development		1	[134] patient 3

c.118-2A>G; skipping exon 2	IVS 1	c.2524G>T; p.Val842Phe	23	ALF	PHA not assesed	no	Short stature	Normal psychomotor development	Hypoglicemia	1	[121] patient 10
c.2708T>; p.Leu903Arg	24	c.2708T>G; p.Leu903Arg	24	ALF	no PHA	no	Short stature	Epilepsy, learning disability, borderline QI (77)		1	[121] patient 2
c.2827G>T; p.Glu943*	25	c.2708T>G; p.Leu903Arg	24	ALF	no PHA	no	Short stature	Intellectual disability (QI 50), mild coordination deficit		1	[121] patient 4
c.2819A>C; p. His940Pro	25	c.2819A>C; p. His940Pro	25	ALF, hepatomegaly	PHA not assesed	Not assesed	Poor growth	Normal psychomotor development		1	[135]
c.1533_1545del; p.Ile 512Thrfs*4	15	c.2951T>G; p.Ile984Ser	26	ALF	PHA not assesed	no	Short stature	Mild developmental delay with subsequent normal intelligence		1	[114] patient 6
c.603_605delCCT; p.Leu202del	8	c.3164T>C; p.Leu1055Pro	28	ALF	no PHA, Celiac disease	no	Short stature	Normal psychomotor and development, normal intelligence		1	[121] patient 3
c.686dupT; p.230Qfs*4	9	c.3164T>C; p.Leu1055Pro	28	ALF	PHA not assesed	no	Short stature	Normal psychomotor and development, normal intelligence		1	[121] patient 11
c.3010C>T; p.Arg1004*	26	c.3164T>C; p.Leu1055Pro	28	ALF	no PHA	no	NO short stature	Normal psychomotor and development, normal intelligence	Cardiomyopathy	1	[121] patient 5
c.173-2A>G; skipping exon 3	IVS 2	c.3363A>G; p.Ile1121Met	30	ALF	PHA not assesed	No	NO short stature	Normal psychomotor and development, normal intelligence		1	[121] patient 14
c.209+1G>A; skipping exon 3	IVS 3	c.3596G>A; p.Cys1199Tyr	31	ALF	PHA not assesed	Not assesed	Unreported			1	[132]
c.6611_6612insCA; p.M2204Ifs*3	50	c.3596G>A; p.Cys1199Tyr	31	ALF	PHA not assesed	Not assesed	Unreported	Normal psychomotor development	Intrahepatic cholestasis during pregnancy	1	[134] patient 1
c.586C>T; p.Gln196*	8	c.3596G>A; p.Cys1199Tyr	31	ALF	PHA not assesed	Not assesed	Unreported	Normal psychomotor development		1	[134] patient 2

c.3928A>G; p.Thr1310Ala	33	c.4228 A>G; p.Thr1410Ala	36	ALF	PHA not assesed	Not assesed	Unreported	Unreported		1	Semenova et al. [133]
c.2827G>T; p.Glu943*	25	deletion exons 39-40; p.Val2145_Glu2237del	39-40	ALF	PHA, hypogammaglobulinemia, lymphopenia during crisis	Optic atrophy	Short stature, skeletal dysplasia	Mild psichomotor delay, epilepsy, neuroblastoma		1	[121] patient 12
c.2032C>T; p.Gln678*	19	c.5741G>A; p.Arg1914His	45	ELT	PHA, hypogammaglobulinaemia	Optic atrophy, nystagmus	Large anterior fontanelle, short stature, reduced bone density, fractures, pamidronate therapy	Mild intellectual disability	Episodes of ketotic hypoglycaemia, bilateral 5th finger clinodactyly with bulbous tips to his fingers and toes, high-pitched voice	1	[118] patient 2
c.2827G>T; p.Glu943*	25	c.5741G>A; p.Arg1914His	45	ELT	PHA, hypogammaglobulinemia, neutropenia, no response to vaccinations, reduced B cells	Optic atrophy, progressive visual loss, strabismus	Large anterior fontanelle, short stature, skeletal dysplasia, delayed bone age, multiple Wormian bones	Hypotonia, developmental delay with normal intelligence	IUGR, oligohydramnios, reduced subcutaneous fat, contractures	1	[120]
c.3010C>T; p.Arg1004*	26	c.5741G>A; p.Arg1914His	45	ELT	PHA, hypogammaglobulinaemia, progressive lymphopenia	Optic atrophy, nystagmus and myopia	Large anterior fontanelle, short stature, skeletal dysplasia, reduced bone density, fractures, multiple Wormian bones	Moderate intellectual disability, autism	Prematurity 33 w, bilateral 5th finger clinodactyly with bulbous tips to his fingers and toes, high-pitched voive	1	[118] patient 1
c.5741G>A; p.Arg1914His	45	c.5741G>A; p.Arg1914His	45	ELT	PHA	Decreased visual acuity, optic atrophy, foveal hypoplasia,	Short stature	Normal intelligence		2	[119]

						achromatopsia, nystagmus, thickness of the retinal nerve fiber layer					
c.5741G>A; p.Arg1914His	45	c.5741G>A; p.Arg1914His	45	ELT not assesed	PHA	Optic atrophy, strabismus, myopia	Short stature, delayed bone age	Normal intelligence	High pitched voice	34	[115]
c.6237-3C>G; skipping exon 48	48	c.6237-3C>G; skipping exon 48	48	no ELT	PHA not assesed	Optic atrophy, severe visual deficit, exotropia	Large fontanelles, skeletal dysplasia	Extreme hypotonia, severe neuropsychomotor delay, EEG abnormalities, epilepsy, thin corpus callosum, severe intellectual disability	Palatoschisis, brevity of arms with cutaneous folds, clinodactyly, contractures, sacral dimple, mixed hearing defect	2	[116, 117]
c.686dupT; p.230Qfs*4	9	c.6840G>A; p.Thr2280Thr	51	ELT	PHA, hypogammaglobulinemia, coeliac disease	Congenital glaucoma	Short stature, skeletal dysplasia, reduced bone density	Developmental delay with normal intelligence	Congenital hypothyroidism, small hands with V finger clinodactyly, sandal gap	1	Present study, patient 1
c.1501C>T; p.Arg501*	15	c.6840G>A; p.Thr2280Thr	51	ELT	PHA, hypogammaglobulinemia	Retinopathy of prematurity, severe myopia	Short stature	Developmental delay with normal intelligence	Prematurity 28 w	1	Present study, patient 2

A total of 36 patients have been reported to carry the homozygous p.Arg1914His change associated with the SOPH phenotype [115, 119], while two patients were reported to have a skeletal phenotype associated with the homozygous c.6237−3C>G splice-site change [116, 116]. We evaluated the remaining 37 cases with biallelic *NBAS* variants for possible genotype–phenotype correlations. Pathogenic variants included 24 sequence changes with predicted loss-of-function (LOF; nonsense, frameshift, out-of-frame splicing changes); 21 missense variants; three splice-site changes leading to in-frame deletions, and two changes predicting single amino acid deletions. Of note, genotypes could be divided into two major categories. A first group (8 cases) was characterized by the combination of two missense variants or a missense and an in-frame deletion (Figure 13 g, top), whereas a second group (27 cases) was characterized by compound heterozygosity for a LOF variant and a missense or in-frame splicing/deletion (Figure 13 g, bottom). The phenotype associated with biallelic *NBAS* pathogenic variants mainly affects the liver, with immunodeficiency, skeletal defects, and ophthalmologic and neurologic anomalies also representing recurrent features. Of note, all patients from Group 1 were found to present with acute liver failure (ALF) in the absence of immunodeficiency as a concomitant associated feature. Based on this observation, and assuming an equivalent inactivating effect for each of the reported nonsense and frameshift variants, independently from the type of change and its location, we explored any possible correlation between phenotype and position of the second pathogenic variant. Remarkably, a relationship between liver involvement and variant position was observed as all patients who experienced ALF episodes were found to carry pathogenic variant(s) between exons 7 and 40, the majority causing amino acid changes within the NBAS-Nter and Sec39 functional domains. The only two patients in which both elevated liver transaminases (ELT) and ALF had been formally ruled out were the two sisters affected by acrofrontofacionasal dysostosis type 1 caused by the homozygous c.6237−3C>G change (skipping exon 48), resulting in the production of an aberrant protein [116, 117]. The 34 SOPH patients, homozygotes for the c.5741G>A missense change (p.Arg1914His), had not been investigated for hepatic involvement. However, two siblings with the same genotype presented with skeletal, ocular,

possible immunological involvement (frequent infections had not been investigated), and mild hepatic involvement with persistent ELT without episodes of ALF [119]. This suggests that patients with SOPH may have a subclinical hepatic involvement that should be investigated. Among the reported *NBAS* genotypes, skipping of exon21/c.1042C>T (p.Pro348Ser) has been described in two siblings [121] presenting with severe hepatic involvement with ALF and differing only in the short stature of one. Of note, immunodeficiency is the only other clinical feature that seems to strictly correlate with the location of pathogenic variants, with a pattern reverse to liver failure: cases with immunodeficiency have missense variants at the N-terminal or C-terminal regions of the protein. The p.Glu447Lys and p.Cys426Trp variants in exon 14, just downstream of the NBAS-Nter domain, were the only exceptions, and were both associated with a combined ALF and immunodeficiency. Despite the occurrence of correlations, we however noted the presence of a discordant neurodevelopmental phenotype in two unrelated patients with the same genotype (p.Glu943*/p.Leu903Arg) presenting with ALF, short stature and without immunological or ocular involvement. One presented mild intellectual disability (ID) and epilepsy, the other presented severe ID. It remains to be established whether this is a feature of variable expressivity associated with p.Leu903Arg, or if it is due to the different genetic backgrounds, or if it is a complication of severe ALF-related hepatic encephalopathy [121]. In this context, in addition to immunologic, ocular, and skeletal features being commonly reported in patients with biallelic *NBAS* pathogenic variants, shared features of the two affected subjects in this study included bilateral glaucoma, hypothyroidism, and a celiac disease in patient 1, and a sacral cleft with tethered spinal cord in patient 2. Reanalysis of WES data did not identify variants in genes that could be related to these phenotypes, suggesting a possible contribution of defective NBAS function and an expansion of NBAS-related phenotypes.

A notable finding of this study is the identification of a recurrent pathogenic synonymous variant demonstrated to affect proper *NBAS* transcript processing and resulting in skipping of an exon encoding part of the C-terminal tail. A different variant causing skipping of a different exon coding

for an adjacent portion of the protein has previously been reported (Figure 13 g), further documenting the functional relevance of this still structurally uncharacterized region of the protein. It is now well-established that synonymous variants may alter gene expression through modulation of splicing, mRNA stability, and translation, and disturbing these processes may contribute to human disease [136, 137]. This finding further highlights the current need to optimize the bioinformatics workflow required to attain an accurate functional annotation of the large number of variants that are routinely identified by genome-wide sequencing, as well as the importance of not underestimating synonymous variations when screening for disease-causing variants [138–140].

In conclusion, we report two unrelated subjects with a trait associated with defective NBAS function sharing a previously unreported pathogenic "synonymous" change demonstrated to affect proper *NBAS* transcript processing. Assessing the clinical features and signs of affected subjects with biallelic *NBAS* variants documents the occurrence of a recognizable facial profile for these patients, and provide the first evidence for the occurrence of clinically relevant genotype–phenotype correlations in diseases associated with *NBAS* pathogenic variants.

6 New therapeutic approaches

RASopathies share the molecular mechanisms with cancer, and recently MEK inhibitors targeted drugs, developed in oncology research have been proposed for treatment in RASopathy patients through drug repositioning [141]. One of the first therapeutic approaches with MEK inhibitor in a patient with RASopathy, treated at the Regina Margherita Children's Hospital of Torino in 2019 will be discussed in this chapter [15].

6.1 MEK Inhibition in a Newborn with RAF1-Associated Noonan Syndrome Ameliorates Hypertrophic Cardiomyopathy but Is Insufficient to Revert Pulmonary Vascular Disease

6.1.1 Introduction

Noonan syndrome (NS) is an autosomal dominant disorder affecting development and growth with a prevalence of 1 in 2000 live births. Major clinical features of the disorder include cardiac defects, mostly pulmonary valve stenosis and hypertrophic cardiomyopathy (HCM), postnatal short stature and failure to thrive, distinctive gestalt, cryptorchidism, skeletal and lymphatic anomalies, variable neurodevelopmental involvement, and bleeding diathesis [9]. NS is the most common among the RASopathies, a clinically variable family group of genetic conditions characterized by overlapping features and caused by upregulation of intracellular signalling through the Ras/mitogen-activated protein kinase (RAS-MAPK) pathway [142]. Specific genotype/phenotype correlations have been described in NS. Patients harboring pathogenic *PTPN11* or *SOS1* variants have a low prevalence of hypertrophic cardiomyopathy [143], while those with disease-causing *RAF1, RIT1* and *MRAS* variants are expected to develop this cardiac defect (~85%, 70%, and 100%, respectively) [144–146], showing the strongest association with HCM among RASopathies [147]. *RAF1* variants represent approximately 5% of the gene defects in NS, but account for many of the most severe cases [148]. Notably, the *RAF1*(NM_002880):c.770C>T (p.Ser257Leu) variant is associated with a severe clinical phenotype of NS with neonatal HCM and pulmonary hypertension [146, 149]. Early-onset HCM represents the major determinant in the outcome of patients with RASopathies and is associated with cardiac failure, worse outcome and high risk of cardiac death [147, 148, 150].

Recently, precision medicine offered interesting treatment opportunities in the RASopathies. The RAS-MAPK pathway has a well-defined role in cancer biology and has been extensively studied as an important target in the development of targeted therapies. Several small-molecule inhibitors

targeting the mitogen-activated protein/extracellular signal-regulated kinases 1 and 2 (MEK1 and MEK2), which are key signal transducers of the MAPK cascade, have been developed. Reducing the perturbed signal transduction of the RAS/MAPK pathway has been presented as promising for RASopathy-associated cardiomyopathies [148]. The use of a MEK inhibitor (MEKi) in a murine model of *RAF1*-related NS showed encouraging results, since inhibition of MEK was able to revert multiple features of the disease, including HCM [141]. Furthermore, Trametinib, a selective reversible inhibitor of MEK1/2 activity approved for treatment of cancers with RAS/MAPK pathway activation, was successfully employed in two *RIT1*-mutated newborns with NS and severe HCM, inducing reversal of cardiac failure and valvular obstruction [6].

Here, we report on a *RAF1*-mutated patient with severe NS, including neonatal HCM and pulmonary hypertension, treated with selective MEK inhibition by Trametinib.

6.1.2 Materials and Methods

6.1.2.1 RNA Extraction

Blood samples from the patient have been collected in sodium-heparin tubes at days 0, 7, 16, 30, and 37 of Trametinib treatment. Peripheral blood mononuclear cells (PBMCs) have been isolated by Ficoll-Hypaque density gradient centrifugation (Histopaque-1077, Sigma-Aldrich, St. Louis, MO, USA). Total RNA was extracted from PBMCs preserved in TRI Reagent using the Direct-zol RNA miniprep kit (Zymo Research, Irvine, California, USA), according to the manufacturer's instructions. RNA concentration was quantified using the Qubit Fluorometer (Thermo Fisher Scientific, Waltham, MA, USA). RNA quality was assessed by verifying the RNA integrity number (RIN) and percentage of RNA fragments >200 nucleotides in size (DV200) with Agilent RNA Kits on a Bioanalyzer 2100 (Agilent, Santa Clara, CA, USA).

6.1.2.2 RNA Sequencing

Total RNA was processed for RNA-seq analysis with the TruSeq RNA Library Prep Kit v2 (Illumina, San Diego, CA, USA) following manufacturer's instructions. Furthermore, it is quantified using the Qubit Fluorometer (Thermo Fisher Scientific). Library correct size and purity were checked on a Bioanalyzer 2100 (Agilent), using Agilent DNA High Sensitivity kit. Libraries were sequenced on a NextSeq 500 system (Illumina).

6.1.2.3 Gene Expression Quantification

Each fastq file was aligned using STAR [151] to version HG38 of the human genome. Gencode 27 was used as the transcriptome reference database and gene quantification was performed with feature counts [152]. To avoid noise from low-detection genes, genes not reaching 4 counts in at least one sample were removed, and a thresholding was applied by assigning a random value between 3 and 4 counts to values below 4 counts. The final processing step was trimmed mean of M values (TMM) normalization using the EdgeR package [153].

6.1.2.4 Gene Set Enrichment Analysis

The two samples at Day 7 were averaged, then for each gene the log2 ratio vs Day 0 was calculated at each time point. For each time point, log2ratio values were used to rank genes for pre-ranked GSEA, using standard parameters [154, 155]. Log2 ratio between average expression at all treatment points vs Day 0 was also calculated and used for pre-ranked GSEA. To identify a core set of representative genes for the various modulated pathways, we selected genes that were in the GSEA leading edge of the respective signature at all time points. Among these, we further prioritized MKI67, a known reporter of cell proliferation [156], and genes potentially involved in cardiomyocyte physiopathology based on literature search.

6.1.3 Results

6.1.3.1 Clinical Report

A female preterm infant was born at 33+6 weeks of gestation, after a pregnancy characterized by polyhydramnios (amniotic fluid index at 31 + 2 weeks of gestation 133 mm) and HCM (septal thickness 9 mm, thoracic index 0.5), from healthy and non-consanguineous parents. Prenatal measurement of nuchal translucency, biochemical pregnancy screening and foetal biometry were normal. Apgar score was 3/5 at 1 and 5 minutes, respectively, with poor initiation of breathing, cyanosis, hypotonia and hyporeflexia. The patient required urgent intubation and mechanical ventilation. Neonatal weight was 2150 g (+0.4 SDS), length 49.0 cm (+2.4 SDS), OFC 32.1 cm (+0.9 SDS). Clinical features were dominated by facial and nuchal dysmorphisms, highly suggestive for NS.

Echocardiography, performed shortly after birth, confirmed severe biventricular obstructive HCM with minimal left intraventricular gradient, mild mitral regurgitation, aortic valve with thickened cusps and dysplastic pulmonary valve with normal origin and caliber of the pulmonary branches. No direct or indirect signs of pulmonary hypertension were present and β-blockade treatment with propranolol was started.

At the 2nd day of life, she underwent a routine transfontanellar ultrasound demonstrating a grade II cerebral ventricular hemorrhage. Blood tests, including clotting tests, were normal. On blood extracted DNA, a next generation sequencing gene panel targeted to the RASopathy genes revealed a de novo c.770C>T (p.Ser257Leu) pathogenic variant in *RAF1* (NM_002880), confirming the clinical diagnosis of NS.

In the next days, she progressively developed severe congestive heart failure (CHF) characterized by profound hypoxic crises with moderate hypercarbia and requiring incremental ventilator support with high-frequency oscillatory ventilation and CHF drugs introduction (furosemide and spironolactone). She progressively developed a post-hemorrhagic hydrocephalus and an external ventricular drain was placed at 21 days subsequently replaced at 39 days of life. In the next week, her ventilatory and

inotrope requirements continuously increased. Given the near-terminal CHF, having no other treatment options besides cardiac transplant, Trametinib was introduced (0.022 mg/kg/day) as an off-label prescription with parents' consent and under approval of the local Ethical Committee for off-label prescriptions (47th day of life, treatment day +0).

After treatment initiation there was a prompt improvement in clinical conditions (ROSS score from IV to III), allowing progressive and rapid withdrawal of inotropes in the next 4 days and weaning from mechanical ventilation a week later. Consistent with HCM stabilization, nt-pro-BNP decreased from 30,805 to 2355 pg/mL, and the patient was placed in non-invasive ventilator support and restricted fluid intake, with furosemide administration "as needed". During the next month, treatment with Trametinib was continued without relevant side effects. ROSS score was II at 1 month. Liver enzymes, complete blood count, clotting tests, electrolytes, renal function were regularly monitored with no substantial modifications from baseline nor effects attributable to Trametinib administration. Echocardiography showed a tendency to HCM improvement with reduction of the septal thickness from treatment start to day +23. We also noted sudden dilation of the pulmonary artery dilation (14 mm, +3.5 SDS) at day 23. Despite of this finding, clinical conditions were stable in the following days and non-invasive ventilatory support was progressively reduced in terms of oxygen flow and fraction.

At day +46, a ventriculoperitoneal shunt was placed in order to manage the intraventricular hemorrhage and a red blood cell unit was transfused. After surgery, we observed rapid worsening of CHF (nt-pro-BNP increased from 2049 pg/mL to 47,000 pg/mL) as well as respiratory deterioration, requiring again mechanical ventilator support. Pulmonary artery dilation, stable until then, increased to 18 mm (+5.7 SDS) and death from untreatable CHF with hypoxic respiratory failure occurred on day +57. Figure 14 recapitulates the time course with septal thickness changes, left ventricular outflow (LVO) gradient and nt-pro-BNP changes across treatment. Figure 15 shows the ultrasound HCM evolution over time.

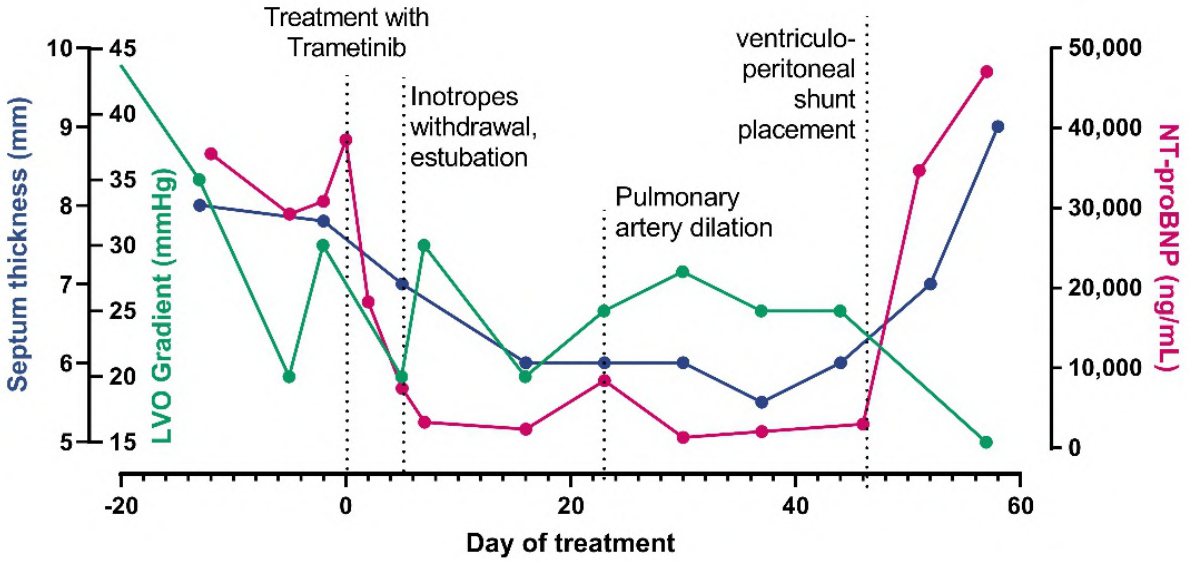

Figure 14. Treatment time course. The picture shows changes in nt-pro-BNP, Left Ventricular Outflow (LVO) gradient and septal thickness at ultrasound before and after treatment initiation and related to the major clinical events in our patient.

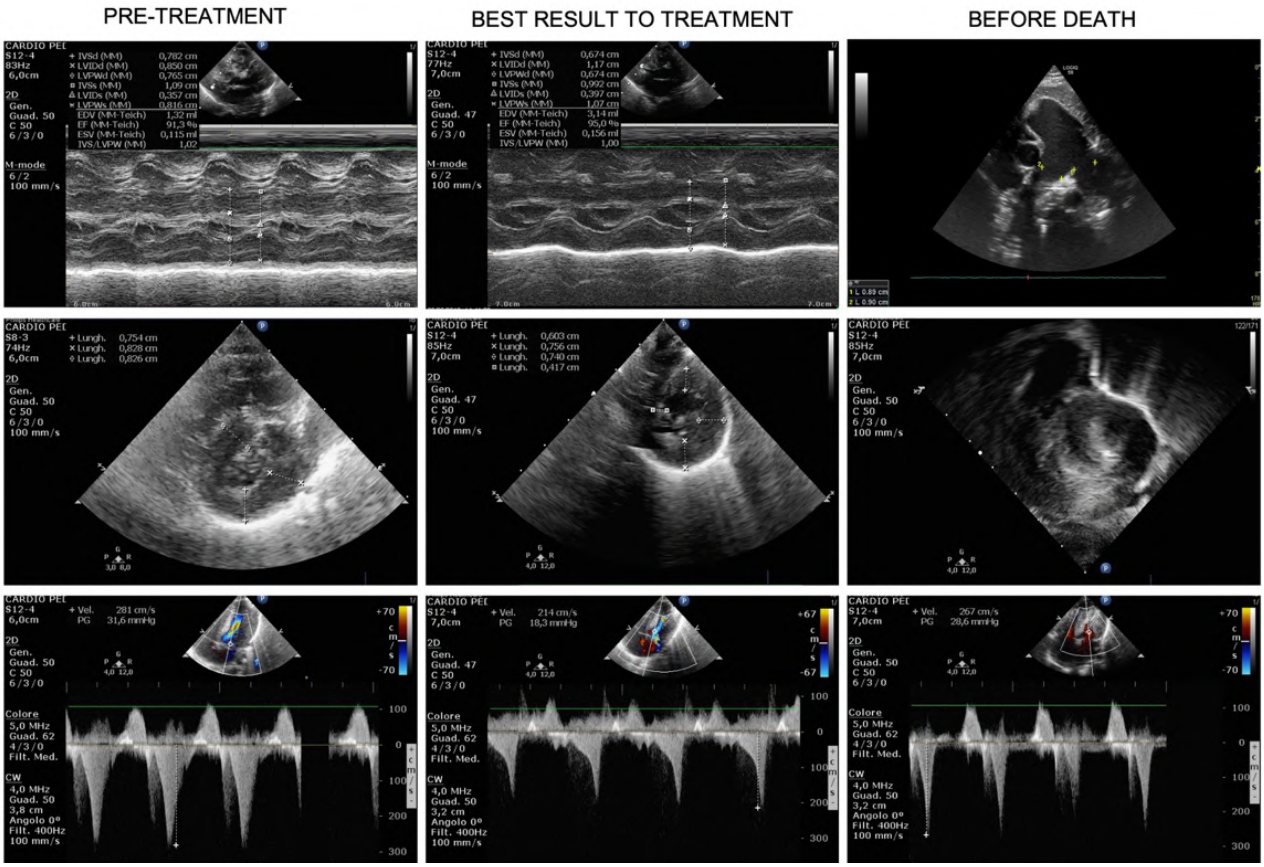

Figure 15. Evolution over time of hypertrophic cardiomyopathy (HCM). Pre-treatment US (first column) shows severe HCM at M-mode Left Ventricle (Mm-LV, first row), short-axis LV (second row) and LV outflow track obstruction (CW-Doppler, third row), few days before treatment start. The

best result under treatment is shown in the middle column: Mm-LV in first row, short-axis LV (second row) and LV outflow track obstruction (third row) demonstrated a consistent reduction of LV thickness and improvement of LV outflow track obstruction. The third column shows cardiac US three days before death: pulmonary artery dilatation is evident in the first row (2D), the rapid worsening of HCM, both in terms of LV thickness and obstruction are depicted in the last 2 rows (short- axis LV and CW-Doppler, respectively).

Autopsy confirmed a severe obstructive HCM as well as dilation of pulmonary artery trunk and branches (Figure 16). Pulmonary histology showed a complete disarray of both gross and fine pulmonary vascular anatomy consistent with diffuse blood congestion and alveolar damage, alveolar lumens with exudate and foamy histiocytes containing hemosiderin, septal fibrosis, thick-walled pulmonary arteries, thickened inter-alveolar septum with proliferation of blood vessels and capillaries randomly arranged and spaced apart from the alveolar lumen (Figure 17). The histologic features were consistent with an aberrant and excessive capillary proliferation and layering consistent with a diagnosis of pulmonary capillary hemangiomatosis.

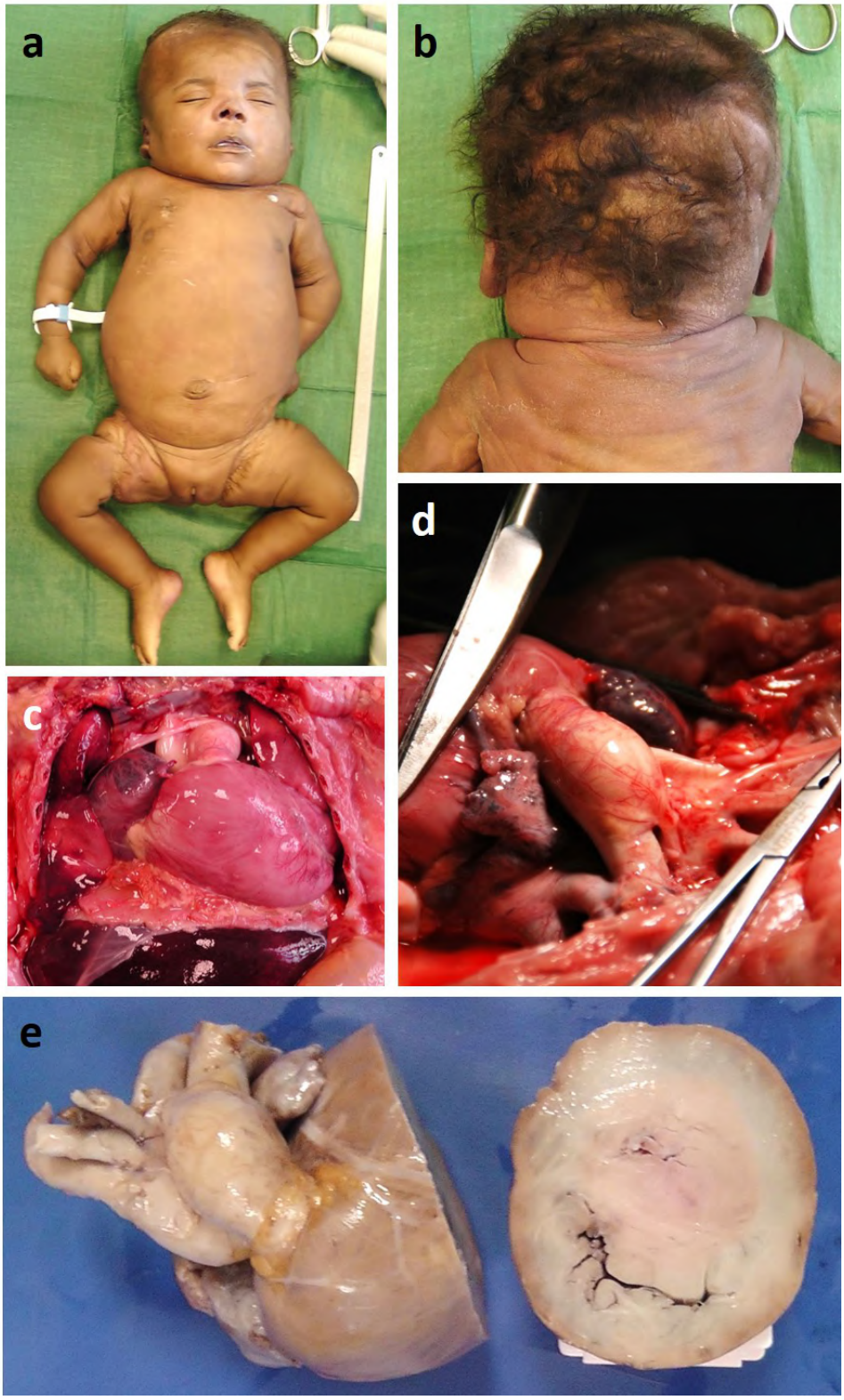

Figure 16. Gross pathology findings. Autopsy showed typical Noonan syndrome (NS) features with low-set posteriorly rotated ears, high anterior hairline with wide forehead and narrow temples, mild hypertelorism, downslanting palpebral fissures, broad nose, full tip with deeply grooved philtrum (a), pterigium colli, short webbed neck (b), severe obstructive HCM (c,e), dilation of pulmonary artery trunk and branches (d).

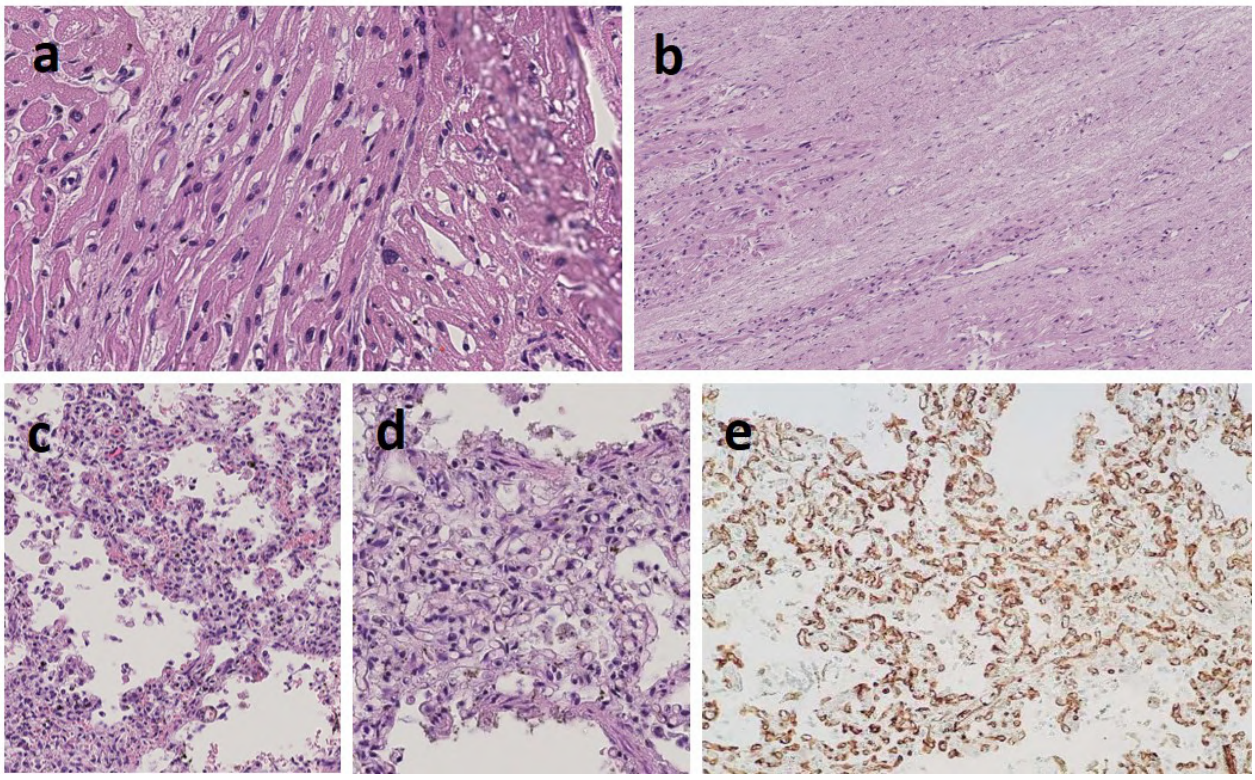

Figure 17. Histology showed a complete disarray of both gross and fine cardiac and pulmonary anatomy. Heart microscopy showed disorientation of muscle fibers and hypertrophic myocells with enlarged ovoid nucleus (a), left ventricle fibrotic and necrotic areas of myocells (long-standing infarction) and limited neighboring areas of more recent ischemic damage (b). Picture of the lungs with arterial hypertension, chronic stasis and alveolar damage: pulmonary capillary hemangiomatosis with peripheral arterioles with stenotic lumen for muscular tunic hypertrophy, intimal tunic thickening, hilar pulmonary vessels of increased caliber and with hypertrophic wall, thickened and hypervascularized interalveolar septa, alveolar lumens with exudate and foamy histiocytes containing hemosiderin (c), and increased thickness of the interalveolar septum with hypercapillarization (d). The capillaries (colored in brown with immunohistochemical staining CD31) were markedly increased in with a chaotic distribution (hemangiomatosis) with most of them not reaching the alveolar surface (e).

6.1.3.2 Transcriptomics

Peripheral blood mononuclear cells (PBMCs) were obtained at days 0, 7, 16, 30, and 37 of Trametinib treatment. Gene expression analysis was performed by global mRNA sequencing, and revealed marked changes in the transcriptional profiles, already apparent at day 7 and generally sustained over the treatment course. To systematically explore functional pathway alterations driven by Trametinib, we employed GeneSet Enrichment Analysis (GSEA) [154, 155], which revealed

sustained downregulation of many gene signatures, excluding the occurrence of adaptive response to the treatment. A particularly large group of signatures was associated with RAS/MAPK signaling (Figure 18a), including EGFR, RAS, RAF, and the previously published signature previously characterized in PBMCs from NS patients with mutated *PTPN11* alleles [19]. Further signatures associated with related pathways were also persistently downregulated, including cell cycle, PI-3 kinase, WNT and YAP/TAZ pathways (Figure 18b). In-depth analysis of representative genes for these pathways highlighted key transcriptional targets of trametinib potentially involved in heart and lung tissue homeostasis.

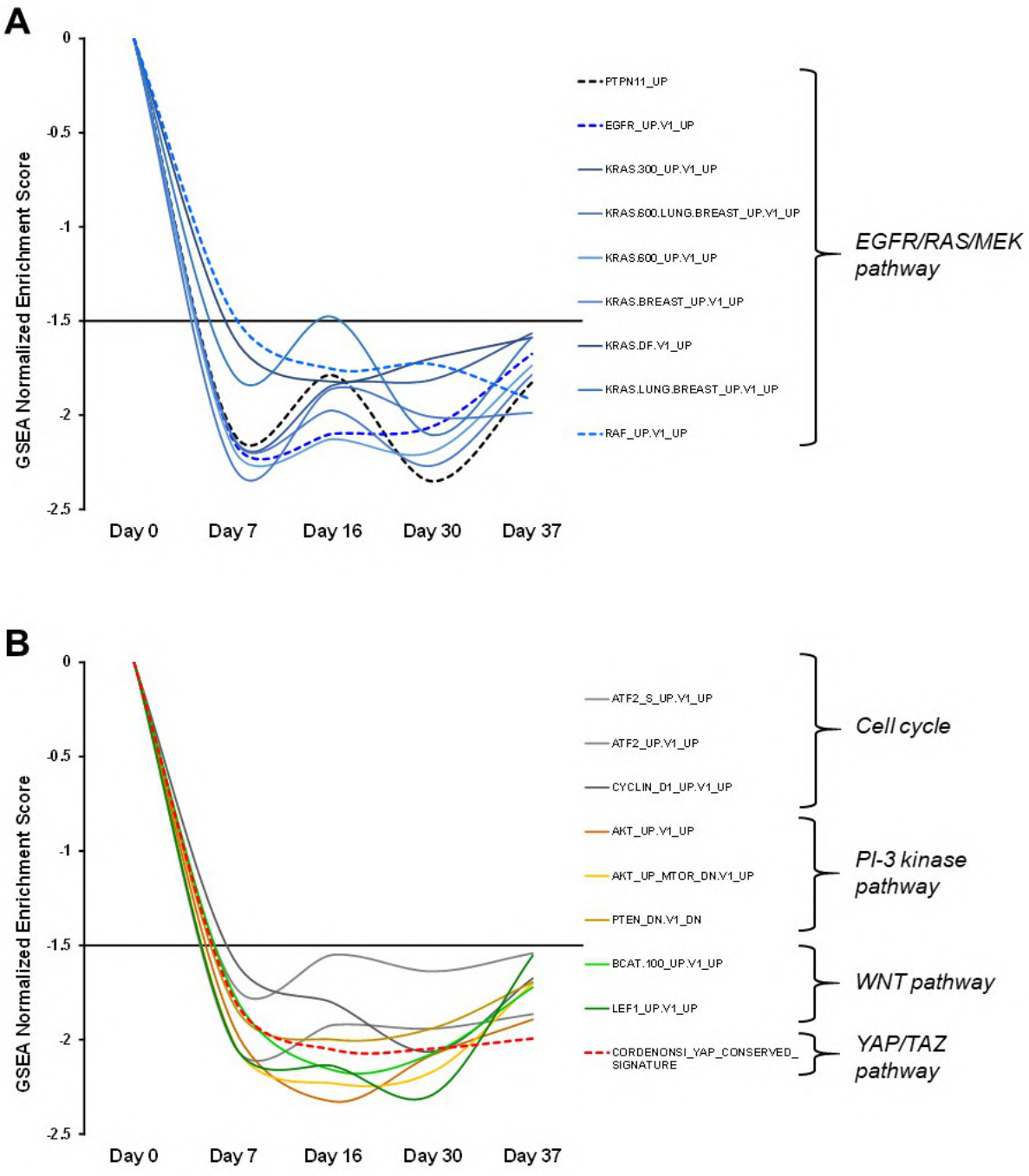

Figure 18. GSEA analysis of trametinib-driven pathway signature dynamics in the PBMC transcriptome. All signatures display a consistently negative Enrichment Score, below the −1.5 significance threshold value, indicating overall down-modulation by trametinib over the entire treatment period. (A) Modulation of signatures related to the EGFR/RAS/RAF/MEK pathway. These include the PTPN11 RASopathy signature, highlighted by the black dashed line. (B) Modulation of signatures associated with additional pathways, including the YAP/TAZ pathway signature highlighted by the red dashed line.

6.1.4 Discussion

Molecular therapy for congenital defects represents one of the most interesting and innovative advancements of precision medicine [20]. RASopathies represent a paradigmatic group of genetic diseases that could benefit from these innovative therapeutic approaches. In a newborn affected by a severe phenotype of NS with progressive HCM and pulmonary hypertension, due to a *RAF1* p.Ser257Leu variant, we reasoned that MEK inhibition might limit the progression of cardiac disease. This assumption relied on the observation of phenotype reversal under MEK inhibition of murine models of severe NS [141] and on the encouraging results obtained in *RIT1*-mutated NS patients with HCM [6]. MEK inhibitor treatment was initially characterized by a rapid and significant improvement in the overall clinical conditions of the patient, associated with a relevant nt-pro-BNP decrease consistent with Trametinib introduction. A clear response to the treatment was observed after a previous progressive negative evolution of the cardiac and pulmonary picture since birth that was evolving to a terminal CHF.

RAS activation is involved in the physiologic and pathologic cardiac hypertrophy, and the p.Ser257Leu and p.Leu613Val pathogenic variants have extensively been studied for their severe impact on myocardial physiology [157, 158]. Indeed, the p.Ser257Leu variant in *RAF1* has been causally associated with severe pulmonary arterial hypertension [159] and progressive HCM [160] with lethal outcome. Several reports link this variant to a particularly severe NS phenotype [146, 161–164], and activating *RAF1* variants are well known to be highly correlated with HCM [146–148, 163, 165–167]. The patient we describe presented a very severe phenotype complicated by prematurity. In addition to progressive HCM, she finally developed pulmonary hypertension, a clinical feature described in several patients with the p.Ser257Leu amino acid substitution in *RAF1* [160] and hydrocephalus, also already reported in association with this variant [160], in this case likely related to intraventricular hemorrhage of prematurity. Pulmonary artery dilation, consistent with an aneurysm, has been rarely observed in NS, reported only in a single newborn and in an adult patient

[168], whereas cardiac and great arteries aneurysms have been sporadically described as part of the NS phenotype [169–174]. The pulmonary artery dilation observed in this patient was likely an epiphenomenon of the pulmonary hypertension (PH) and the histological abnormalities observed in the lungs: histology revealed pulmonary capillary hemangiomatosis (PCH), a very rare cause of PH characterized by extensive proliferation of pulmonary capillaries within alveolar septae [175] never reported in NS. Despite frequent fatal outcomes in severe NS, few pulmonary autopsy reports have been described so far [176, 177]. Our case suggests that one of the most prevalent and deleterious pathogenic *RAF1* variants is characterized by a unique histopathological pulmonary finding, clearly related to the lethal outcome in the context of a respiratory course. The pulmonary findings observed are intriguing, since pulmonary vascular bed remodeling characterizing PCH and carcinogenesis have analogous features, such as the altered crosstalk between cells form different types of tissues and proliferation of pulmonary smooth muscle and endothelial cells [178]. Moreover, MAPK signaling has been identified as a key player in heritable forms of pulmonary arterial hypertension [179], with a role in the control of vascular remodeling. In this case, we suggest that the recurrent postnatal hypoxic episodes played a synergistic effect on the genetic predisposition with hyperactivation of the RAS-MAPK pathway. Thus, hypoxia and CHF could have triggered pulmonary microvascular remodeling, inducing a negative feed-back loop which hesitated to respiratory failure and worsening of the CHF [180].

At the same time of the therapeutic attempt, we collected patient's PBMC at different timepoints and performed whole RNA sequencing. We decided to use PBMC as surrogate target cells to study the effects that can occur in target organs, such as the heart, because PBMC can be easily and repeatedly collected and are suitable for studying expression changes over time. However, as a limitation of this approach, it is not known whether the changes in gene expression levels in PBMCs are a reliable indicator of changes in target organs. We observed marked changes in the transcriptome, with a strong

and sustained downregulation of signatures related to the SHP2 and RAS/MAPK signaling [181], which can be used as surrogate markers to measure Trametinib effect.

Notably, the RAS/MAPK axis was not the only pathway found downmodulated. Further downregulated signatures included those associated with the PI3 kinase, WNT and YAP/TAZ pathways, indicating that MEK inhibition exerted a broad effect on signal transduction. The YAP/TAZ pathway was particularly interesting, because it has been shown to promote cardiomyocyte proliferation during development [182]. Indeed, RASopathy-driven YAP/TAZ hyperactivity could be related to the cardiac hypertrophy observed in the patient, potentially explaining the mechanism for the sudden response to treatment, through trametinib-driven YAP/TAZ downmodulation. Among the most consistently downregulated genes, HB-EGF and SPP1 have been linked to cardiac hypertrophy by ERK pathway activation [183]. THBS1, SPP1 and LGR1 were previously associated with cardiomyocyte fibrosis, and heart failure [184, 185]1/31/22 2:27:00 PM. LMO2 is involved in angiogenesis and endothelial cell proliferation [186].

Several causes can be linked to the fatal outcome of our case. It may be conceivable that some sort of “honeymoon phenomenon” has occurred for the drug. However, we observed that the expression downregulation of the signatures was sustained along the entire treatment course, excluding the occurrence of adaptive response to the treatment. Rather, the negative evolution could be linked to secondary remodeling of the pulmonary vascular bed which could have led to a worsening of the pulmonary perfusion dynamics. Trametinib, despite being effective at the cardiac level, likely failed to control the pulmonary vascular component of the disease process. It is noteworthy that in the model of genetic forms of pulmonary hypertension-BMPR2 loss-of function-ERK1/2 are constitutively activated and two Raf inhibitors (Sorafenib and AZ628) as well as Nintedanib (a triple receptor tyrosine kinase inhibitor acting upstream) reversed the invasive proliferation of the pulmonary artery endothelial cells [179]. Imatinib, a tyrosine kinase inhibitor, has been observed to be efficient in

reversing the cardiopulmonary remodeling in pulmonary hypertension, representing a potential candidate for a combined therapy [187], which has shown synergistic effects in cancer models [188].

The timing and rapidity of the terminal clinical worsening observed connects the deteriorating clinical condition with the surgery for ventriculoperitoneal shunt placement. Undoubtedly, the extremely precarious clinical conditions have been disturbed in their delicate balance by such concomitant factors complicating its management.

In our opinion, the prompt improvement and subsequent clinical stability that characterized our case from the moment of the introduction of the MEK inhibitor until the final rapidly evolving CHF makes this experience encouraging despite the outcome. The use of MEK inhibitors remains a promising therapeutic option for HCM in the RASopathies and further experience in this area, in patients with associated pulmonary hypertension, is needed. Finally, the unique histopathological pulmonary finding highlights the connection between pulmonary vascular disease and the severe clinical outcome generally associated with the *RAF1* p.Ser257Leu amino acid substitution, besides underlying the paucity of data on the pulmonary issues of RASopathy patients and suggesting that this should be looked at more frequently.

7 Discussion

The rapid evolution of diagnostic techniques and the increasing discovery of new genes allow the etiological diagnosis in an increasing number of patients. Molecular diagnosis represents the end of the diagnostic odyssey but the beginning of the treatment pathway for these patients who often face the lack of knowledge on rare and recently discovered diseases. This implies the lack of guidelines, the lack of knowledge on the natural history of the disease and on the underlying pathogenetic mechanisms [2]. Clinical research on the clinical characteristics of diseases, namely deep phenotyping, and basic research on the pathogenetic mechanisms of the disease are essential for acquiring knowledge to define the best strategy of care and cure. In rare diseases, to reach a significant number of patients for clinical studies it is often necessary to develop international collaborations, gathered by dedicated services and patient's associations [189]. An example of the potential of this approach is given by RASopathies, a group of diseases first clinically described in 1883 [7] and whose molecular basis was discovered in 2001 [8]. Research on RASopathies is favored by the relative high frequency of the disease, about 1 in 2000, that is one of the most frequent rare diseases in the world [190], which allowed the collection of numerous patients' cohort with a broad and detailed description of the natural history of the disease and of possible complications. RASopathies are in fact one of the few rare diseases for which shared guidelines, indications for follow-up, dedicated growth curves and structured treatment pathways are available [190]. Furthermore, the molecular mechanism underlying RASopathies is one of the mechanisms most implicated in the development of cancer [10], and research on RASopathies was also favored by the extensive basic research conducted on the RAS/MAPK pathway in the field of oncology, which led to the development of specific drugs, such as MEK inhibitors [10]. Over the past 10 years, it has been demonstrated the potential efficacy of these drugs on RASopathies cellular and animal models [141] and over the past 2 years the first treatments have been attempted on patients with RASopathy [6], such as the one described in the present study [15]. The example of RASopathies demonstrates how much the

increasing clinical and molecular knowledge on rare diseases can change treatment options and improve patients' quality of life and confirms clinical genetics as a paradigm of personalized medicine.

8 References

1 Suwinski P, Ong C, Ling MHT, Poh YM, Khan AM, Ong HS. Advancing Personalized Medicine Through the Application of Whole Exome Sequencing and Big Data Analytics. *Front Genet* 2019;**10**:49.

2 Manickam K, McClain MR, Demmer LA, Biswas S, Kearney HM, Malinowski J, Massingham LJ, Miller D, Yu TW, Hisama FM. Exome and genome sequencing for pediatric patients with congenital anomalies or intellectual disability: an evidence-based clinical guideline of the American College of Medical Genetics and Genomics (ACMG). *Genet Med* 2021;**23**:2029–37.

3 Lelieveld SH, Spielmann M, Mundlos S, Veltman JA, Gilissen C. Comparison of Exome and Genome Sequencing Technologies for the Complete Capture of Protein-Coding Regions. *Human Mutation* 2015;**36**:815–22.

4 Zurynski Y, Gonzalez A, Deverell M, Phu A, Leonard H, Christodoulou J, Elliott E. Rare disease: a national survey of paediatricians' experiences and needs. *BMJ Paediatr Open* 2017;**1**:e000172.

5 Venot Q, Blanc T, Rabia SH, Berteloot L, Ladraa S, Duong J-P, Blanc E, Johnson SC, Hoguin C, Boccara O, Sarnacki S, Boddaert N, Pannier S, Martinez F, Magassa S, Yamaguchi J, Knebelmann B, Merville P, Grenier N, Joly D, Cormier-Daire V, Michot C, Bole-Feysot C, Picard A, Soupre V, Lyonnet S, Sadoine J, Slimani L, Chaussain C, Laroche-Raynaud C, Guibaud L, Broissand C, Amiel J, Legendre C, Terzi F, Canaud G. Targeted therapy in patients with PIK3CA-related overgrowth syndrome. *Nature* 2018;**558**:540–6.

6 Andelfinger G, Marquis C, Raboisson M-J, Théoret Y, Waldmüller S, Wiegand G, Gelb BD, Zenker M, Delrue M-A, Hofbeck M. Hypertrophic Cardiomyopathy in Noonan Syndrome Treated by MEK-Inhibition. *J Am Coll Cardiol* 2019;**73**:2237–9.

7 Marcinowski F. Oskar Kobyliński (1856-1926) and the first description of Noonan syndrome in the medical literature. *J Med Biogr* 2020;**28**:202–7.

8 Tartaglia M, Mehler EL, Goldberg R, Zampino G, Brunner HG, Kremer H, van der Burgt I, Crosby AH, Ion A, Jeffery S, Kalidas K, Patton MA, Kucherlapati RS, Gelb BD. Mutations in PTPN11, encoding the protein tyrosine phosphatase SHP-2, cause Noonan syndrome. *Nat Genet* 2001;**29**:465–8.

9 Roberts AE, Allanson JE, Tartaglia M, Gelb BD. Noonan syndrome. *Lancet* 2013;**381**:333–42.

10 Santarpia L, Lippman SM, El-Naggar AK. Targeting the MAPK-RAS-RAF signaling pathway in cancer therapy. *Expert Opin Ther Targets* 2012;**16**:103–19.

11 Bergqvist C, Wolkenstein P. MEK inhibitors in RASopathies. *Curr Opin Oncol* 2021;**33**:110–9.

12 Bryant L, Li D, Cox SG, Marchione D, Joiner EF, Wilson K, Janssen K, Lee P, March ME, Nair D, Sherr E, Fregeau B, Wierenga KJ, Wadley A, Mancini GMS, Powell-Hamilton N, van de Kamp J, Grebe T, Dean J, Ross A, Crawford HP, Powis Z, Cho MT, Willing MC, Manwaring L, Schot R, Nava C, Afenjar A, Lessel D, Wagner M, Klopstock T, Winkelmann J, Catarino CB, Retterer K, Schuette JL, Innis JW, Pizzino A, Lüttgen S, Denecke J, Strom TM, Monaghan KG, DDD Study, Yuan Z-F, Dubbs H, Bend R, Lee JA, Lyons MJ, Hoefele J, Günthner R, Reutter H, Keren B, Radtke K, Sherbini O, Mrokse C, Helbig KL, Odent S, Cogne B, Mercier S, Bezieau S, Besnard T, Kury S, Redon R, Reinson K, Wojcik MH, Õunap K, Ilves P, Innes AM, Kernohan KD, Care4Rare Canada Consortium, Costain G, Meyn MS, Chitayat D, Zackai E, Lehman A, Kitson

H, CAUSES Study, Martin MG, Martinez-Agosto JA, Undiagnosed Diseases Network, Nelson SF, Palmer CGS, Papp JC, Parker NH, Sinsheimer JS, Vilain E, Wan J, Yoon AJ, Zheng A, Brimble E, Ferrero GB, Radio FC, Carli D, Barresi S, Brusco A, Tartaglia M, Thomas JM, Umana L, Weiss MM, Gotway G, Stuurman KE, Thompson ML, McWalter K, Stumpel CTRM, Stevens SJC, Stegmann APA, Tveten K, Vøllo A, Prescott T, Fagerberg C, Laulund LW, Larsen MJ, Byler M, Lebel RR, Hurst AC, Dean J, Schrier Vergano SA, Norman J, Mercimek-Andrews S, Neira J, Van Allen MI, Longo N, Sellars E, Louie RJ, Cathey SS, Brokamp E, Heron D, Snyder M, Vanderver A, Simon C, de la Cruz X, Padilla N, Crump JG, Chung W, Garcia B, Hakonarson HH, Bhoj EJ. Histone H3.3 beyond cancer: Germline mutations in Histone 3 Family 3A and 3B cause a previously unidentified neurodegenerative disorder in 46 patients. *Sci Adv* 2020;**6**:eabc9207.

13 Gazzin A, Carli D, Sirchia F, Molinatto C, Cardaropoli S, Palumbo G, Zampino G, Ferrero GB, Mussa A. Phenotype evolution and health issues of adults with Beckwith-Wiedemann syndrome. *Am J Med Genet A* 2019;**179**:1691–702.

14 Carli D, Giorgio E, Pantaleoni F, Bruselles A, Barresi S, Riberi E, Licciardi F, Gazzin A, Baldassarre G, Pizzi S, Niceta M, Radio FC, Molinatto C, Montin D, Calvo PL, Ciolfi A, Fleischer N, Ferrero GB, Brusco A, Tartaglia M. NBAS pathogenic variants: Defining the associated clinical and facial phenotype and genotype-phenotype correlations. *Hum Mutat* 2019;**40**:721–8.

15 Mussa A, Carli D, Giorgio E, Villar AM, Cardaropoli S, Carbonara C, Campagnoli MF, Galletto P, Palumbo M, Olivieri S, Isella C, Andelfinger G, Tartaglia M, Botta G, Brusco A, Medico E, Ferrero GB. MEK Inhibition in a Newborn with RAF1-Associated Noonan Syndrome Ameliorates Hypertrophic Cardiomyopathy but Is Insufficient to Revert Pulmonary Vascular Disease. *Genes (Basel)* 2021;**13**:6.

16 Meng L, Pammi M, Saronwala A, Magoulas P, Ghazi AR, Vetrini F, Zhang J, He W, Dharmadhikari AV, Qu C, Ward P, Braxton A, Narayanan S, Ge X, Tokita MJ, Santiago-Sim T, Dai H, Chiang T, Smith H, Azamian MS, Robak L, Bostwick BL, Schaaf CP, Potocki L, Scaglia F, Bacino CA, Hanchard NA, Wangler MF, Scott D, Brown C, Hu J, Belmont JW, Burrage LC, Graham BH, Sutton VR, Craigen WJ, Plon SE, Lupski JR, Beaudet AL, Gibbs RA, Muzny DM, Miller MJ, Wang X, Leduc MS, Xiao R, Liu P, Shaw C, Walkiewicz M, Bi W, Xia F, Lee B, Eng CM, Yang Y, Lalani SR. Use of Exome Sequencing for Infants in Intensive Care Units: Ascertainment of Severe Single-Gene Disorders and Effect on Medical Management. *JAMA Pediatr* 2017;**171**:e173438.

17 Tan TY, Dillon OJ, Stark Z, Schofield D, Alam K, Shrestha R, Chong B, Phelan D, Brett GR, Creed E, Jarmolowicz A, Yap P, Walsh M, Downie L, Amor DJ, Savarirayan R, McGillivray G, Yeung A, Peters H, Robertson SJ, Robinson AJ, Macciocca I, Sadedin S, Bell K, Oshlack A, Georgeson P, Thorne N, Gaff C, White SM. Diagnostic Impact and Cost-effectiveness of Whole-Exome Sequencing for Ambulant Children With Suspected Monogenic Conditions. *JAMA Pediatr* 2017;**171**:855–62.

18 Retterer K, Juusola J, Cho MT, Vitazka P, Millan F, Gibellini F, Vertino-Bell A, Smaoui N, Neidich J, Monaghan KG, McKnight D, Bai R, Suchy S, Friedman B, Tahiliani J, Pineda-Alvarez D, Richard G, Brandt T, Haverfield E, Chung WK, Bale S. Clinical application of whole-exome sequencing across clinical indications. *Genet Med* 2016;**18**:696–704.

19 Trujillano D, Bertoli-Avella AM, Kumar Kandaswamy K, Weiss ME, Köster J, Marais A, Paknia O, Schröder R, Garcia-Aznar JM, Werber M, Brandau O, Calvo del Castillo M, Baldi C, Wessel K, Kishore S, Nahavandi N, Eyaid W, Al Rifai MT, Al-Rumayyan A, Al-Twaijri W, Alothaim A, Alhashem A, Al-Sannaa N, Al-Balwi M, Alfadhel M, Rolfs A, Abou Jamra R. Clinical exome sequencing: results from 2819 samples reflecting 1000 families. *Eur J Hum Genet* 2017;**25**:176–82.

20 Lee H, Deignan JL, Dorrani N, Strom SP, Kantarci S, Quintero-Rivera F, Das K, Toy T, Harry B, Yourshaw M, Fox M, Fogel BL, Martinez-Agosto JA, Wong DA, Chang VY, Shieh PB, Palmer CGS, Dipple KM, Grody WW, Vilain E, Nelson SF. Clinical Exome Sequencing for Genetic Identification of Rare Mendelian Disorders. *JAMA* 2014;**312**:1880–7.

21 Yang Y, Muzny DM, Reid JG, Bainbridge MN, Willis A, Ward PA, Braxton A, Beuten J, Xia F, Niu Z, Hardison M, Person R, Bekheirnia MR, Leduc MS, Kirby A, Pham P, Scull J, Wang M, Ding Y, Plon SE, Lupski JR, Beaudet AL, Gibbs RA, Eng CM. Clinical whole-exome sequencing for the diagnosis of mendelian disorders. *N Engl J Med* 2013;**369**:1502–11.

22 Lionel AC, Costain G, Monfared N, Walker S, Reuter MS, Hosseini SM, Thiruvahindrapuram B, Merico D, Jobling R, Nalpathamkalam T, Pellecchia G, Sung WWL, Wang Z, Bikangaga P, Boelman C, Carter MT, Cordeiro D, Cytrynbaum C, Dell SD, Dhir P, Dowling JJ, Heon E, Hewson S, Hiraki L, Inbar-Feigenberg M, Klatt R, Kronick J, Laxer RM, Licht C, MacDonald H, Mercimek-Andrews S, Mendoza-Londono R, Piscione T, Schneider R, Schulze A, Silverman E, Siriwardena K, Snead OC, Sondheimer N, Sutherland J, Vincent A, Wasserman JD, Weksberg R, Shuman C, Carew C, Szego MJ, Hayeems RZ, Basran R, Stavropoulos DJ, Ray PN, Bowdin S, Meyn MS, Cohn RD, Scherer SW, Marshall CR. Improved diagnostic yield compared with targeted gene sequencing panels suggests a role for whole-genome sequencing as a first-tier genetic test. *Genet Med* 2018;**20**:435–43.

23 Stavropoulos DJ, Merico D, Jobling R, Bowdin S, Monfared N, Thiruvahindrapuram B, Nalpathamkalam T, Pellecchia G, Yuen RKC, Szego MJ, Hayeems RZ, Shaul RZ, Brudno M, Girdea M, Frey B, Alipanahi B, Ahmed S, Babul-Hirji R, Porras RB, Carter MT, Chad L, Chaudhry A, Chitayat D, Doust SJ, Cytrynbaum C, Dupuis L, Ejaz R, Fishman L, Guerin A, Hashemi B, Helal M, Hewson S, Inbar-Feigenberg M, Kannu P, Karp N, Kim R, Kronick J, Liston E, MacDonald H, Mercimek-Mahmutoglu S, Mendoza-Londono R, Nasr E, Nimmo G, Parkinson N, Quercia N, Raiman J, Roifman M, Schulze A, Shugar A, Shuman C, Sinajon P, Siriwardena K, Weksberg R, Yoon G, Carew C, Erickson R, Leach RA, Klein R, Ray PN, Meyn MS, Scherer SW, Cohn RD, Marshall CR. Whole Genome Sequencing Expands Diagnostic Utility and Improves Clinical Management in Pediatric Medicine. *NPJ Genom Med* 2016;**1**:15012.

24 Willig LK, Petrikin JE, Smith LD, Saunders CJ, Thiffault I, Miller NA, Soden SE, Cakici JA, Herd SM, Twist G, Noll A, Creed M, Alba PM, Carpenter SL, Clements MA, Fischer RT, Hays JA, Kilbride H, McDonough RJ, Rosterman JL, Tsai SL, Zellmer L, Farrow EG, Kingsmore SF. Whole-genome sequencing for identification of Mendelian disorders in critically ill infants: a retrospective analysis of diagnostic and clinical findings. *Lancet Respir Med* 2015;**3**:377–87.

25 Bick D, Fraser PC, Gutzeit MF, Harris JM, Hambuch TM, Helbling DC, Jacob HJ, Kersten JN, Leuthner SR, May T, North PE, Prisco SZ, Schuler BA, Shimoyama M, Strong KA, Van Why SK, Veith R, Verbsky J, Weborg AM, Wilk BM, Willoughby RE, Worthey EA, Dimmock DP. Successful Application of Whole Genome Sequencing in a Medical Genetics Clinic. *J Pediatr Genet* 2017;**6**:61–76.

26 McKenna A, Hanna M, Banks E, Sivachenko A, Cibulskis K, Kernytsky A, Garimella K, Altshuler D, Gabriel S, Daly M, DePristo MA. The Genome Analysis Toolkit: a MapReduce framework for analyzing next-generation DNA sequencing data. *Genome Res* 2010;**20**:1297–303.

27 Li H, Durbin R. Fast and accurate short read alignment with Burrows-Wheeler transform. *Bioinformatics* 2009;**25**:1754–60.

28 Cingolani P, Platts A, Wang LL, Coon M, Nguyen T, Wang L, Land SJ, Lu X, Ruden DM. A program for annotating and predicting the effects of single nucleotide polymorphisms, SnpEff: SNPs in the genome of

Drosophila melanogaster strain w1118; iso-2; iso-3. *Fly (Austin)* 2012;**6**:80–92.

29 Lord J, McMullan DJ, Eberhardt RY, Rinck G, Hamilton SJ, Quinlan-Jones E, Prigmore E, Keelagher R, Best SK, Carey GK, Mellis R, Robart S, Berry IR, Chandler KE, Cilliers D, Cresswell L, Edwards SL, Gardiner C, Henderson A, Holden ST, Homfray T, Lester T, Lewis RA, Newbury-Ecob R, Prescott K, Quarrell OW, Ramsden SC, Roberts E, Tapon D, Tooley MJ, Vasudevan PC, Weber AP, Wellesley DG, Westwood P, White H, Parker M, Williams D, Jenkins L, Scott RH, Kilby MD, Chitty LS, Hurles ME, Maher ER, Prenatal Assessment of Genomes and Exomes Consortium. Prenatal exome sequencing analysis in fetal structural anomalies detected by ultrasonography (PAGE): a cohort study. *Lancet* 2019;**393**:747–57.

30 Rehm HL, Bale SJ, Bayrak-Toydemir P, Berg JS, Brown KK, Deignan JL, Friez MJ, Funke BH, Hegde MR, Lyon E, Working Group of the American College of Medical Genetics and Genomics Laboratory Quality Assurance Commitee. ACMG clinical laboratory standards for next-generation sequencing. *Genet Med* 2013;**15**:733–47.

31 Kircher M, Witten DM, Jain P, O'Roak BJ, Cooper GM, Shendure J. A general framework for estimating the relative pathogenicity of human genetic variants. *Nat Genet* 2014;**46**:310–5.

32 Jagadeesh KA, Wenger AM, Berger MJ, Guturu H, Stenson PD, Cooper DN, Bernstein JA, Bejerano G. M-CAP eliminates a majority of variants of uncertain significance in clinical exomes at high sensitivity. *Nat Genet* 2016;**48**:1581–6.

33 Li Q, Wang K. InterVar: Clinical Interpretation of Genetic Variants by the 2015 ACMG-AMP Guidelines. *Am J Hum Genet* 2017;**100**:267–80.

34 Eberle MA, Fritzilas E, Krusche P, Källberg M, Moore BL, Bekritsky MA, Iqbal Z, Chuang H-Y, Humphray SJ, Halpern AL, Kruglyak S, Margulies EH, McVean G, Bentley DR. A reference data set of 5.4 million phased human variants validated by genetic inheritance from sequencing a three-generation 17-member pedigree. *Genome Res* 2017;**27**:157–64.

35 Richards S, Aziz N, Bale S, Bick D, Das S, Gastier-Foster J, Grody WW, Hegde M, Lyon E, Spector E, Voelkerding K, Rehm HL, ACMG Laboratory Quality Assurance Committee. Standards and guidelines for the interpretation of sequence variants: a joint consensus recommendation of the American College of Medical Genetics and Genomics and the Association for Molecular Pathology. *Genet Med* 2015;**17**:405–24.

36 Zhao Z, Shilatifard A. Epigenetic modifications of histones in cancer. *Genome Biol* 2019;**20**:245.

37 Kim J-H, Lee JH, Lee I-S, Lee SB, Cho KS. Histone Lysine Methylation and Neurodevelopmental Disorders. *International Journal of Molecular Sciences* 2017;**18**:1404.

38 Peter CJ, Akbarian S. Balancing histone methylation activities in psychiatric disorders. *Trends Mol Med* 2011;**17**:372–9.

39 Bagchi RA, Weeks KL. Histone deacetylases in cardiovascular and metabolic diseases. *J Mol Cell Cardiol* 2019;**130**:151–9.

40 Wickramasekara RN, Stessman HAF. Histone 4 Lysine 20 Methylation: A Case for Neurodevelopmental Disease. *Biology* 2019;**8**:11.

41 Schwartzentruber J, Korshunov A, Liu X-Y, Jones DTW, Pfaff E, Jacob K, Sturm D, Fontebasso AM, Quang D-AK, Tönjes M, Hovestadt V, Albrecht S, Kool M, Nantel A, Konermann C, Lindroth A, Jäger N,

Rausch T, Ryzhova M, Korbel JO, Hielscher T, Hauser P, Garami M, Klekner A, Bognar L, Ebinger M, Schuhmann MU, Scheurlen W, Pekrun A, Frühwald MC, Roggendorf W, Kramm C, Dürken M, Atkinson J, Lepage P, Montpetit A, Zakrzewska M, Zakrzewski K, Liberski PP, Dong Z, Siegel P, Kulozik AE, Zapatka M, Guha A, Malkin D, Felsberg J, Reifenberger G, von Deimling A, Ichimura K, Collins VP, Witt H, Milde T, Witt O, Zhang C, Castelo-Branco P, Lichter P, Faury D, Tabori U, Plass C, Majewski J, Pfister SM, Jabado N. Driver mutations in histone H3.3 and chromatin remodelling genes in paediatric glioblastoma. *Nature* 2012;**482**:226–31.

42 Maver A, Čuturilo G, Ruml SJ, Peterlin B. Clinical Next Generation Sequencing Reveals an H3F3A Gene as a New Potential Gene Candidate for Microcephaly Associated with Severe Developmental Delay, Intellectual Disability and Growth Retardation. *Balkan J Med Genet* 2019;**22**:65–8.

43 Ederveen THA, Mandemaker IK, Logie C. The human histone H3 complement anno 2011. *Biochim Biophys Acta* 2011;**1809**:577–86.

44 Jang C-W, Shibata Y, Starmer J, Yee D, Magnuson T. Histone H3.3 maintains genome integrity during mammalian development. *Genes Dev* 2015;**29**:1377–92.

45 Bush KM, Yuen BT, Barrilleaux BL, Riggs JW, O'Geen H, Cotterman RF, Knoepfler PS. Endogenous mammalian histone H3.3 exhibits chromatin-related functions during development. *Epigenetics Chromatin* 2013;**6**:7.

46 Sakai A, Schwartz BE, Goldstein S, Ahmad K. Transcriptional and developmental functions of the H3.3 histone variant in Drosophila. *Curr Biol* 2009;**19**:1816–20.

47 Lim KK, Ong TYR, Tan YR, Yang EG, Ren B, Seah KS, Yang Z, Tan TS, Dymock BW, Chen ES. Mutation of histone H3 serine 86 disrupts GATA factor Ams2 expression and precise chromosome segregation in fission yeast. *Sci Rep* 2015;**5**:14064.

48 Karch KR, Sidoli S, Garcia BA. Identification and Quantification of Histone PTMs Using High-Resolution Mass Spectrometry. *Methods Enzymol* 2016;**574**:3–29.

49 Walker MB, Kimmel CB. A two-color acid-free cartilage and bone stain for zebrafish larvae. *Biotech Histochem* 2007;**82**:23–8.

50 Piovesan D, Minervini G, Tosatto SCE. The RING 2.0 web server for high quality residue interaction networks. *Nucleic Acids Res* 2016;**44**:W367-374.

51 Lek M, Karczewski KJ, Minikel EV, Samocha KE, Banks E, Fennell T, O'Donnell-Luria AH, Ware JS, Hill AJ, Cummings BB, Tukiainen T, Birnbaum DP, Kosmicki JA, Duncan LE, Estrada K, Zhao F, Zou J, Pierce-Hoffman E, Berghout J, Cooper DN, Deflaux N, DePristo M, Do R, Flannick J, Fromer M, Gauthier L, Goldstein J, Gupta N, Howrigan D, Kiezun A, Kurki MI, Moonshine AL, Natarajan P, Orozco L, Peloso GM, Poplin R, Rivas MA, Ruano-Rubio V, Rose SA, Ruderfer DM, Shakir K, Stenson PD, Stevens C, Thomas BP, Tiao G, Tusie-Luna MT, Weisburd B, Won H-H, Yu D, Altshuler DM, Ardissino D, Boehnke M, Danesh J, Donnelly S, Elosua R, Florez JC, Gabriel SB, Getz G, Glatt SJ, Hultman CM, Kathiresan S, Laakso M, McCarroll S, McCarthy MI, McGovern D, McPherson R, Neale BM, Palotie A, Purcell SM, Saleheen D, Scharf JM, Sklar P, Sullivan PF, Tuomilehto J, Tsuang MT, Watkins HC, Wilson JG, Daly MJ, MacArthur DG, Exome Aggregation Consortium. Analysis of protein-coding genetic variation in 60,706 humans. *Nature* 2016;**536**:285–91.

52 Pepenella S, Murphy KJ, Hayes JJ. Intra- and inter-nucleosome interactions of the core histone tail domains in higher-order chromatin structure. *Chromosoma* 2014;**123**:3–13.

53 Sidoli S, Garcia BA. Properly reading the histone code by MS-based proteomics. *Proteomics* 2015;**15**:2901–2.

54 Papillon-Cavanagh S, Lu C, Gayden T, Mikael LG, Bechet D, Karamboulas C, Ailles L, Karamchandani J, Marchione DM, Garcia BA, Weinreb I, Goldstein D, Lewis PW, Dancu OM, Dhaliwal S, Stecho W, Howlett CJ, Mymryk JS, Barrett JW, Nichols AC, Allis CD, Majewski J, Jabado N. Impaired H3K36 methylation defines a subset of head and neck squamous cell carcinomas. *Nat Genet* 2017;**49**:180–5.

55 Lewis PW, Müller MM, Koletsky MS, Cordero F, Lin S, Banaszynski LA, Garcia BA, Muir TW, Becher OJ, Allis CD. Inhibition of PRC2 activity by a gain-of-function H3 mutation found in pediatric glioblastoma. *Science* 2013;**340**:857–61.

56 Cox SG, Kim H, Garnett AT, Medeiros DM, An W, Crump JG. An essential role of variant histone H3.3 for ectomesenchyme potential of the cranial neural crest. *PLoS Genet* 2012;**8**:e1002938.

57 Lowe BR, Maxham LA, Hamey JJ, Wilkins MR, Partridge JF. Histone H3 Mutations: An Updated View of Their Role in Chromatin Deregulation and Cancer. *Cancers* 2019;**11**:660.

58 Ricketts MD, Frederick B, Hoff H, Tang Y, Schultz DC, Singh Rai T, Grazia Vizioli M, Adams PD, Marmorstein R. Ubinuclein-1 confers histone H3.3-specific-binding by the HIRA histone chaperone complex. *Nat Commun* 2015;**6**:7711.

59 Wen H, Li Y, Xi Y, Jiang S, Stratton S, Peng D, Tanaka K, Ren Y, Xia Z, Wu J, Li B, Barton MC, Li W, Li H, Shi X. ZMYND11 links histone H3.3K36me3 to transcription elongation and tumour suppression. *Nature* 2014;**508**:263–8.

60 Moskowitz AM, Belnap N, Siniard AL, Szelinger S, Claasen AM, Richholt RF, De Both M, Corneveaux JJ, Balak C, Piras IS, Russell M, Courtright AL, Rangasamy S, Ramsey K, Craig DW, Narayanan V, Huentelman MJ, Schrauwen I. A de novo missense mutation in ZMYND11 is associated with global developmental delay, seizures, and hypotonia. *Cold Spring Harb Mol Case Stud* 2016;**2**:a000851.

61 Johnson P, Mitchell V, McClure K, Kellems M, Marshall S, Allison MK, Lindley H, Nguyen H-TT, Tackett JE, Duina AA. A systematic mutational analysis of a histone H3 residue in budding yeast provides insights into chromatin dynamics. *G3 (Bethesda)* 2015;**5**:741–9.

62 Norris A, Bianchet MA, Boeke JD. Compensatory interactions between Sir3p and the nucleosomal LRS surface imply their direct interaction. *PLoS Genet* 2008;**4**:e1000301.

63 Matsubara K, Sano N, Umehara T, Horikoshi M. Global analysis of functional surfaces of core histones with comprehensive point mutants. *Genes Cells* 2007;**12**:13–33.

64 Hake SB, Allis CD. Histone H3 variants and their potential role in indexing mammalian genomes: the 'H3 barcode hypothesis'. *Proc Natl Acad Sci U S A* 2006;**103**:6428–35.

65 Schulmeister A, Schmid M, Thompson EM. Phosphorylation of the histone H3.3 variant in mitosis and meiosis of the urochordate Oikopleura dioica. *Chromosome Res* 2007;**15**:189–201.

66 Lau PNI, Cheung P. Histone code pathway involving H3 S28 phosphorylation and K27 acetylation

activates transcription and antagonizes polycomb silencing. *Proc Natl Acad Sci U S A* 2011;**108**:2801–6.

67 Sawicka A, Seiser C. Histone H3 phosphorylation - a versatile chromatin modification for different occasions. *Biochimie* 2012;**94**:2193–201.

68 Chang FTM, Chan FL, R McGhie JD, Udugama M, Mayne L, Collas P, Mann JR, Wong LH. CHK1-driven histone H3.3 serine 31 phosphorylation is important for chromatin maintenance and cell survival in human ALT cancer cells. *Nucleic Acids Res* 2015;**43**:2603–14.

69 Burgess RJ, Zhang Z. Histone chaperones in nucleosome assembly and human disease. *Nat Struct Mol Biol* 2013;**20**:14–22.

70 Maze I, Wenderski W, Noh K-M, Bagot RC, Tzavaras N, Purushothaman I, Elsässer SJ, Guo Y, Ionete C, Hurd YL, Tamminga CA, Halene T, Farrelly L, Soshnev AA, Wen D, Rafii S, Birtwistle MR, Akbarian S, Buchholz BA, Blitzer RD, Nestler EJ, Yuan Z-F, Garcia BA, Shen L, Molina H, Allis CD. Critical Role of Histone Turnover in Neuronal Transcription and Plasticity. *Neuron* 2015;**87**:77–94.

71 Lepack AE, Bagot RC, Peña CJ, Loh Y-HE, Farrelly LA, Lu Y, Powell SK, Lorsch ZS, Issler O, Cates HM, Tamminga CA, Molina H, Shen L, Nestler EJ, Allis CD, Maze I. Aberrant H3.3 dynamics in NAc promote vulnerability to depressive-like behavior. *Proc Natl Acad Sci U S A* 2016;**113**:12562–7.

72 Tatton-Brown K, Loveday C, Yost S, Clarke M, Ramsay E, Zachariou A, Elliott A, Wylie H, Ardissone A, Rittinger O, Stewart F, Temple IK, Cole T, Childhood Overgrowth Collaboration, Mahamdallie S, Seal S, Ruark E, Rahman N. Mutations in Epigenetic Regulation Genes Are a Major Cause of Overgrowth with Intellectual Disability. *Am J Hum Genet* 2017;**100**:725–36.

73 Tessadori F, Giltay JC, Hurst JA, Massink MP, Duran K, Vos HR, van Es RM, Deciphering Developmental Disorders Study, Scott RH, van Gassen KLI, Bakkers J, van Haaften G. Germline mutations affecting the histone H4 core cause a developmental syndrome by altering DNA damage response and cell cycle control. *Nat Genet* 2017;**49**:1642–6.

74 Forsythe LP, Szydlowski V, Murad MH, Ip S, Wang Z, Elraiyah TA, Fleurence R, Hickam DH. A Systematic Review of Approaches for Engaging Patients for Research on Rare Diseases. *J GEN INTERN MED* 2014;**29**:788–800.

75 Mussa A, Russo S, De Crescenzo A, Chiesa N, Molinatto C, Selicorni A, Richiardi L, Larizza L, Silengo MC, Riccio A, Ferrero GB. Prevalence of beckwith–wiedemann syndrome in North West of Italy. *American Journal of Medical Genetics Part A* 2013;**161**:2481–6.

76 Mussa A, Molinatto C, Cerrato F, Palumbo O, Carella M, Baldassarre G, Carli D, Peris C, Riccio A, Ferrero GB. Assisted Reproductive Techniques and Risk of Beckwith-Wiedemann Syndrome. *Pediatrics* 2017;**140**. doi:10.1542/peds.2016-4311

77 Shuman C, Beckwith JB, Weksberg R. Beckwith-Wiedemann Syndrome. In: Adam MP, Ardinger HH, Pagon RA, Wallace SE, Bean LJ, Stephens K, Amemiya A, eds. *GeneReviews®*. Seattle (WA): : University of Washington, Seattle 1993. http://www.ncbi.nlm.nih.gov/books/NBK1394/ (accessed 16 Jan2019).

78 Mussa A, Russo S, Larizza L, Riccio A, Ferrero GB. Epi)genotype–phenotype correlations in Beckwith–Wiedemann syndrome: a paradigm for genomic medicine. *Clinical Genetics* 2016;**89**:403–15.

79 Mussa A, Russo S, De Crescenzo A, Freschi A, Calzari L, Maitz S, Macchiaiolo M, Molinatto C,

Baldassarre G, Mariani M. (Epi) genotype–phenotype correlations in Beckwith–Wiedemann syndrome. *European Journal of Human Genetics* 2016;**24**:183–90.

80 Mussa A, Russo S, De Crescenzo A, Freschi A, Calzari L, Maitz S, Macchiaiolo M, Molinatto C, Baldassarre G, Mariani M, Tarani L, Bedeschi MF, Milani D, Melis D, Bartuli A, Cubellis MV, Selicorni A, Silengo MC, Larizza L, Riccio A, Ferrero GB. Fetal growth patterns in Beckwith–Wiedemann syndrome. *Clinical Genetics* 2016;**90**:21–7.

81 Mussa A, Molinatto C, Baldassarre G, Riberi E, Russo S, Larizza L, Riccio A, Ferrero GB. Cancer Risk in Beckwith-Wiedemann Syndrome: A Systematic Review and Meta-Analysis Outlining a Novel (Epi)Genotype Specific Histotype Targeted Screening Protocol. *The Journal of Pediatrics* 2016;**176**:142-149.e1.

82 Maas SM, Vansenne F, Kadouch DJM, Ibrahim A, Bliek J, Hopman S, Mannens MM, Merks JHM, Maher ER, Hennekam RC. Phenotype, cancer risk, and surveillance in Beckwith-Wiedemann syndrome depending on molecular genetic subgroups. *Am J Med Genet A* 2016;**170**:2248–60.

83 Brioude F, Kalish JM, Mussa A, Foster AC, Bliek J, Ferrero GB, Boonen SE, Cole T, Baker R, Bertoletti M, Cocchi G, Coze C, De Pellegrin M, Hussain K, Ibrahim A, Kilby MD, Krajewska-Walasek M, Kratz CP, Ladusans EJ, Lapunzina P, Le Bouc Y, Maas SM, Macdonald F, Õunap K, Peruzzi L, Rossignol S, Russo S, Shipster C, Skórka A, Tatton-Brown K, Tenorio J, Tortora C, Grønskov K, Netchine I, Hennekam RC, Prawitt D, Tümer Z, Eggermann T, Mackay DJG, Riccio A, Maher ER. Expert consensus document: Clinical and molecular diagnosis, screening and management of Beckwith-Wiedemann syndrome: an international consensus statement. *Nat Rev Endocrinol* 2018;**14**:229–49.

84 Mussa A, Di Candia S, Russo S, Catania S, De Pellegrin M, Di Luzio L, Ferrari M, Tortora C, Meazzini MC, Brusati R, Milani D, Zampino G, Montirosso R, Riccio A, Selicorni A, Cocchi G, Ferrero GB. Recommendations of the Scientific Committee of the Italian Beckwith–Wiedemann Syndrome Association on the diagnosis, management and follow-up of the syndrome. *European Journal of Medical Genetics* 2016;**59**:52–64.

85 Greer KJ, Kirkpatrick SJ, Weksberg R, Pauli RM. Beckwith-Wiedemann syndrome in adults: observations from one family and recommendations for care. *Am J Med Genet A* 2008;**146A**:1707–12.

86 Cacciari E, Milani S, Balsamo A, Spada E, Bona G, Cavallo L, Cerutti F, Gargantini L, Greggio N, Tonini G, Cicognani A. Italian cross-sectional growth charts for height, weight and BMI (2 to 20 yr). *J Endocrinol Invest* 2006;**29**:581–93.

87 Chiesa N, De Crescenzo A, Mishra K, Perone L, Carella M, Palumbo O, Mussa A, Sparago A, Cerrato F, Russo S, Lapi E, Cubellis MV, Kanduri C, Cirillo Silengo M, Riccio A, Ferrero GB. The KCNQ1OT1 imprinting control region and non-coding RNA: new properties derived from the study of Beckwith-Wiedemann syndrome and Silver-Russell syndrome cases. *Hum Mol Genet* 2012;**21**:10–25.

88 Zollino M, Orteschi D, Marangi G, De Crescenzo A, Pecile V, Riccio A, Neri G. A case of Beckwith-Wiedemann syndrome caused by a cryptic 11p15 deletion encompassing the centromeric imprinted domain of the BWS locus. *J Med Genet* 2010;**47**:429–32.

89 Sparago A, Cerrato F, Vernucci M, Ferrero GB, Silengo MC, Riccio A. Microdeletions in the human H19 DMR result in loss of IGF2 imprinting and Beckwith-Wiedemann syndrome. *Nat Genet* 2004;**36**:958–60.

90 Valente FM, Sparago A, Freschi A, Hill-Harfe K, Maas SM, Frints SGM, Alders M, Pignata L, Franzese M, Angelini C, Carli D, Mussa A, Gazzin A, Gabbarini F, Acurzio B, Ferrero GB, Bliek J, Williams CA, Riccio A, Cerrato F. Transcription alterations of KCNQ1 associated with imprinted methylation defects in the Beckwith-Wiedemann locus. *Genet Med* Published Online First: 12 January 2019. doi:10.1038/s41436-018-0416-7

91 Clouston WM, Cannell GC, Fryar BG, Searle JW, Martin NI, Mortimer RH. Virilizing adrenal adenoma in an adult with the Beckwith-Wiedemann syndrome: paradoxical response to dexamethasone. *Clin Endocrinol (Oxf)* 1989;**31**:467–73.

92 Kulkarni R, Wolf JS, Padiyar N, Zuckerman L, Gera R, Scott-Emuakpor AB. Severe intrarenal fibrosis, infundibular stenosis, renal cysts, and persistent perilobar nephrogenic rests in a patient with Beckwith-Wiedemann syndrome 27 years after diffuse nephroblastomatosis and Wilms tumor: natural progression or a consequence of treatment? *J Pediatr Hematol Oncol* 2002;**24**:389–93.

93 Hopsu E, Aarnisalo A, Pitkaranta A. Progressive stapedial fixation in Beckwith-Wiedemann syndrome. *Arch Otolaryngol Head Neck Surg* 2003;**129**:1131–4.

94 Aleck KA, Hadro TA. Dominant inheritance of Wiedemann-Beckwith syndrome: further evidence for transmission of 'unstable premutation' through carrier women. *Am J Med Genet* 1989;**33**:155–60.

95 Brioude F, Nicolas C, Marey I, Gaillard S, Bernier M, Das Neves C, Le Bouc Y, Touraine P, Netchine I. Hypercortisolism due to a Pituitary Adenoma Associated with Beckwith-Wiedemann Syndrome. *Horm Res Paediatr* 2016;**86**:206–11.

96 Gurrieri F, Zollino M, Oliva A, Pascali V, Orteschi D, Pietrobono R, Camporeale A, Coll Vidal M, Partemi S, Brugada R, Bellocci F, Neri G. Mild Beckwith-Wiedemann and severe long-QT syndrome due to deletion of the imprinting center 2 on chromosome 11p. *Eur J Hum Genet* 2013;**21**:965–9.

97 Romanelli V, Belinchón A, Benito-Sanz S, Martínez-Glez V, Gracia-Bouthelier R, Heath KE, Campos-Barros A, García-Miñaur S, Fernandez L, Meneses H, López-Siguero JP, Guillén-Navarro E, Gómez-Puertas P, Wesselink J-J, Mercado G, Esteban-Marfil V, Palomo R, Mena R, Sánchez A, Del Campo M, Lapunzina P. CDKN1C (p57(Kip2)) analysis in Beckwith-Wiedemann syndrome (BWS) patients: Genotype-phenotype correlations, novel mutations, and polymorphisms. *Am J Med Genet A* 2010;**152A**:1390–7.

98 Cardarelli L, Sparago A, De Crescenzo A, Nalesso E, Zavan B, Cubellis MV, Selicorni A, Cavicchioli P, Pozzan GB, Petrella M, Riccio A. Silver-Russell syndrome and Beckwith-Wiedemann syndrome phenotypes associated with 11p duplication in a single family. *Pediatr Dev Pathol* 2010;**13**:326–30.

99 Tomlinson JK, Morse SA, Bernard SPL, Greensmith AL, Meara JG. Long-term outcomes of surgical tongue reduction in Beckwith-Wiedemann syndrome. *Plast Reconstr Surg* 2007;**119**:992–1002.

100 Matsumoto K, Morita K-I, Jinno S, Omura K. Sensory changes after tongue reduction for macroglossia. *Oral Surg Oral Med Oral Pathol Oral Radiol* 2014;**117**:e1-2.

101 Mussa A, Peruzzi L, Chiesa N, Crescenzo A, Russo S, Melis D, Tarani L, Baldassarre G, Larizza L, Riccio A, Silengo M, Ferrero G. Nephrological findings and genotype–phenotype correlation in Beckwith–Wiedemann syndrome. *Pediatric Nephrology* 2012;**27**:397–406.

102 Elliott M, Bayly R, Cole T, Temple IK, Maher ER. Clinical features and natural history of

Beckwith-Wiedemann syndrome: presentation of 74 new cases. *Clin Genet* 1994;**46**:168–74.

103 Pettenati MJ, Haines JL, Higgins RR, Wappner RS, Palmer CG, Weaver DD. Wiedemann-Beckwith syndrome: presentation of clinical and cytogenetic data on 22 new cases and review of the literature. *Hum Genet* 1986;**74**:143–54.

104 Canavese F, Mussa A, Manenti M, Cortese MG, Ferrero L, Tuli G, Macchieraldo R, Lala R. Sperm count of young men surgically treated for cryptorchidism in the first and second year of life: fertility is better in children treated at a younger age. *Eur J Pediatr Surg* 2009;**19**:388–91.

105 Feyles F, Peiretti V, Mussa A, Manenti M, Canavese F, Cortese MG, Lala R. Improved sperm count and motility in young men surgically treated for cryptorchidism in the first year of life. *Eur J Pediatr Surg* 2014;**24**:376–80.

106 Chan E, Wayne C, Nasr A, FRCSC for Canadian Association of Pediatric Surgeon Evidence-Based Resource. Ideal timing of orchiopexy: a systematic review. *Pediatr Surg Int* 2014;**30**:87–97.

107 Gianotten J, van der Veen F, Alders M, Leschot NJ, Tanck MWT, Land JA, Kremer JAM, Hoefsloot LH, Mannens MM, Lombardi MP, Hoffer MJV. Chromosomal region 11p15 is associated with male factor subfertility. *Mol Hum Reprod* 2003;**9**:587–92.

108 Hayward NK, Little MH, Mortimer RH, Clouston WM, Smith PJ. Generation of homozygosity at the c-Ha-ras-1 locus on chromosome 11p in an adrenal adenoma from an adult with Wiedemann-Beckwith syndrome. *Cancer Genet Cytogenet* 1988;**30**:127–32.

109 Bémurat L, Gosse P, Ballanger P, Tauzin-Fin P, Barat P, Lacombe D, Lemétayer P, Clémenty J. Successful laparoscopic operation of bilateral pheochromocytoma in a patient with Beckwith-Wiedemann syndrome. *J Hum Hypertens* 2002;**16**:281–4.

110 Houtenbos I, Ossenkoppele GJ. Acute myeloid leukemia in a 23-year-old patient with Beckwith-Wiedemann syndrome. *Cancer Genet Cytogenet* 2002;**136**:90–1.

111 Bertoin F, Letouzé E, Grignani P, Patey M, Rossignol S, Libé R, Pasqual C, Lardière-Deguelte S, Hoeffel-Fornes C, Gaillard D, Previderè C, Delemer B, Lalli E. Genome-wide paternal uniparental disomy as a cause of Beckwith-Wiedemann syndrome associated with recurrent virilizing adrenocortical tumors. *Horm Metab Res* 2015;**47**:497–503.

112 Romanelli V, Nevado J, Fraga M, Trujillo AM, Mori MÁ, Fernández L, Pérez de Nanclares G, Martínez-Glez V, Pita G, Meneses H, Gracia R, García-Miñaur S, García de Miguel P, Lecumberri B, Rodríguez JI, González Neira A, Monk D, Lapunzina P. Constitutional mosaic genome-wide uniparental disomy due to diploidisation: an unusual cancer-predisposing mechanism. *J Med Genet* 2011;**48**:212–6.

113 Fleisher AS, Meltzer SJ, James SP. Colon polyps in Beckwith-Wiedmann syndrome: role of imprinted genes. *Gastroenterology* 2000;**118**:637.

114 Haack TB, Staufner C, Köpke MG, Straub BK, Kölker S, Thiel C, Freisinger P, Baric I, McKiernan PJ, Dikow N, Harting I, Beisse F, Burgard P, Kotzaeridou U, Kühr J, Himbert U, Taylor RW, Distelmaier F, Vockley J, Ghaloul-Gonzalez L, Zschocke J, Kremer LS, Graf E, Schwarzmayr T, Bader DM, Gagneur J, Wieland T, Terrile C, Strom TM, Meitinger T, Hoffmann GF, Prokisch H. Biallelic Mutations in NBAS Cause Recurrent Acute Liver Failure with Onset in Infancy. *Am J Hum Genet* 2015;**97**:163–9.

115 Maksimova N, Hara K, Nikolaeva I, Chun-Feng T, Usui T, Takagi M, Nishihira Y, Miyashita A, Fujiwara H, Oyama T, Nogovicina A, Sukhomyasova A, Potapova S, Kuwano R, Takahashi H, Nishizawa M, Onodera O. Neuroblastoma amplified sequence gene is associated with a novel short stature syndrome characterised by optic nerve atrophy and Pelger-Huët anomaly. *J Med Genet* 2010;**47**:538–48.

116 Palagano E, Zuccarini G, Prontera P, Borgatti R, Stangoni G, Elisei S, Mantero S, Menale C, Forlino A, Uva P, Oppo M, Vezzoni P, Villa A, Merlo GR, Sobacchi C. Mutations in the Neuroblastoma Amplified Sequence gene in a family affected by Acrofrontofacionasal Dysostosis type 1. *Bone* 2018;**114**:125–36.

117 Prontera P, Urciuoli R, Siliquini S, Macone S, Stangoni G, Donti E, Cantisani TA, Elia M, Belcastro V. Acrofrontofacionasal dysostosis 1 in two sisters of Indian origin. *Am J Med Genet A* 2011;**155A**:3125–7.

118 Balasubramanian M, Hurst J, Brown S, Bishop NJ, Arundel P, DeVile C, Pollitt RC, Crooks L, Longman D, Caceres JF, Shackley F, Connolly S, Payne JH, Offiah AC, Hughes D, DDD Study, Parker MJ, Hide W, Skerry TM. Compound heterozygous variants in NBAS as a cause of atypical osteogenesis imperfecta. *Bone* 2017;**94**:65–74.

119 Park JW, Lee SJ. Foveal hypoplasia in short stature with optic atrophy and Pelger-Huët anomaly syndrome with neuroblastoma-amplified sequence (NBAS) gene mutation. *J AAPOS* 2021;**25**:257-259.e2.

120 Kortüm F, Marquardt I, Alawi M, Korenke GC, Spranger S, Meinecke P, Kutsche K. Acute Liver Failure Meets SOPH Syndrome: A Case Report on an Intermediate Phenotype. *Pediatrics* 2017;**139**:e20160550.

121 Staufner C, Haack TB, Köpke MG, Straub BK, Kölker S, Thiel C, Freisinger P, Baric I, McKiernan PJ, Dikow N, Harting I, Beisse F, Burgard P, Kotzaeridou U, Lenz D, Kühr J, Himbert U, Taylor RW, Distelmaier F, Vockley J, Ghaloul-Gonzalez L, Ozolek JA, Zschocke J, Kuster A, Dick A, Das AM, Wieland T, Terrile C, Strom TM, Meitinger T, Prokisch H, Hoffmann GF. Recurrent acute liver failure due to NBAS deficiency: phenotypic spectrum, disease mechanisms, and therapeutic concepts. *J Inherit Metab Dis* 2016;**39**:3–16.

122 Sunwoo Y, Kim Y-M, Kim EN, Oh S-H, Lee BH. Severe form of neuroblastoma amplified sequence deficiency in an infant with recurrent acute liver failure. *Pediatr Int* 2018;**60**:302–4.

123 Capo-Chichi J-M, Mehawej C, Delague V, Caillaud C, Khneisser I, Hamdan FF, Michaud JL, Kibar Z, Mégarbané A. Neuroblastoma Amplified Sequence (NBAS) mutation in recurrent acute liver failure: Confirmatory report in a sibship with very early onset, osteoporosis and developmental delay. *Eur J Med Genet* 2015;**58**:637–41.

124 Mégarbané A, Samaras L, Chédid R, Chouery E, Chrétien D, Caillaud C, Abou-Ghoch J, Jalkh N. Developmental delay, dysmorphic features, neonatal spontaneous fractures, wrinkled skin, and hepatic failure: a new metabolic syndrome? *Am J Med Genet A* 2008;**146A**:3198–201.

125 Flex E, Niceta M, Cecchetti S, Thiffault I, Au MG, Capuano A, Piermarini E, Ivanova AA, Francis JW, Chillemi G, Chandramouli B, Carpentieri G, Haaxma CA, Ciolfi A, Pizzi S, Douglas GV, Levine K, Sferra A, Dentici ML, Pfundt RR, Le Pichon J-B, Farrow E, Baas F, Piemonte F, Dallapiccola B, Graham JM, Saunders CJ, Bertini E, Kahn RA, Koolen DA, Tartaglia M. Biallelic Mutations in TBCD, Encoding the

Tubulin Folding Cofactor D, Perturb Microtubule Dynamics and Cause Early-Onset Encephalopathy. *Am J Hum Genet* 2016;**99**:962–73.

126 Kortüm F, Caputo V, Bauer CK, Stella L, Ciolfi A, Alawi M, Bocchinfuso G, Flex E, Paolacci S, Dentici ML, Grammatico P, Korenke GC, Leuzzi V, Mowat D, Nair LDV, Nguyen TTM, Thierry P, White SM, Dallapiccola B, Pizzuti A, Campeau PM, Tartaglia M, Kutsche K. Mutations in KCNH1 and ATP6V1B2 cause Zimmermann-Laband syndrome. *Nat Genet* 2015;**47**:661–7.

127 Niceta M, Stellacci E, Gripp KW, Zampino G, Kousi M, Anselmi M, Traversa A, Ciolfi A, Stabley D, Bruselles A, Caputo V, Cecchetti S, Prudente S, Fiorenza MT, Boitani C, Philip N, Niyazov D, Leoni C, Nakane T, Keppler-Noreuil K, Braddock SR, Gillessen-Kaesbach G, Palleschi A, Campeau PM, Lee BHL, Pouponnot C, Stella L, Bocchinfuso G, Katsanis N, Sol-Church K, Tartaglia M. Mutations Impairing GSK3-Mediated MAF Phosphorylation Cause Cataract, Deafness, Intellectual Disability, Seizures, and a Down Syndrome-like Facies. *Am J Hum Genet* 2015;**96**:816–25.

128 Gurovich Y, Hanani Y, Bar O, Nadav G, Fleischer N, Gelbman D, Basel-Salmon L, Krawitz PM, Kamphausen SB, Zenker M, Bird LM, Gripp KW. Identifying facial phenotypes of genetic disorders using deep learning. *Nat Med* 2019;**25**:60–4.

129 Regateiro FS, Belkaya S, Neves N, Ferreira S, Silvestre P, Lemos S, Venâncio M, Casanova J-L, Gonçalves I, Jouanguy E, Diogo L. Recurrent elevated liver transaminases and acute liver failure in two siblings with novel bi-allelic mutations of NBAS. *Eur J Med Genet* 2017;**60**:426–32.

130 Segarra NG, Ballhausen D, Crawford H, Perreau M, Campos-Xavier B, van Spaendonck-Zwarts K, Vermeer C, Russo M, Zambelli P-Y, Stevenson B, Royer-Bertrand B, Rivolta C, Candotti F, Unger S, Munier FL, Superti-Furga A, Bonafé L. NBAS mutations cause a multisystem disorder involving bone, connective tissue, liver, immune system, and retina. *Am J Med Genet A* 2015;**167A**:2902–12.

131 Calvo PL, Tandoi F, Haak TB, Brunati A, Pinon M, Olio DD, Romagnoli R, Spada M. NBAS mutations cause acute liver failure: when acetaminophen is not a culprit. *Ital J Pediatr* 2017;**43**:88.

132 Wang J, Pu Z, Lu Z. Targeted next-generation sequencing reveals two novel mutations of NBAS in a patient with infantile liver failure syndrome-2. *Mol Med Rep* 2018;**17**:2245–50.

133 Abstracts from the 51st European Society of Human Genetics Conference: Electronic Posters. *Eur J Hum Genet* 2019;**27**:870–1041.

134 Li J-Q, Qiu Y-L, Gong J-Y, Dou L-M, Lu Y, Knisely AS, Zhang M-H, Luan W-S, Wang J-S. Novel NBAS mutations and fever-related recurrent acute liver failure in Chinese children: a retrospective study. *BMC Gastroenterol* 2017;**17**:77.

135 Hasosah MY, Iskandarani AI, Shawli AI, Alsahafi AF, Sukkar GA, Qurashi MA. Neuroblastoma amplified sequence gene mutation: A rare cause of recurrent liver failure in children. *Saudi J Gastroenterol* 2017;**23**:206–8.

136 Mueller WF, Larsen LSZ, Garibaldi A, Hatfield GW, Hertel KJ. The Silent Sway of Splicing by Synonymous Substitutions. *J Biol Chem* 2015;**290**:27700–11.

137 Supek F, Miñana B, Valcárcel J, Gabaldón T, Lehner B. Synonymous mutations frequently act as driver mutations in human cancers. *Cell* 2014;**156**:1324–35.

138 Gelfman S, Wang Q, McSweeney KM, Ren Z, La Carpia F, Halvorsen M, Schoch K, Ratzon F, Heinzen EL, Boland MJ, Petrovski S, Goldstein DB. Annotating pathogenic non-coding variants in genic regions. *Nat Commun* 2017;**8**:236.

139 Livingstone M, Folkman L, Yang Y, Zhang P, Mort M, Cooper DN, Liu Y, Stantic B, Zhou Y. Investigating DNA-, RNA-, and protein-based features as a means to discriminate pathogenic synonymous variants. *Hum Mutat* 2017;**38**:1336–47.

140 Pantaleoni F, Lev D, Cirstea IC, Motta M, Lepri FR, Bottero L, Cecchetti S, Linger I, Paolacci S, Flex E, Novelli A, Carè A, Ahmadian MR, Stellacci E, Tartaglia M. Aberrant HRAS transcript processing underlies a distinctive phenotype within the RASopathy clinical spectrum. *Hum Mutat* 2017;**38**:798–804.

141 Wu X, Simpson J, Hong JH, Kim K-H, Thavarajah NK, Backx PH, Neel BG, Araki T. MEK-ERK pathway modulation ameliorates disease phenotypes in a mouse model of Noonan syndrome associated with the Raf1(L613V) mutation. *J Clin Invest* 2011;**121**:1009–25.

142 Tartaglia M, Zampino G, Gelb BD. Noonan syndrome: clinical aspects and molecular pathogenesis. *Mol Syndromol* 2010;**1**:2–26.

143 Tartaglia M, Kalidas K, Shaw A, Song X, Musat DL, van der Burgt I, Brunner HG, Bertola DR, Crosby A, Ion A, Kucherlapati RS, Jeffery S, Patton MA, Gelb BD. PTPN11 mutations in Noonan syndrome: molecular spectrum, genotype-phenotype correlation, and phenotypic heterogeneity. *Am J Hum Genet* 2002;**70**:1555–63.

144 Aoki Y, Niihori T, Banjo T, Okamoto N, Mizuno S, Kurosawa K, Ogata T, Takada F, Yano M, Ando T, Hoshika T, Barnett C, Ohashi H, Kawame H, Hasegawa T, Okutani T, Nagashima T, Hasegawa S, Funayama R, Nagashima T, Nakayama K, Inoue S-I, Watanabe Y, Ogura T, Matsubara Y. Gain-of-function mutations in RIT1 cause Noonan syndrome, a RAS/MAPK pathway syndrome. *Am J Hum Genet* 2013;**93**:173–80.

145 Motta M, Giancotti A, Mastromoro G, Chandramouli B, Pinna V, Pantaleoni F, Di Giosaffatte N, Petrini S, Mazza T, D'Ambrosio V, Versacci P, Ventriglia F, Chillemi G, Pizzuti A, Tartaglia M, De Luca A. Clinical and functional characterization of a novel RASopathy-causing SHOC2 mutation associated with prenatal-onset hypertrophic cardiomyopathy. *Hum Mutat* Published Online First: 6 May 2019. doi:10.1002/humu.23767

146 Pandit B, Sarkozy A, Pennacchio LA, Carta C, Oishi K, Martinelli S, Pogna EA, Schackwitz W, Ustaszewska A, Landstrom A, Bos JM, Ommen SR, Esposito G, Lepri F, Faul C, Mundel P, López Siguero JP, Tenconi R, Selicorni A, Rossi C, Mazzanti L, Torrente I, Marino B, Digilio MC, Zampino G, Ackerman MJ, Dallapiccola B, Tartaglia M, Gelb BD. Gain-of-function RAF1 mutations cause Noonan and LEOPARD syndromes with hypertrophic cardiomyopathy. *Nat Genet* 2007;**39**:1007–12.

147 Gelb BD, Roberts AE, Tartaglia M. Cardiomyopathies in Noonan syndrome and the other RASopathies. *Prog Pediatr Cardiol* 2015;**39**:13–9.

148 Calcagni G, Adorisio R, Martinelli S, Grutter G, Baban A, Versacci P, Digilio MC, Drago F, Gelb BD, Tartaglia M, Marino B. Clinical Presentation and Natural History of Hypertrophic Cardiomyopathy in RASopathies. *Heart Fail Clin* 2018;**14**:225–35.

149 Jaouadi H, Chehida AB, Kraoua L, Etchevers HC, Argiro L, Kasdallah N, Blibech S, Delague

V, Lévy N, Tebib N, Mrad R, Abdelhak S, Benkhalifa R, Zaffran S. A severe clinical phenotype of Noonan syndrome with neonatal hypertrophic cardiomyopathy in the second case worldwide with RAF1 S259Y neomutation. *Genet Res (Camb)* 2019;**101**:e6.

150 Calcagni G, Limongelli G, D'Ambrosio A, Gesualdo F, Digilio MC, Baban A, Albanese SB, Versacci P, De Luca E, Ferrero GB, Baldassarre G, Agnoletti G, Banaudi E, Marek J, Kaski JP, Tuo G, Russo MG, Pacileo G, Milanesi O, Messina D, Marasini M, Cairello F, Formigari R, Brighenti M, Dallapiccola B, Tartaglia M, Marino B. Cardiac defects, morbidity and mortality in patients affected by RASopathies. CARNET study results. *Int J Cardiol* 2017;**245**:92–8.

151 Dobin A, Davis CA, Schlesinger F, Drenkow J, Zaleski C, Jha S, Batut P, Chaisson M, Gingeras TR. STAR: ultrafast universal RNA-seq aligner. *Bioinformatics* 2013;**29**:15–21.

152 Liao Y, Smyth GK, Shi W. featureCounts: an efficient general purpose program for assigning sequence reads to genomic features. *Bioinformatics* 2014;**30**:923–30.

153 Robinson MD, McCarthy DJ, Smyth GK. edgeR: a Bioconductor package for differential expression analysis of digital gene expression data. *Bioinformatics* 2010;**26**:139–40.

154 Liberzon A, Subramanian A, Pinchback R, Thorvaldsdóttir H, Tamayo P, Mesirov JP. Molecular signatures database (MSigDB) 3.0. *Bioinformatics* 2011;**27**:1739–40.

155 Subramanian A, Tamayo P, Mootha VK, Mukherjee S, Ebert BL, Gillette MA, Paulovich A, Pomeroy SL, Golub TR, Lander ES, Mesirov JP. Gene set enrichment analysis: a knowledge-based approach for interpreting genome-wide expression profiles. *Proc Natl Acad Sci U S A* 2005;**102**:15545–50.

156 Sun X, Kaufman PD. Ki-67: more than a proliferation marker. *Chromosoma* 2018;**127**:175–86.

157 Dhandapany PS, Fabris F, Tonk R, Illaste A, Karakikes I, Sorourian M, Sheng J, Hajjar RJ, Tartaglia M, Sobie EA, Lebeche D, Gelb BD. Cyclosporine attenuates cardiomyocyte hypertrophy induced by RAF1 mutants in Noonan and LEOPARD syndromes. *J Mol Cell Cardiol* 2011;**51**:4–15.

158 Savoia P, Fava P, Casoni F, Cremona O. Targeting the ERK Signaling Pathway in Melanoma. *Int J Mol Sci* 2019;**20**. doi:10.3390/ijms20061483

159 Hopper RK, Feinstein JA, Manning MA, Benitz W, Hudgins L. Neonatal pulmonary arterial hypertension and Noonan syndrome: two fatal cases with a specific RAF1 mutation. *Am J Med Genet A* 2015;**167A**:882–5.

160 Thompson D, Patrick-Esteve J, Surcouf JW, Rivera D, Castellanos B, Desai P, Lilje C, Lacassie Y, Marble M, Zambrano R. RAF1 variants causing biventricular hypertrophic cardiomyopathy in two preterm infants: further phenotypic delineation and review of literature. *Clin Dysmorphol* 2017;**26**:195–9.

161 Carcavilla A, Santomé JL, Pinto I, Sánchez-Pozo J, Guillén-Navarro E, Martín-Frías M, Lapunzina P, Ezquieta B. LEOPARD syndrome: a variant of Noonan syndrome strongly associated with hypertrophic cardiomyopathy. *Rev Esp Cardiol (Engl Ed)* 2013;**66**:350–6.

162 Gelb BD, Tartaglia M. Noonan Syndrome with Multiple Lentigines. In: Adam MP, Ardinger HH, Pagon RA, Wallace SE, Bean LJ, Mirzaa G, Amemiya A, eds. *GeneReviews®*. Seattle (WA): : University of Washington, Seattle 1993. http://www.ncbi.nlm.nih.gov/books/NBK1383/ (accessed 14 Jun2021).

163 Razzaque MA, Nishizawa T, Komoike Y, Yagi H, Furutani M, Amo R, Kamisago M, Momma K, Katayama H, Nakagawa M, Fujiwara Y, Matsushima M, Mizuno K, Tokuyama M, Hirota H, Muneuchi J, Higashinakagawa T, Matsuoka R. Germline gain-of-function mutations in RAF1 cause Noonan syndrome. *Nat Genet* 2007;**39**:1013–7.

164 Zarate YA, Lichty AW, Champion KJ, Clarkson LK, Holden KR, Matheus MG. Unique cerebrovascular anomalies in Noonan syndrome with RAF1 mutation. *J Child Neurol* 2014;**29**:NP13-17.

165 Dhandapany PS, Razzaque MdA, Muthusami U, Kunnoth S, Edwards JJ, Mulero-Navarro S, Riess I, Pardo S, Sheng J, Rani DS, Rani B, Govindaraj P, Flex E, Yokota T, Furutani M, Nishizawa T, Nakanishi T, Robbins J, Limongelli G, Hajjar RJ, Lebeche D, Bahl A, Khullar M, Rathinavel A, Sadler KC, Tartaglia M, Matsuoka R, Thangaraj K, Gelb BD. RAF1 mutations in childhood-onset dilated cardiomyopathy. *Nat Genet* 2014;**46**:635–9.

166 Ko JM, Kim J-M, Kim G-H, Yoo H-W. PTPN11, SOS1, KRAS, and RAF1 gene analysis, and genotype-phenotype correlation in Korean patients with Noonan syndrome. *J Hum Genet* 2008;**53**:999–1006.

167 Wilkinson JD, Lowe AM, Salbert BA, Sleeper LA, Colan SD, Cox GF, Towbin JA, Connuck DM, Messere JE, Lipshultz SE. Outcomes in children with Noonan syndrome and hypertrophic cardiomyopathy: a study from the Pediatric Cardiomyopathy Registry. *Am Heart J* 2012;**164**:442–8.

168 Brown JR, Plotnick G. Pulmonary artery aneurysm as a cause for chest pain in a patient with Noonan's syndrome: a case report. *Cardiology* 2008;**110**:249–51.

169 Morgan JM, Coupe MO, Honey M, Miller GA. Aneurysms of the sinuses of Valsalva in Noonan's syndrome. *Eur Heart J* 1989;**10**:190–3.

170 Ogihara Y, Fujimoto N, Ohashi H, Yamamoto N, Ito H, Mitani Y, Aoki Y, Imanaka-Yosida K, Ito M, Dohi K. Case of Noonan Syndrome With an Expanding Coronary Arterial Aneurysm. *Circ Cardiovasc Imaging* 2019;**12**:e009429.

171 Purnell R, Williams I, Von Oppell U, Wood A. Giant aneurysms of the sinuses of Valsalva and aortic regurgitation in a patient with Noonan's syndrome. *Eur J Cardiothorac Surg* 2005;**28**:346–8.

172 Tahir RA, Asmaro K, Pabaney A, Kole M, Nypaver T, Marin H. Separate origins of the left internal and external carotid arteries from the aortic arch and cervical internal carotid artery aneurysm in a patient with Noonan syndrome. *J Neurointerv Surg* 2017;**9**:e11.

173 Wong CK, Cheng CH, Lau CP, Leung WH. Congenital coronary artery anomalies in Noonan's syndrome. *Am Heart J* 1990;**119**:396–400.

174 Yanli Z, Xiaocong W, Liping P, Yan M, Wei Y, Shu J. Diagnosis of a giant left atrial appendage aneurysm by contrast-enhanced echocardiography: Case report and literature review. *J Clin Ultrasound* 2021;**49**:293–7.

175 Weatherald J, Dorfmüller P, Perros F, Ghigna M-R, Girerd B, Humbert M, Montani D. Pulmonary capillary haemangiomatosis: a distinct entity? *Eur Respir Rev* 2020;**29**. doi:10.1183/16000617.0168-2019

176 Lee DH, Kim WB, Choi JH, Lee SN. A Case of Congenital Pulmonary Lymphangiectasia in Noonan Syndrome. Journal of the Korean Pediatric Society. 2014;**40**:877–82.

177 Puvabanditsin S, Abellar R, Madubuko A, Mehta R, Walzer L. Pulmonary Vasculitis and a Horseshoe Kidney in Noonan Syndrome. *Case Rep Pathol* 2018;**2018**:6829586.

178 Guignabert C, Tu L, Le Hiress M, Ricard N, Sattler C, Seferian A, Huertas A, Humbert M, Montani D. Pathogenesis of pulmonary arterial hypertension: lessons from cancer. *Eur Respir Rev* 2013;**22**:543–51.

179 Awad KS, Elinoff JM, Wang S, Gairhe S, Ferreyra GA, Cai R, Sun J, Solomon MA, Danner RL. Raf/ERK drives the proliferative and invasive phenotype of BMPR2-silenced pulmonary artery endothelial cells. *Am J Physiol Lung Cell Mol Physiol* 2016;**310**:L187-201.

180 Oviedo A, Abramson LP, Worthington R, Dainauskas JR, Crawford SE. Congenital pulmonary capillary hemangiomatosis: Report of two cases and review of the literature. *Pediatr Pulmonol* 2003;**36**:253–6.

181 Ferrero GB, Picco G, Baldassarre G, Flex E, Isella C, Cantarella D, Corà D, Chiesa N, Crescenzio N, Timeus F, Merla G, Mazzanti L, Zampino G, Rossi C, Silengo M, Tartaglia M, Medico E. Transcriptional hallmarks of Noonan syndrome and Noonan-like syndrome with loose anagen hair. *Hum Mutat* 2012;**33**:703–9.

182 Chen X, Li Y, Luo J, Hou N. Molecular Mechanism of Hippo-YAP1/TAZ Pathway in Heart Development, Disease, and Regeneration. *Front Physiol* 2020;**11**:389.

183 Lee K-S, Park J-H, Lim H-J, Park H-Y. HB-EGF induces cardiomyocyte hypertrophy via an ERK5-MEF2A-COX2 signaling pathway. *Cell Signal* 2011;**23**:1100–9.

184 Liu C, Lim ST, Teo MHY, Tan MSY, Kulkarni MD, Qiu B, Li A, Lal S, Dos Remedios CG, Tan NS, Wahli W, Ferenczi MA, Song W, Hong W, Wang X. Collaborative Regulation of LRG1 by TGF-β1 and PPAR-β/δ Modulates Chronic Pressure Overload-Induced Cardiac Fibrosis. *Circ Heart Fail* 2019;**12**:e005962.

185 López B, González A, Lindner D, Westermann D, Ravassa S, Beaumont J, Gallego I, Zudaire A, Brugnolaro C, Querejeta R, Larman M, Tschöpe C, Díez J. Osteopontin-mediated myocardial fibrosis in heart failure: a role for lysyl oxidase? *Cardiovasc Res* 2013;**99**:111–20.

186 Gratzinger D, Zhao S, West R, Rouse RV, Vogel H, Gil EC, Levy R, Lossos IS, Natkunam Y. The transcription factor LMO2 is a robust marker of vascular endothelium and vascular neoplasms and selected other entities. *Am J Clin Pathol* 2009;**131**:264–78.

187 Leong ZP, Okida A, Higuchi M, Yamano Y, Hikasa Y. Reversal effects of low-dose imatinib compared with sunitinib on monocrotaline-induced pulmonary and right ventricular remodeling in rats. *Vascul Pharmacol* 2018;**100**:41–50.

188 Subbiah V, Baik C, Kirkwood JM. Clinical Development of BRAF plus MEK Inhibitor Combinations. *Trends Cancer* 2020;**6**:797–810.

189 Julkowska D, Austin CP, Cutillo CM, Gancberg D, Hager C, Halftermeyer J, Jonker AH, Lau LPL, Norstedt I, Rath A, Schuster R, Simelyte E, van Weely S. The importance of international collaboration for rare diseases research: a European perspective. *Gene Ther* 2017;**24**:562–71.

190 Roberts AE. Noonan Syndrome. In: Adam MP, Ardinger HH, Pagon RA, Wallace SE, Bean

LJ, Gripp KW, Mirzaa GM, Amemiya A, eds. *GeneReviews*®. Seattle (WA): : University of Washington, Seattle 1993. http://www.ncbi.nlm.nih.gov/books/NBK1124/ (accessed 30 Jan2022).